Towards the controlled destabilisation of aggregates

Simon Welsh

Towards the Controlled Destabilisation of Aggregates

by

Simon Welsh

A thesis submitted in part-fulfilment of the degree of Doctor of Philosophy of the University of Durham
February 2003

Research carried out at the Department of Chemistry
1999-2002

Towards the Controlled Destabilisation of Aggregates

Simon Welsh

Abstract

Lipid based non-viral delivery systems are potentially of great importance to the development of an effective and versatile therapeutic gene treatment. Many difficulties are faced in designing efficient lipid based gene delivery systems and addressing the problem of endosomal escape is one key area where efficiency could be greatly improved

Molecules aimed at inducing aggregate disruption in response to changes in pH, or metal ion concentration, have been synthesised. Series of compounds were prepared based on cationic 5-alkyl-2-methylaminoalkyl pyridine amphiphiles and amphiphilic C_8-C_{16} EDTA dialkylamides.

The critical aggregation concentration of each species was measured and a series of experiments undertaken, designed to assess the extent of pH, or metal ion concentration, induced aggregate disruption effects. The experiments were carried out by including the molecules to be examined as small mole percent co-aggregates in micellar and liposome model systems.

Each group of compounds appears to exhibit disruption effects on the more strongly ordered bilayer membrane systems, with the EDTA based compounds displaying the most consistent pH dependent disruption. However, the more dynamic micellar aggregate models were less sensitive to disruption using the particular observation method employed.

University of Durham

February 2003

Declaration

The contents of this thesis, represents the work of the author unless indicated to the contrary or acknowledged by reference. The thesis describes results of research carried out in the Department of Chemistry at the University of Durham between October 1999 and October 2002. This work has not been submitted for a higher degree in any other academic institution.

Statement of Copyright

Acknowledgements

I would like to take this opportunity to thank more people than I can possibly hope to name in a single page. I will try my best to include everyone under some heading or another.

To begin, I would like to express my sincere gratitude to my supervisor Professor David Parker who has provided scientific and technical knowledge, support, discussion, carrot and stick with perfect balance and timing throughout my experimental work and writing up.

The work carried out by Dr. Justin Perry, his experience, assistance and eventually his bench space were of great benefit to my work and scientific development. The Liposomal expertise of Dr. John M. Sanderson, along with certain pieces of his equipment, were also of significant help in this work. Other members of the department to be singled out are Dr. Andrew Beeby, Dr Ritu Kataky, Dr Mike Jones, and Dr Alan Kenwright. Many thanks must go to all the technical, analytical and support staff of the department, who have salvaged, repaired, imported/exported, ordered, cleaned, trained me, and even served me hot beverages during my research.

I also thank *every* member of the Parker group, past and present who worked with me. They *all* deserve note for their help, support and their friendship along the way. In particular I will name; Dr James Bruce whose knowledge of fluorimetry and goon show scripts was invaluable, Dr Mark O'Halloran who inspired the search for my ring forming routes and Dr Horst Pushmann 'that man' in crystallography.

The financial support of the EPSRC is gratefully acknowledged, as is the financial and more general and whole hearted support of my parents.

Finally I must thank Suzi for being there for me throughout my research and write up and for her love.

There is a single light of science, and to brighten it anywhere is to brighten it everywhere.

Isaac Asimov

Table of Contents.

List of Abbreviations

AIBN	2,2'-azobis (2-methylpropionitrile)
ANTS	8-aminonaphthalene-1,3,6-trisulfonic acid
Boc	*tert*-butyl carbamate/carbonate
^{t}Bu	*tert*-butyl
CAC	critical aggregation concentration
CCD	charge coupled device
CDOPE	N-citraconyl-dioleoylphosphatidylethanolamine
CF	carboxyfluorescein
ChIm	cholesterol-(3-imidazol-1-yl propyl) carbamate
CTAB	cetyltrimethylammonium bromide
CMC	critical micelle concentration
DCM	dichloromethane
DIPEA	diisopropylethyl amine
DMF	dimethylformamide
DMPC	dimyristoylphosphatidylcholine
DOIm	4-(2,3-bis-oleoyloxy-propyl)-1-methyl-1H-imidazole
DOPE	dioleoylphosphatidylethanolamine
DPAPy	2,3-bis-palmytoyloxy-propyl-pyridine-4-yl-amine
DPIm	4-(2,3-bis-palmitoyloxy-propyl)-1-methyl-1H-imidazole
DPX	*p*-xylene-bis-pyridinium bromide
DTPA	diethylenetriaminepentaacetic acid

EDC EDCI	1-(3-dimethylaminopropyl)-3-ethylcarbodiimide
EDTA	ethylenediaminetetraacetic acid
Et	ethyl
FTIR	fourier transform infra red
IR	infra red
Me	methyl
Ms	methanesulfonyl
Mp	melting point
MS	mass spectroscopy
	DCI desorbed chemical ionisation
	ESMS electrospray mass spectrometry
	ES+/- electrospray positive/negative
	FAB fast atom bombardment
	m molecular ion
Naph	naphthalene
NBS	N-bromosuccinimide
NMR	nuclear magnetic resonance
	s singlet
	d doublet
	dd doublet of doublets
	m multiplet
	t triplet
	q quartet
	pent. pentet
	br broad
PBS	phosphate buffered saline
PEI	polyethylenimine
PLL	poly-(L)-lysine
^{i}Pr	*iso*-propyl
Py	pyridine

SANS	small angle neutron scattering
SDS	sodium dodecyl sulfate
SEM	scanning electron microscope / micrograph
TFA	trifluoroacetic acid
THF	tetrahydrofuran
TLC	thin layer chromatography
UV	ultra violet
Vis	visible

Chapter 1

1 Introduction

After a brief introduction to the area of gene therapy and in particular gene delivery, this chapter addresses problems encountered by synthetic lipid based delivery systems. The work presented in this thesis is aimed at overcoming one of the problems encountered by synthetic transfection systems, namely the controlled destabilisation of an endosome vesicle or related aggregate structures.

Gene therapy is the use of genetic material from an external source to express a protein or peptide which will have a beneficial effect on a patient's condition. The conditions which are treatable could be inherited genetic disorders or acquired conditions which will be relieved by the production and release of a specific protein. There is, therefore, great potential for gene therapies to eliminate diseases such as cystic fibrosis, diabetes and other conditions which are believed to arise from the failure or absence of a specific gene. There is also scope for the treatment of cancers, by using targeted gene therapies to slow cell division, reverse mutations which cause tumour growth or cause the targeted tumour cells to die. This large number of potential applications along with the serious nature of many of the conditions potentially treatable has made gene therapy a widely researched area, as teams around the world strive to produce efficient and safe methods for gene therapy.

With the completion of the first draft of the human genome project in 2000[1], the increasing ease of DNA synthesis, and the function of more and more genes being identified, the production of appropriate therapeutic genetic material is rapidly becoming the least of a gene therapist's worries. Gene delivery, however, is the key to effective gene therapy and is still a problem which has to be faced and overcome before the envisaged "magic bullet" gene treatments can

become a reality in everyday clinical use. At present, the few gene therapies in clinical use, whilst having some observable effect, do not represent efficient treatments for any human disease.

Gene therapy systems are based on a wide range of delivery routes and strategies, some of the most commonly used and researched, along with the main problems which they encounter are discussed in the following pages.

1.1 Gene Delivery

1.3.1 DNA/RNA

DNA or RNA is the core of every gene delivery vehicle. Both molecules are large polymeric molecules made up of a phosphate linked strand. From this strand deoxyribose (DNA) or ribose (RNA) sugar moieties are appended. Each DNA sugar unit carries one of four heterocyclic bases adenine, guanine, thymine and cytosine (Figure 1). In RNA, thymine is replaced by uracil, a similar structure to thymine but lacking the methyl group on the ring.

DNA and RNA strands can link *via* hydrogen bonds, forming a double stranded structure. DNA is normally found as a double strand which can adopt a number of conformations. The most famous and more common conformation *in vivo* is the double-helix. The structure of DNA allows for the encoding of information through different arrangements of the four bases. This information when decoded through the binding of RNA in a process known as transcription, leads to the production of proteins, peptides and ultimately the construction and maintenance of complex multi-celled organisms. RNA is usually a single strand polymer which binds to DNA in the transcription process. The DNA and RNA molecules are susceptible to degradation in acid conditions and digestion by the action of nuclease enzymes.

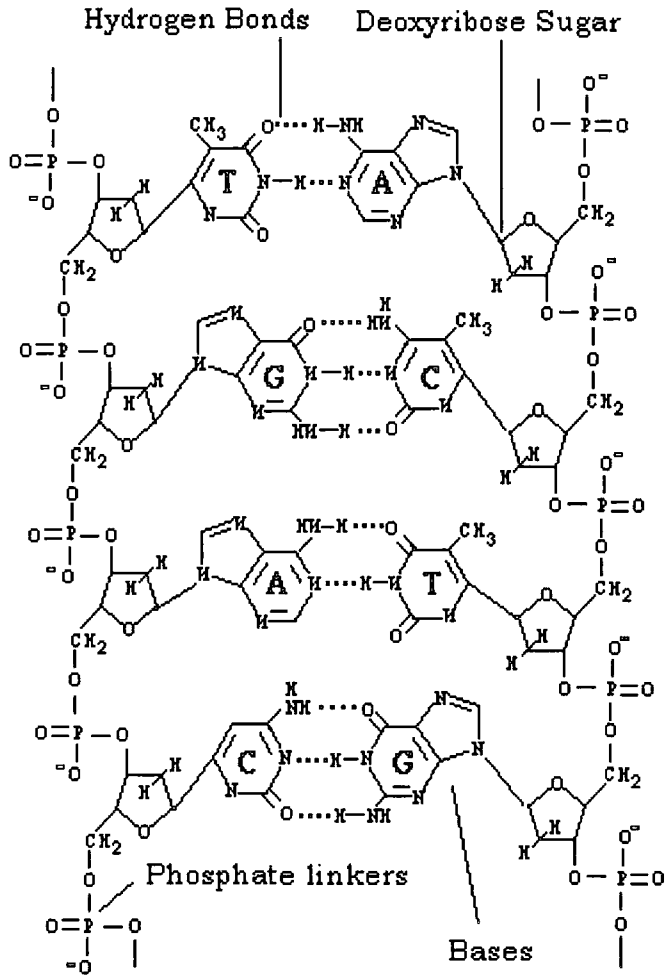

Figure 1 DNA Structure

Base structure labels
A=Adenine T=Thymine G=Guanine C=Cytosine

The charges along the phosphate linked 'backbone' of the DNA repel each other and this electrostatic influence increases the size of the DNA molecule as well as playing a part in determining the conformations adopted by the double strand systems. The size of the DNA molecule is a major factor which needs to be considered before delivery systems can be designed. Large molecules are difficult to carry across cell membranes and may even become trapped in narrow blood vessels. Neutralisation of the phosphate charges by cationic species, such as spermine and related polyamines, allows compaction

of the DNA structure[2,3,4]. These species are important in the design of systems to allow the transport of DNA through the body.

1.2 Transfection and Expression

Transfection and expression are the key goals for gene delivery. Transfection is the crossing of the cell and nuclear membranes and release of the new genetic material to be expressed by the cell. Expression is the action of the DNA being transcribed into a protein. However this process is not one which occurs easily and spontaneously with any great efficiency. Some of the underlying difficulties faced in trying to achieve effective transfection are detailed below.

1.3.1 Barriers to be Crossed

There are several 'barriers' to achieving transfection and ultimately expression of genetic material within a cell. In general, the human system has evolved over thousands of years to prevent the damage and alteration of the genetic material at the core of every cell. These highly evolved survival mechanisms which reduce mutations and try to prevent the inclusion of foreign DNA into the human genome, pose significant obstacles to the inclusion of therapeutic genetic material and therefore to gene therapy[5]. These barriers can be separated into two categories: extracellular barriers and intracellular barriers[6]. Intracellular barriers, apart from the obvious and physical barrier of crossing the cell membrane, include instability of DNA in the cytoplasm, DNA escape from endosomes and the resulting degradation of DNA in the lysosome if this is not achieved. Translocation of DNA to the nucleus once inside the cell, is another intracellular obstacle. Extracellular barriers are linked with systemic survival, targeting and administration routes. DNA is degraded or cleared from the system

rapidly by blood plasma and trapped by the capillary beds found in the reticuloendothelial system. The oral administration route is almost completely ineffective and transfection of cells within the body is suppressed by mucosal coatings found in various tissues. If not addressed, each of these obstacles will reduce the level of expression and if several of these barriers are not effectively addressed then they can quickly reduce the levels of transfection and expression to zero.

1.3.2 Transport and Protection

DNA is susceptible to attack and degradation by nuclease enzymes as well as acidic environments encountered within the human system. In order for destruction or mutation of the therapeutic DNA to be averted, exposure to any of these environments must be avoided. To prevent damage during transport through the body and so increase the transport range of DNA, gene therapy systems almost always employ some form of protective coat to the genetic material. This varies from proteins to lipids [4,6,7] and even inorganic layered clays[8].

These coatings allow the possibility of overcoming another transportation barrier, the targeting of gene therapies. Effectively, targeted gene therapy agents could be administered in lower doses and would produce fewer unwanted side effects as less 'chance expression' would occur.

Targeting generally relies on the recognition of receptors or other features on the target cell's surface. By adding moieties which bind these receptors or recognise proteins present on specific cell surfaces, the uptake of the delivery vehicles by that cell type can be increased. If the receptor also triggers the internalisation of the delivery system, a secondary advantage can be received. Targeting can also be achieved on a physical, macro-scale basis by the injection

or delivery of the gene therapy agent only to the target tissue. This direct injection approach of tissue targeting has become increasingly viable as development of 'keyhole' surgical techniques has allowed accurate and direct access to the internal organs without the need for highly invasive surgery. (See section 1.3.3).

1.3.3 Endocytosis

Endocytosis is the natural mechanism by which cells internalise any large particle which cannot diffuse across their membrane[9]. The mechanism can be triggered by molecules binding to specific receptors on the cell surface, or can be a more spontaneous process when particles fall into preformed pits on the membrane surface (Figure 2.) In each case the steps of the mechanism are almost identical. In the early stages of endocytosis, the particle to be internalised binds to the receptor or enters the pit on the cell membrane's surface. In the receptor mediated case, binding initiates the process of pit formation. The pit then begins to deepen and the outer edges of the pit close together over the particle encapsulating it within a pouch attached to the cell membrane. This pouch pinches off from the inner wall of the cell to become a free 'mini-cell' or endosome containing the particle.

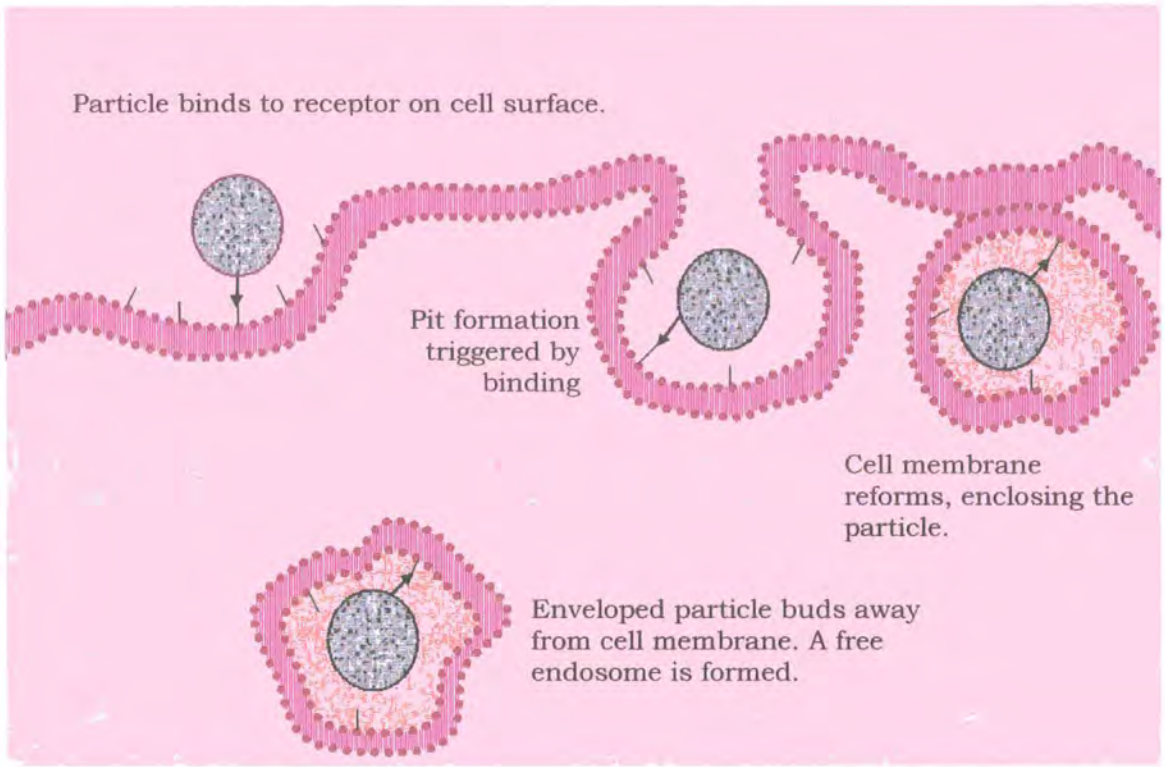

Figure 2 Diagram showing particle internalisation by receptor mediated endocytosis

1.3.4 Endosomal Properties

Due to their small size, endosomes lack the proteins which act as channels and 'ion pumps' through cell membranes to maintain constant concentrations of various ionic species. In particular, endosomes lack the ability to maintain pH at the usual physiological levels. As a result of this, endosomes begin to acidify from the moment they become separated from the cell membrane[9]. Endosomes acidify from their initial ambient physiological pH of 7.24. The pH within the endosomal compartment drops to as low as pH 4 as the endosome ages and moves into the cell. In addition to the change in pH, the lack of active transport across the endosomal membrane results in increased metal ion concentrations [M^{n+}], particularly levels of Ca^{2+} and Zn^{2+} are thought to increase. Endosomal packages often fuse

with other endosomes within the cell, as they age. Eventually these ageing endosomes fuse with, or develop into lysosomes. These structures are larger cellular organs which contain not only an acidic environment but also digestive enzymes. Lysosomes can be thought of as cell stomachs. The lysosome breaks down the particle brought in *via* endocytosis and recycles any useful nutrient constituents into the cell's metabolism.

1.3 Delivery Systems and Strategies

1.3.1 Viral Delivery

Viruses are the benchmark for targeted DNA delivery. With millions of years of evolutionary development behind them, they have routes to effectively move through their host, enter its cells and deliver their own genetic material to the nucleus of those cells for expression[10]. The structure of viruses varies greatly between the different classifications and is usually linked to the target host's biology and the type of genetic material[5]. Viruses are based on proteins which form the protective coating for the DNA, known as the capsid (Figure 3). Viral capsids come in various shapes and can contain structures to aid cell recognition and mechanisms to stimulate cell entry and release of their cargo of genetic material. Some viruses make use of the cell membrane of their last host as an extra layer of protection around their capsid[9]. These enveloped viruses make use of their outer membranous coating as a means of gaining entry to their next host cell *via* membrane fusion.

Spherical/
Icosahedral
capsid

Micrograph of
icosahedral virus
particles

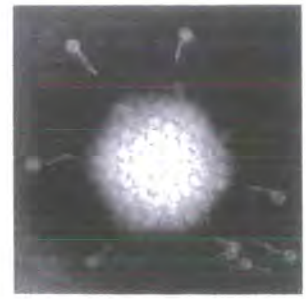

Human adenovirus
(icosahedral) with the fibres
involved in cell binding and
recognition visible

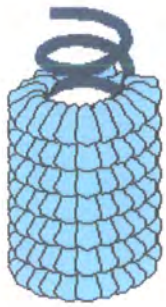

Helical
Capsid

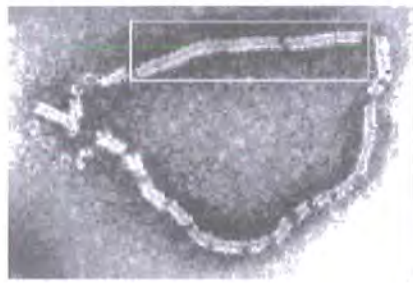

Micrographs of human
paramyxovirus which
causes mumps.

Figure 3 Diagrams and micrographs showing different viral capsid structures[11].

Research into viral gene delivery vectors makes use of highly infectious virus types: retroviruses which carry RNA and of which HIV the human immunodeficiency virus is a member, adenoviruses which include the common cold and herpes based viruses [12,13].

The viruses to be used as vectors have their original DNA replaced or deactivated and the therapeutic strand inserted. In order to then produce large quantities of the therapeutic agents, cell cultures are infected with the virus and used to produce large numbers of replicated genetically modified viruses[14]. The major issues facing the use of viruses therapeutically, are the response of the immune system *in vivo* to the presence of the viral proteins, as

well as receptors on the viral surface. This response reduces the efficiency of treatment in patients who may have encountered the strain of virus hijacked for the therapy. As well as this potential for existing resistance, there is the problem of the active immune system of a patient creating a resistance and reducing the effectiveness of subsequent treatments using that viral gene therapy agent. This problem could be overcome using immune suppression treatments in parallel but the benefits of the gene therapy would need to be significant and proven to justify such a drastic treatment.

In addition to resistance, problems can be envisaged with incomplete deactivation or replacement of the original viral genetic material. In these circumstances, patients could contract the original virus. This could be serious if the patient was already in a weakened condition, or if immune suppression were being used to prevent the problems of resistance to the viral gene therapy.

Viruses are effective transfection systems which are used successfully in *ex vivo* treatments and show high activity in *in vitro* experiments[12,13,15,16]. Some viral strains make use of endocytotic pathways to enter the cell and have evolved mechanisms which respond to the changing conditions within the endosome to trigger release into the cytoplasm. Certain viruses have also evolved methods of hijacking the natural systems within the cell to transport their genetic material to the nucleus, although others replicate and express their DNA in the cytoplasm.

1.3.2 Synthetic Vectors

Synthetic vectors encompass a range of different strategies for protection and delivery. These systems can be based on polymers, liposomes, or polypeptides and proteins. Each of the systems lacks the complete package offered by viral systems, but each has the advantage of not triggering an immune response, or posing an

infection risk, although immune recognition could be an issue with protein based systems. Another advantage of synthetic systems is the potential ease of their production. Viral vectors require the use of cell cultures in their production and this leads to higher cost and greater difficulty in producing precisely reproducible results.

1.3.3 Polymer Delivery Systems

Polymer based delivery systems most commonly consist of cationic polymers which interact electrostatically with the negatively charged phosphate backbone of DNA. The polymers bind and compact DNA, giving protection from the hazards encountered during delivery and reduce the size of the DNA molecule allowing easier transport and cell entry[17,18,19,20]. Straight chain and branched polymers have been used, as have dendrimers[21], block co-polymers and grafted co-polymers [22,23,24]. All polymer systems give the opportunity of attaching targeting ligands which are designed to bind to specific features on the cell surface, maximising contact time and stimulating internalisation by receptor mediated endocytosis[25].

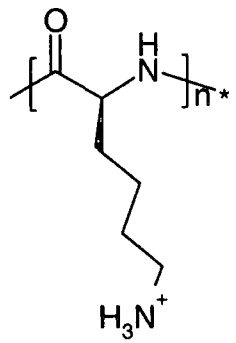

Figure 4 Structure of poly(L-lysine) at pH 7.4

Poly(L-lysine) (PLL) (Figure 4) is the oldest example of a polymer delivery system. This polymer has been shown to have the ability to

form a complex that protects DNA from attack by nucleases. It also leads to significant transfection ability *in vitro* when used with endosomolytic agents such as chloroquine. (Figure 5). Chloroquine is thought to act as a buffer to the pH drop within the endosome and may also act to destabilise DNA complexes with polycationic species[7,26]. PLL also shows activity when modified with targeting ligands. However, the significance of these observations is moderated by the high percentage of cell death in the *in vitro* experiments and the short *in vivo* circulation half life observed with rodents[27]. Lower molecular weight PLL systems, which show no toxic effects to cells, also show little or no transfection activity and a reduced ability to protect their bound DNA[7].

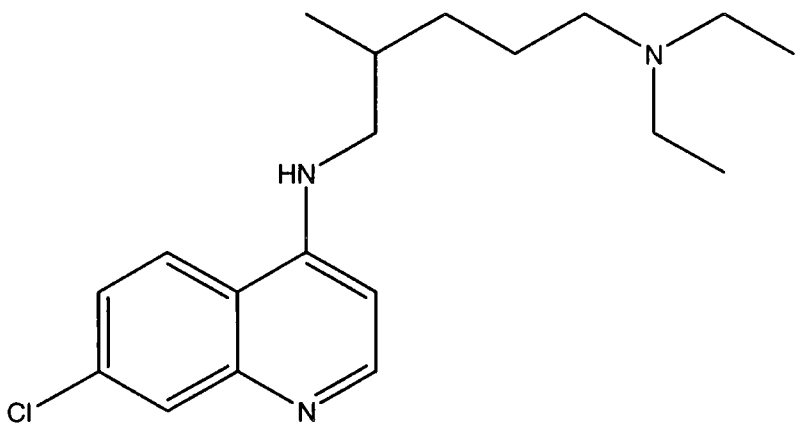

Figure 5 Structure of chloroquine (pK_a 8.4 and 10.8[26])

Polyethylenimine (PEI) (Figure 6) based systems have proved more efficient delivery systems than PLL as they do not require endosomolytic agents in order to have transfecting abilities[28,29]. This is thought to be due to protonatable amine groups present on the PEI chains. PEI efficiency is also affected by molecular weight, although some literature sources differ as to what those affects actually are [6,29]. Despite advantages over PLL, PEI does however share some of the PLL

associated toxicity problems and hence is unlikely to be used clinically unless these issues can be addressed properly.

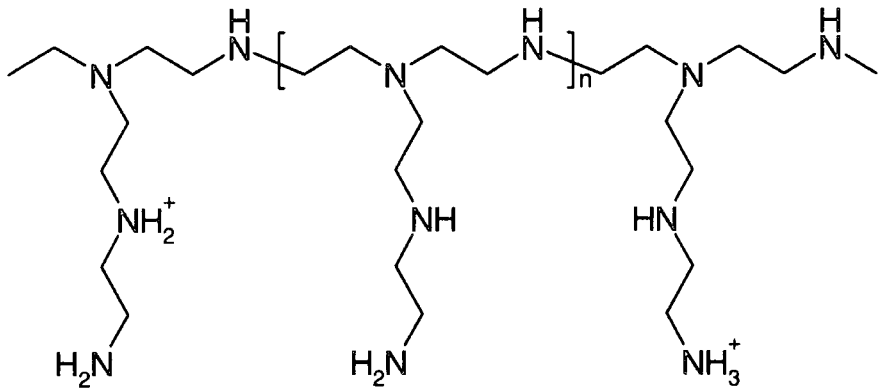

Figure 6 Structure of branched polyethylenimine (PEI). The level of protonation of the amine groups is ~20% at pH 7 and ~50% at pH 5; straight chain and more highly branched structures are also possible

Biodegradable polymers may offer a balance between toxicity and transfection ability. The main problem which is faced by researchers designing biodegradable polymer delivery vehicles is in striking a balance between the time taken for the polymer to decay, once transfection has occurred, and the stability of the polymer structure to both intra and extracellular environments[30,31]. The breakdown of biodegradable polymers within the cell, can prevent the build of potentially damaging polymer molecules, which can lead to cell death *via* membrane damage. The action of polymer degradation may also help to increase the expression of the therapeutic DNA, by promoting the release of any genetic material complexed by the polymer, either within the endosome or cytoplasm. Polymer systems can also make use of the pH change which occurs within the endosomal compartment[22,32], as this is the route thought to be followed to gain cell entry. These pH sensitive polymers, which include PEI and polyamidoamine systems, are thought to operate by

the 'proton sponge' mechanism. The multiple protonation presumably triggers an influx of counterions and subsequently water, causing osmotic swelling and eventually endosome rupture, followed by release of the polymer-DNA complex into the cytoplasm. If increased stability, reduced toxicity and good targeting features can be built into polymeric systems which bind and compact DNA, then an effective and versatile therapeutic vector could be synthesized.

1.3.4 Lipid Vectors

Cationic lipid based vectors allow for a range of different approaches to gene delivery depending on lipid structure and formulation of the final delivery vehicle[33,34,35]. Liposome based systems encapsulate compacted DNA inside vesicles with bilayer membranes[7]. Lipoplexes (lipid complexes) are formed by lipid molecules incorporating DNA binding moieties. Lipoplexes can form systems with a functionallised 'tail', or the charged (cationic) 'head' surface of the lipid binding to the DNA[36,37]. There are a wide range of variations in structure and formulation of lipid based vectors. This allows for optimisation of transfection ability, stability and cell specificity to be attempted, by modifying the structure of the lipid molecules used, or by combining mixtures of lipids to achieve a specific property[7,38,39]. Lipofectin is a commercial transfection product for *in vitro* delivery which uses a 1:1 mixture of N-[1-(2,3-di-olyloxyproyl]-N,N,N-trimethylammonium chloride : 1,2-dioleoylphosphatidylethonolamine (or DOPE). One of the lipofectin components, DOPE, has been used independently in gene delivery research[40,41]. DOPE is believed to facilitate membrane fusion during transfection and has been used in combination with many other lipids. It has also been modified to include pH cleaved moieties which are removed at late endosomal pH[42], thereby allowing the fusogenic

properties of DOPE to take effect only when the delivery vehicle is within the endosome and acid cleavage has taken place (Figure 7).

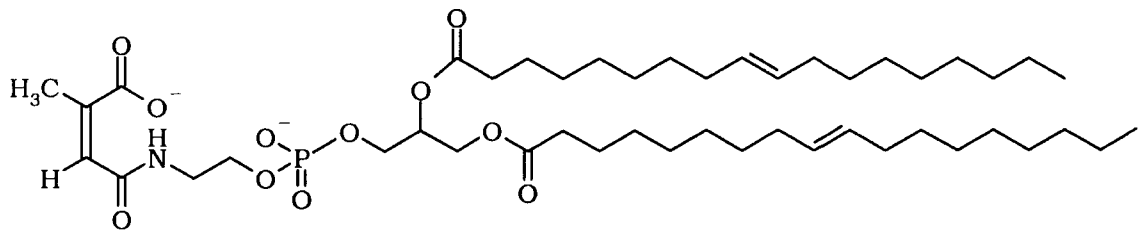

CDOPE

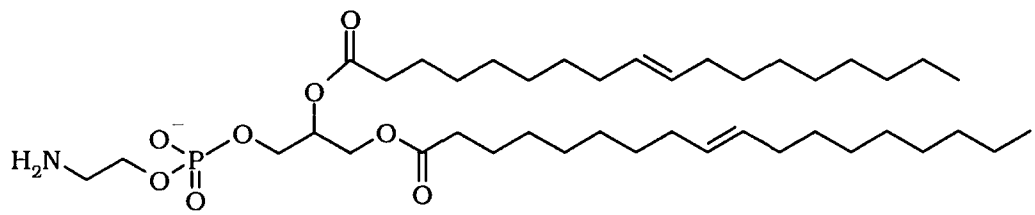

DOPE

Figure 7 Structures of N-citraconyl-dioleoylphosphatidylethanolamine (CDOPE) and dioleoylphosphatidylethanolamine (DOPE)[42].

Previous research carried out, within the group at Durham and in association with the biotechnology company Celltech plc., led to the design and synthesis of a novel amphiphilic bola-lipid based delivery vehicle which contained multiple amine groups in a double tail for DNA binding (Figure 8) and formed toroidal lipoplex particles with radii of ~41-50nm (measured by photon correlation spectroscopy and a combined field-flow fractionation and multi-angle laser light scattering method) when condensed with DNA[43]. The aggregate bolasomes were stable from pH 3.5 – 7.5 and resisted attack from DNAse I and Protease XIV (37°C, pH 7.4.). The formulation of this lipid delivery system was found to have a significant effect on the transfection ability of the vehicle. The formulation with the highest transfection ability, contained a mixture of the polyethylene glycol (PEG) modified amphiphiles and the amphiphiles with the sugar head group.

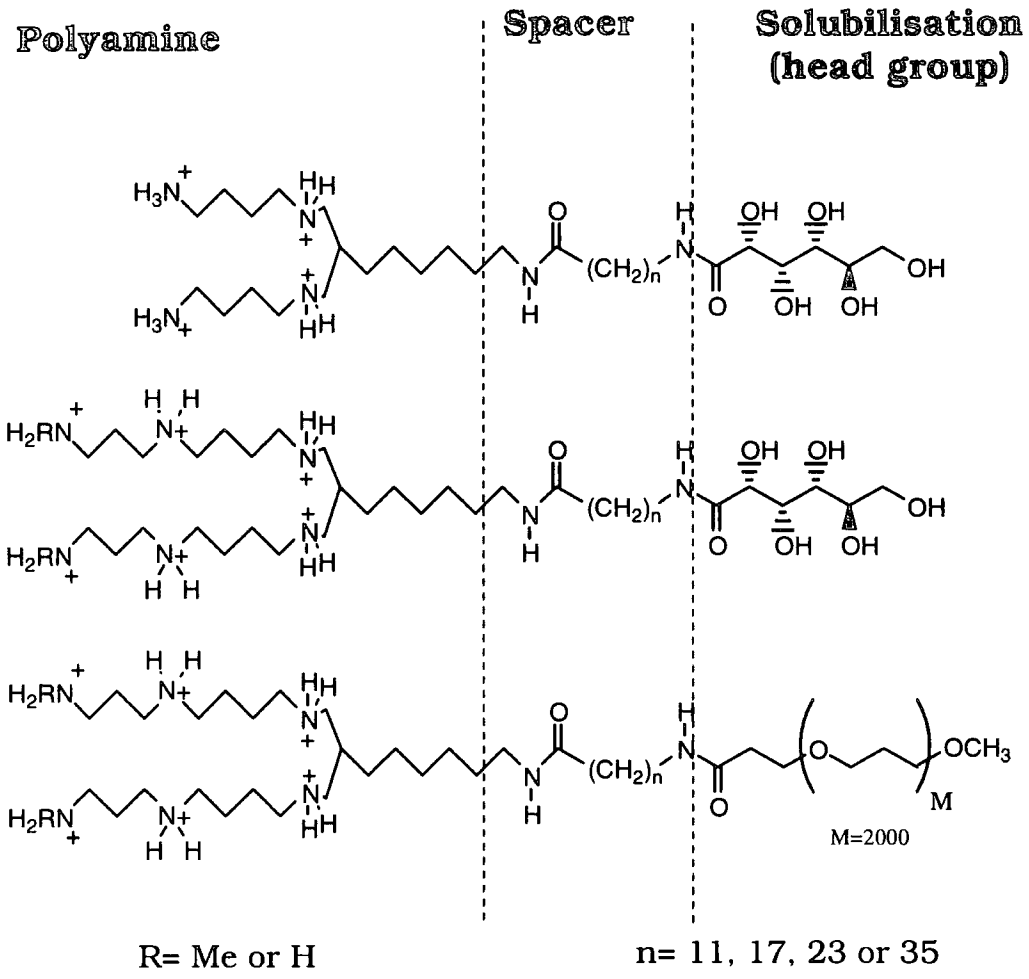

Figure 8 Examples of Bola-amphiphile molecules[43]

This use of PEG groups in gene delivery vehicles is widespread. PEG groups are known to reduce transfection *in vitro*. However, during *in vivo* studies with both polymer and lipid systems, it has been found that inclusion of PEG units reduces the trapping of delivery systems in the lung tissue[6]. This allows longer circulatory lifetimes and increases expression in the liver. The use of ligands or antibodies and PEG groups in delivery systems shows more effective ligand mediated targeting.

1.4 Administration routes

1.3.1 *Ex-Vivo*

The *ex vivo* route involves removal of cells from the patient, followed by incubation of those cells with a gene delivery vector, to produce a line of genetically modified cells, which are then returned to the patient's system[5]. This route is normally associated with blood cells as they are the easiest to remove and replace.

1.3.2 Intravenous injection

Intravenous injection is the administration route aimed for by most of the liposomal species, viral systems and polymer/peptide complexes. Each of these systems attempts to stabilise and protect their DNA cargo for transport through the blood stream. However, at present, a system which offers effective targeting, sufficient stability and low toxicity has yet to be designed. Most *in vivo* trials of gene delivery systems show low expression, with most activity occurring in the lung epithelium where the vectors are 'filtered' out of the bloodstream[6]. Use of targeting ligands has been successful to a certain extent but, in many cases, just leads to the site of activity being moved to the liver.

1.3.3 Injection into tissue

This can be intramuscular, subcutaneous or directly into any accessible tissue. This delivery method is becoming more flexible as keyhole surgery techniques and endoscopic techniques develop. These techniques allow more organs and areas of the body to be accessed for injection. The DNA formulation to be injected could be 'naked' DNA (simply a solution of plasmid DNA with no other species bound or

associated with it). 'Naked' DNA has little or no transfection ability *in vitro* but has shown some activity through *in vivo* studies when injected into solid tissues, such as smooth muscle[6]. Interestingly, application of more complicated delivery systems, in many of these cases, shows no improvement over naked DNA and, in some instances, even reduces transfection. Researchers report that there is also little diffusion from the site of administration for naked DNA, viral or synthetic delivery vectors, when injected into solid tissue[44]. This localisation of action, means that targeting of the therapeutic agent can be achieved physically and without the need for complex modifications to the formulation, for each site or tissue type. Using surgical techniques, this type of application has also shown success in the liver[45]. Clinically, intra-muscular injection has been assessed in DNA vaccination studies, where genetic material coding for a specific antibody is implanted to give instant immune response to a specific pathogen. Injection into solid tissue has been combined with electroporation to improve gene uptake. Electroporation increases the crossing of the cell membrane by the application of a current through the tissue. This encourages pore formation in the cell membrane and makes cell entry, for larger particles, possible.

1.3.4 Inhalation

This route of administration has been successful when used with lipoplex transfecting agents. The delivery system is formulated as an aerosol and has been tested as a treatment for cystic fibrosis, although there are currently no licensed gene treatments available[6,46].

1.5 Lipid Systems

1.3.1 Aggregates, Surfactants, Amphiphiles and Micelles

Many different molecular types form aggregate structures in solution. These molecules can be classified as surface active agents or surfactants. All surfactant systems are amphiphiles, having both lyophilic (or liquid/solvent loving) and lyophobic sections (or liquid/ solvent hating). For aqueous surface activity, an hydrophobic section and an hydrophilic section is required. Amphiphile molecules can be non-ionic, anionic, cationic or amphoteric but they share the same basic structural properties. Some examples of common surface active molecules are shown in Figure 9. All surfactant molecules share certain properties in solution. In dilute solution they behave as normal solutes and, in the case of ionic systems, the expected electrolyte properties are observed. At well defined concentrations, however, distinct and easily observed changes to a number of the solution's physical properties take place. These properties include surface tension, conductivity, turbidity and osmotic pressure. This behaviour has been explained in terms of the formation of organised aggregates, or micelles, of the surfactant molecules. The lyophobic groups associate and orient into the centre of the aggregate away from the bulk solvent and the lyophilic groups remain solvated at the surface of the aggregate.

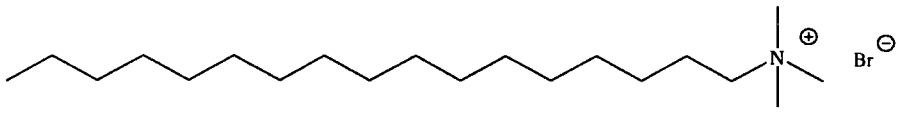

Cetyl Trimethyl Ammonium Bromide (CTAB)

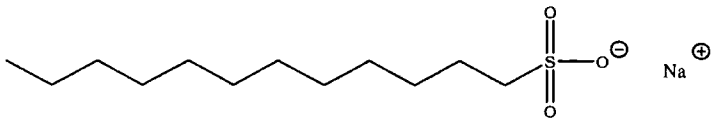

Sodium Dodecyl Sulphate (SDS) or Sodium Lauryl Sulphate (SLS)

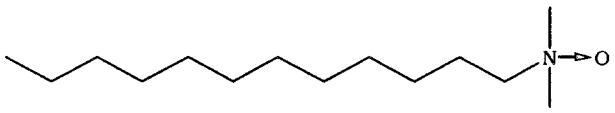

LaurylDimethylAmine-Oxide (LDAO)

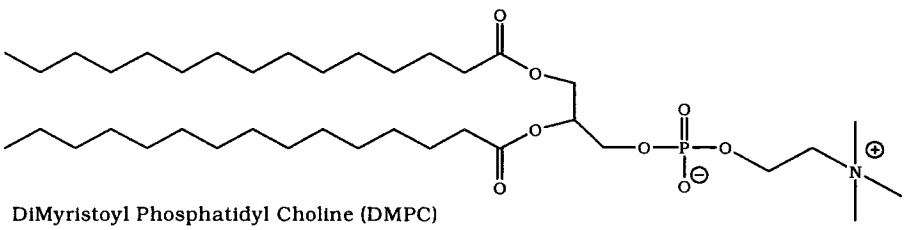

DiMyristoyl Phosphatidyl Choline (DMPC)

Figure 9 Common examples of ionic, non-ionic and amphoteric surfactants

The concentration at which the aforementioned properties change, is defined as the point at which micelle formation becomes appreciable in solution and is termed the critical micelle concentration or CMC[47]. Micelle formation can be thought of as one of four dynamic equilibria occurring in the surfactant solution. The first of these equilibria, is the dissolution of the surfactant from the solid state into free solution. Once in solution, the molecules enter into an equilibrium with micellar vesicles in solution. There are also equilibrium processes between the surfactants in solution and the solvent / atmosphere interface. For completeness, the final equilibrium possible between the solid phase and surfactants adsorbed to the solvent / atmosphere interface should also be included. The stability of these aggregate systems is dependent on the structure of the surfactant molecule, as well as physical conditions such as temperature.

a) Micelles

The structure of micelles has been the topic of much debate. Several models have been proposed; a spherical system, a rod like structure and a lamellar structure. Many variations of the definitive structure, or the combination of structures likely to be present in micellar solutions, were suggested. With the use of various techniques, from NMR and ESR to light and neutron scattering, the structure is now thought, however, to change with increasing concentration. The initial structure is spherical, with a relatively disordered interior in which the hydrophobic alkyl chains are not in a regular array. As the concentration is increased, the micelle shape becomes rod-like with rounded ends. This structure packs into an hexagonal array and eventually an infinite lamellar phase (Figure 10), although some surfactant types may skip a phase[48].

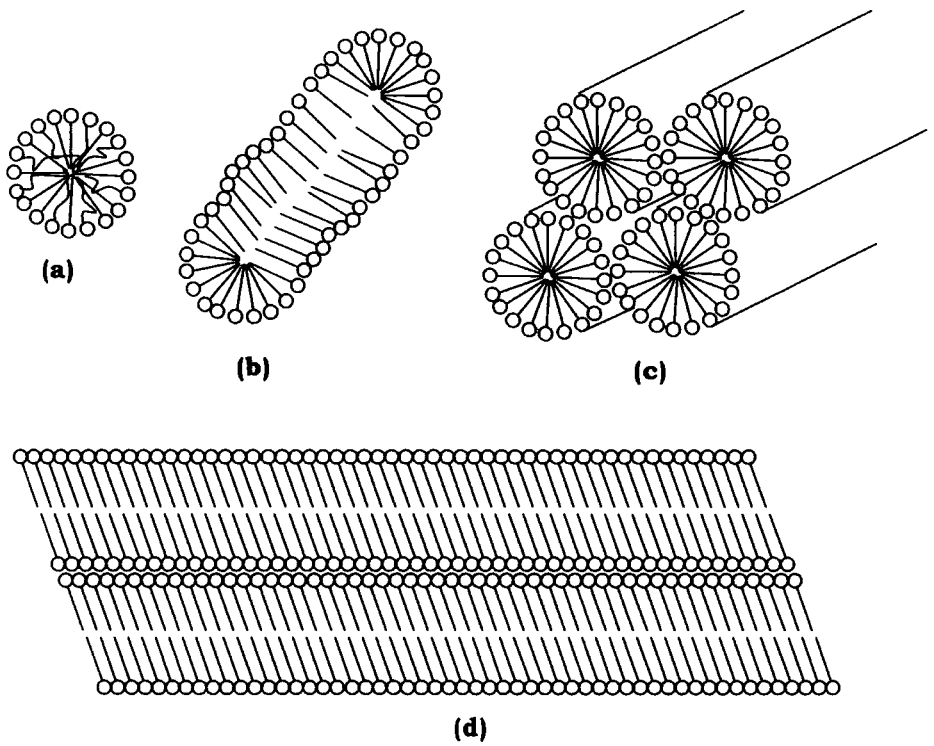

Figure 10 Schematic representation of amphiphile aggregation structures. (a) Spherical Micelle, (b) Cylindrical, (c) Hexagonal, (d) Lamellar

b) Liposomes

Liposomes are more stable, bilayered aggregate structures, which completely enclose a volume of solvent[49]. They are most commonly formed by twin tailed surfactant molecules, specifically phospholipids such as DMPC Figure 9. These phospholipid molecules occur naturally in the wide array of biological membranes and have a number of different structures and features. Because liposomes can be formed which closely resemble cell membranes, they are useful, not only as models of biological bilayers, but also in the transportation and protection of sensitive molecules and preparations through biological systems, as in the case of DNA delivery.

1.3.2 Aggregate Effects

The aggregate structure creates environments differing greatly from those found in a dilute solution. Molecules within these environments exhibit properties specific to the environment type encountered. The polarity and polarisability differ between hydrophobic and hydrophilic areas. These effects mean that some small molecules, which can be trapped or associated with either of the different environments created by the aggregation of the amphiphile molecules, have their physical properties affected. This effect can be used to observe aggregation by using molecules, easily observed spectroscopically, which have their spectroscopic properties altered by the environment in which they find themselves. Fluorescent molecules are used as probes, to determine CMC in micellar systems and to detect breaches in liposome membranes. Co-aggregates are formed when two or more different amphiphiles, usually of the same type; cationic and cationic, non-ionic and non-ionic, associate to form a well-defined aggregate structure. The distinguishing properties of co-

aggregates differ from each of the components. The CMC of a binary co-aggregate, usually lies between the CMC's of its components[48].

1.6 Controlled Disruption of Aggregates

1.3.1 Methods of disruption

Aggregate structures can be disrupted by the addition of various substances to the aggregated solution. Adding molecules which alter the solvent polarity or adding differently charged surfactant molecules or amphiphiles of a different structure to the initial aggregate system can cause disruption of aggregates already in the solution. For example, adding cationic liposomes to anionic liposomes causes a reorganisation of the membrane structures and the release of the liposome contents[50].

Several systems have also been devised in which amphiphile molecules in the aggregate react to change their aggregation properties. These systems respond to the solution environment or to external radiation to alter the aggregative properties of the surfactant molecules and cause disruption to the aggregated structure. The remainder of this section deals with such 'internal' disruption systems separated into categories by the conditions which trigger their action.

a) Redox Sensitivity

There are a small number of examples of lipid systems which are destabilised following exposure to reducing conditions [51,52,53]. The active groups within the lipid or lipopolymer chain, tend to be disulfide linking functionalities. The reduction sensitive lipid cleaves at the disulfide bond, altering the chain length of the amphiphile, and/or the charge distribution within the aggregate, causing the system to be destabilised. Disulfide links will however degrade in

ambient biological conditions over time and so the stability and targeting efficiency of these reduction sensitive formulations is called into question.

b) Optical Switching

A number of different systems have been designed which make use of radiation from NIR through the visible to UV, in order to trigger release from liposomes[54,55,56]. The systems make use of either small mole percent additions of a sensitive amphiphile to the membrane or a membrane completely made up of lipids which are engineered to respond to the radiation applied. The strategies employed to bring about destabilisation are photo-induced polymerisation or dimerisation[57,58] of lipids in the membrane, photoionisation often within the hydrophobic environment of the aggregate structure and optically switched isomerisation[59,60]. Work carried out by Ohya et al[59] synthesised a cationic amphiphile molecule carrying the photosensitive spiropyran group as the terminal functionality of the hydrophobic tail section. On irradiation, the spiropyran undergoes isomerisation to its zwitterionic merocyanine form inducing a charged hydrophilic centre at the chain end. Liposomes prepared containing the spiropyran amphiphiles at 5-10 mole percent levels showed leakage triggered by irradiation at the correct wavelength (465nm) thought to be caused by reorientation of the photosensitive lipids within the membrane. Each of the strategies mentioned above aims to cause movement within the membrane and a localised reorganisation of the aggregate, thereby allowing release of the aggregate contents or complete disruption of the aggregate structure.

c) pH/pM

There are a number of published examples of systems which respond to changes in solution pH [61,62,63,64,65]. A series of amphipathic molecules with protonatable functionality (pKs in the range 5-8 Figure 11) in the 'head' group have been studied. These molecules have been combined with DOPE to form cationic liposomes and DNA liposome complexes. The liposomes and complexes have been shown to exhibit significant pH sensitive fusion properties and increased transfection ability when used in *in vitro* transfection experiments[66]. Biodegradable pH-sensitive surfactants have also been investigated for use in the disruption of liposome systems. (e.g. dodecyl 2-(1-imidazoyl) propionate) they are related to lysosomotropic detergents which are known to disrupt phospholipid bilayers and are able to concentrate within intracellular acidic compartments. These species are lipophilic amines with pK_a values between 5 and 9. On protonation their surface activity is enhanced leading to membrane disruption. DNA liposome complexes containing dodecyl 2-(1-imidazoyl) propionate in the membrane have been shown to have significantly increased transfection ability when used *in vitro* for gene transfer[67]. The proliferation of research in this area is linked to the potential of such systems to be triggered by the natural pH drop within an ageing endosome. If systems which make effective use of this drop in pH can be formulated, then lipid based gene delivery or drug delivery systems which make use of an endocytotic route to gain cell entry may become significantly more efficient by responding to the natural environmental changes only encountered during internalisation.

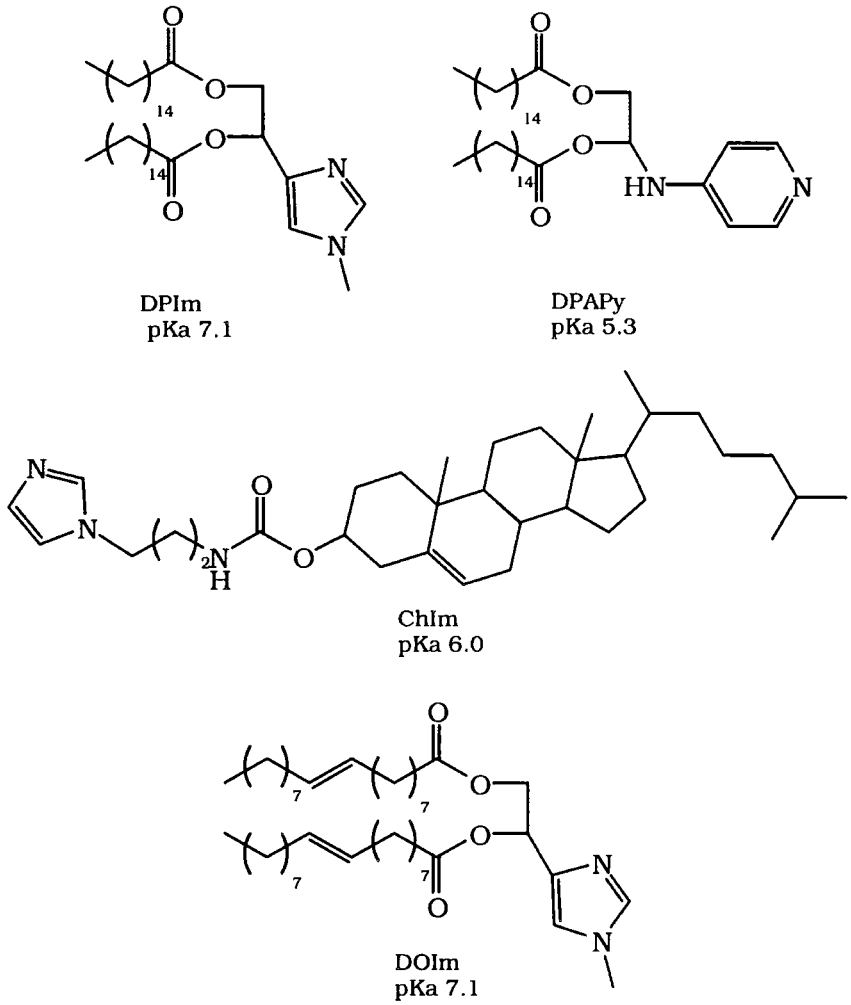

Figure 11 Structures of some pH sensitive lipid molecules[66]

DPIm: 4-(2,3-bis-palmitoyloxy-propyl)-1-methyl-1H-imidazole,

DOIm: 4-(2,3-bis-oleoyloxy-propyl)-1-methyl-1H-imidazole,

ChIm: cholesterol-(3-imidazol-1-yl propyl) carbamate,

DPAPy: 2,3-bis-palmytoyloxy-propyl-pyridine-4-yl-amine.

1.3.2 Focus of Experimental work

The systems investigated in this thesis have been designed to destabilise micellar or liposomal systems when triggered by a pH change, consistent with that occurring within the endosome following endocytosis. The work has focussed on two strategies to achieve destabilisation one of which has the potential to be effected by a

change in metal ion concentration as well as pH. This may also be a useful trigger as the concentration of certain metal ions, most notably Ca^{2+} and Zn^{2+} is reputed to change within the ageing endosomal compartment. The following chapters describe the system design, the synthetic work carried out in the realisation of that design and the analysis undertaken once the molecules under investigation were synthesised.

Chapter 2

2 Design, Synthesis and Properties of Single Chain Cationic Amphiphiles with Mid-Chain Protonatable Functionalities

2.1 System Strategy

A strategy based on the protonation of a single chain cationic amphiphile molecule containing a protonatable functionality approximately half way down the hydrophobic tail section was hypothesised. The molecules are proposed to be used as an additive to form co-aggregates with cationic lipids. The additive species being designed cause destabilisation upon lowering pH, leading to aggregate disruption. The aim of including and positioning this protonatable functionality mid-chain was to introduce a charge centre away from the polar solvent environment, at a given pH. The introduction of this charge centre will attract counter ions and solvent through the aggregate structure and alter the distribution of the hydrophobic and hydrophilic sections of the molecule. It was reasoned, that the combination of these effects may cause the aggregate structure around the protonated molecule to be disrupted (Figure 12). Amine groups were considered the most appropriate functionality for the site of protonation. Amines are affected less by the polarity of their solvating environment than, for example, carboxylate / carboxylic acid functionalites. This is due to the effects of solvating the differently charged species and is shown by the equations and data in Figure 13. The equilibrium relating to amine protonation possesses no overall change in the number of charged species, whereas carboxylate protonation leads to charge neutralisation, which is accompanied by significant changes in the free energy of solvation[68].

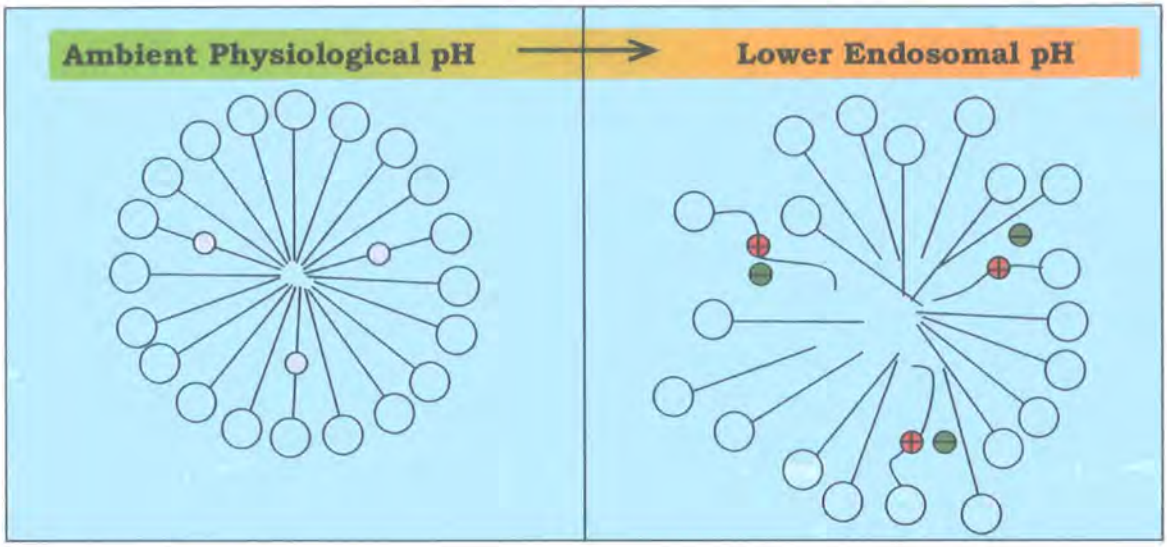

Figure 12. Schematic Diagram Showing The Possible Disruptive Action Of Additive Molecules With Mid-Chain Sites Of Protonation

This low dependence on the polarity of its environment will also tend to reduce any pK_a change undergone by an amine functionality on aggregation. In considering those pK_a changes, the choice of ethanol is made here to model the reputed real micropolarity in the interior of a typical micelle.

$$HA^{Z+1} + SH \rightleftharpoons A^{Z} + SH_2^{+}$$

$$\Delta pK_a = pK_a\,(H_2O) - pK_a\,(EtOH)$$

For Z = 0 pK_a changes little with solvent polarity / dielectric constant
e.g. NH_4^+/NH_3 ΔpK_a (H_2O-EtOH) = -1.2

For Z = -1 or -2 pK_a is reduced significantly as solvent dielectric constant increases
e.g CH_3COOH/CH_3COO^- ΔpK_a (H_2O-EtOH) = -5.4

Figure 13 Information Showing the Effects of Solvent Polarity on the pK_a of Different Functionalities[68].

Prior work in Durham[69] on molecules of this type involved the synthesis of long chain systems with an aniline group at the centre

(Figure 14). The pK_a of these anilines in dilute solution was around 5, so on introduction to an endosome at ambient physiological pH, the molecules would be less than 1 % protonated and would become significantly protonated as the endosome aged and acidified.

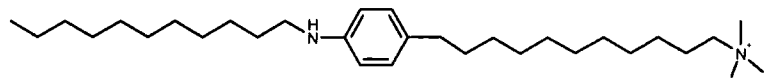

$pK_a = 4.0$ 0.61mM (0.1M Me_4NCl (90%MeOH/10%Water))

$pK_a = 2.7$ 0.36mM + 10mol% CTMAB (0.1M Me_4NCl (aq))

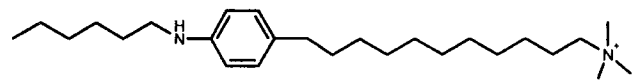

$pK_a = 4.6$ 0.67mM (0.1M Me_4NCl (aq))

$pK_a = 4.9$ 0.07mM (0.1M Me_4NCl (80%MeOH/20%Water))

$pK_a = 3.2$ 0.85mM + 20mol% CTMAB (0.1M Me_4NCl (aq))

$pK_a = 3.1$ 0.085mM + 2mol% CTMAB (0.1M Me_4NCl (aq))

Figure 14 pKa Values determined for aniline systems in free solution and when co-aggregated with CTAB[69]

However, as mentioned in chapter 1, aggregation perturbs the free energy changes that characterise the protonation of a species, with respect to those in dilute homogeneous solution. Despite the choice of the amine functionality, the pK_a of the aniline systems produced was found to be suppressed significantly on aggregation (Figure 14). As a result of this suppression, the pK_a of the anilines was reduced below the pH 5 to 6 range required to be active as an endosome release trigger. In order to overcome this problem, it was decided to investigate species possessing a pK_a value in dilute solution of between 8 and 9. The molecule chosen to fulfil this role was a 2,5 disubstituted pyridine with a methylamine substituent at the 2 position. The effect of having the amine functionality in close proximity to the pyridine ring and the heteroatom, shifts the pK_a of the amine up towards the desired range. This is revealed by examining

literature data for the protonation of simple pyridine-2-methylamines (Figure 15)[70]. The choice of the 2,5 substitution arrangement was to maintain as straight a chain as possible, in order to promote self- and co-aggregation.

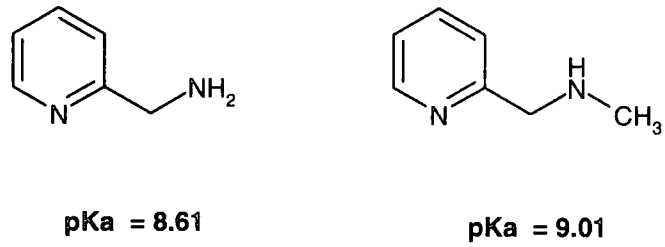

pKa = 8.61 pKa = 9.01

Figure 15 pK_a Values found for simple pyridine-2-methylamines (298 K I= 0.1M NaCl)[70]

2.2 Synthetic Route To 2,5-Difunctionalised Pyridine Systems

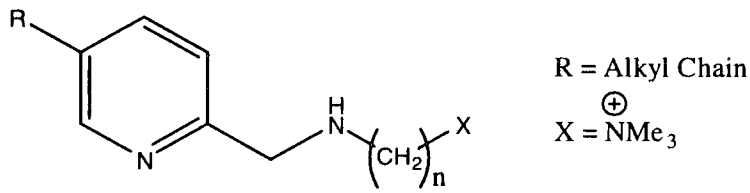

Figure 16 General structure of pyridine based mid-chain protonation species

Initial routes to the general target 2,5-pyridine (Figure 16) were based around modifications of commercially available 2,5-pyridine precursors such as 2,5 lutidine and pyridine-2,5-dicarboxylic acid. In each case, routes designed using these pyridine starting materials encountered significant problems with regard to yield, versatility or selectivity of reaction before the desired product could be synthesised.

The first proposed route from 2,5 lutidine shown in Figure 18 encountered problems with the modification of the methyl group at the 5-position. Selective functionalisation of the 5-methyl group, for

example, was attempted by performing radical bromination on the intermediate amide. With limited availability of the amide intermediate, a readily available model compound 2-bromo-5-methyl pyridine was chosen to be used in attempts to optimise the bromination conditions. This compound could be used to synthesize compound [2] *via* the formation and subsequent hydrolysis of 2-cyano-5-methyl pyridine [1] (Figure 17).

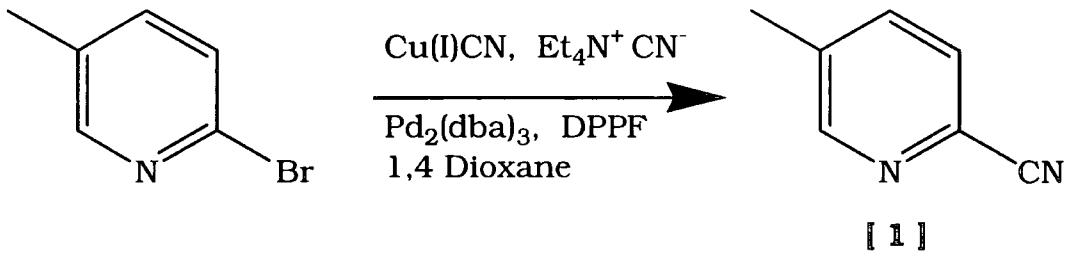

[1]

Figure 17 Formation of 2-cyano-5-methylpyridine **[1]** *via* Pd catalysed cyanation

The radical brominations were carried out in carbon tetrachloride using N-bromosuccinimide to generate the succinimidyl radical and with AIBN as a radical initiator. The bromination reaction when carried out on the model compound, 2-bromo-5-methyl pyridine gave rise to mono- di- and tri-bromo products, which could be separated from each other and the remaining starting material using flash column chromatography. Yields of the more useful mono and di-bromo products were 20% and 25% respectively. However, when bromination of the amide intermediates ([3] and [4]) was attempted there was no observable reaction. This was thought to be due to the effect of the long alkyl chain interfering with the approach of the reacting radical and inhibiting reaction.

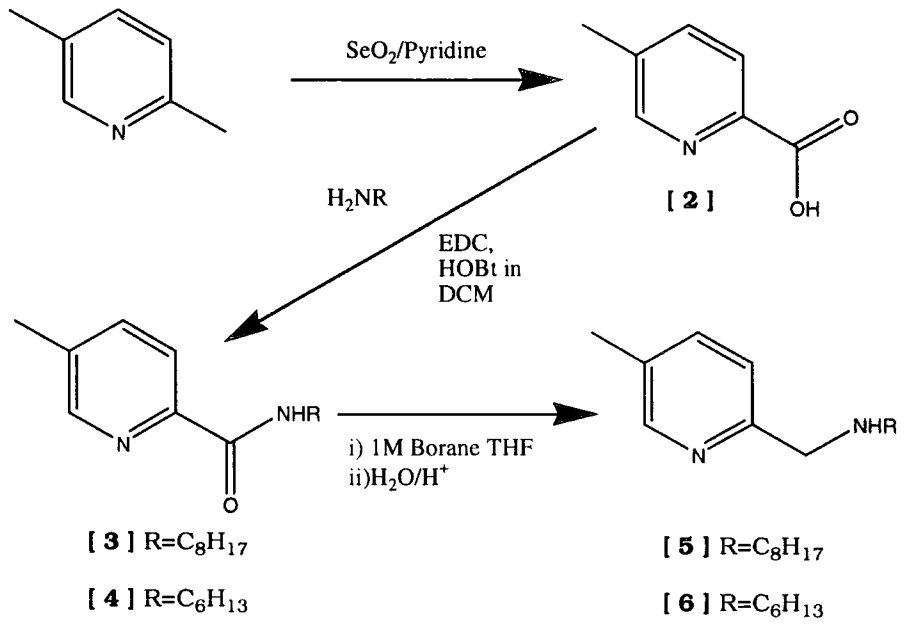

Figure 18 Initial steps in proposed synthetic route from 2,5-lutidine

Routes based around the dicarboxylic acid starting material (Figure 19) used some steps common to the lutidine route, but encountered problems in the reduction of the amide group formed from the coupling reaction. The 5-ester-2-amides, [8] and [9], were reduced using borane THF complex. However, analysis of the mixed products from the reaction by ^{1}H NMR and IR, showed evidence that as well as amide reduction, both the ester and the pyridine ring had undergone reduction. It is thought possible that the pyridine is activated to this borane reduction by the proximity of the ester functionality to the ring. Searches of appropriate literature sources, including Beilstein, Web of Science and SciFinder, failed to identify any previous observations to support this hypothesis.

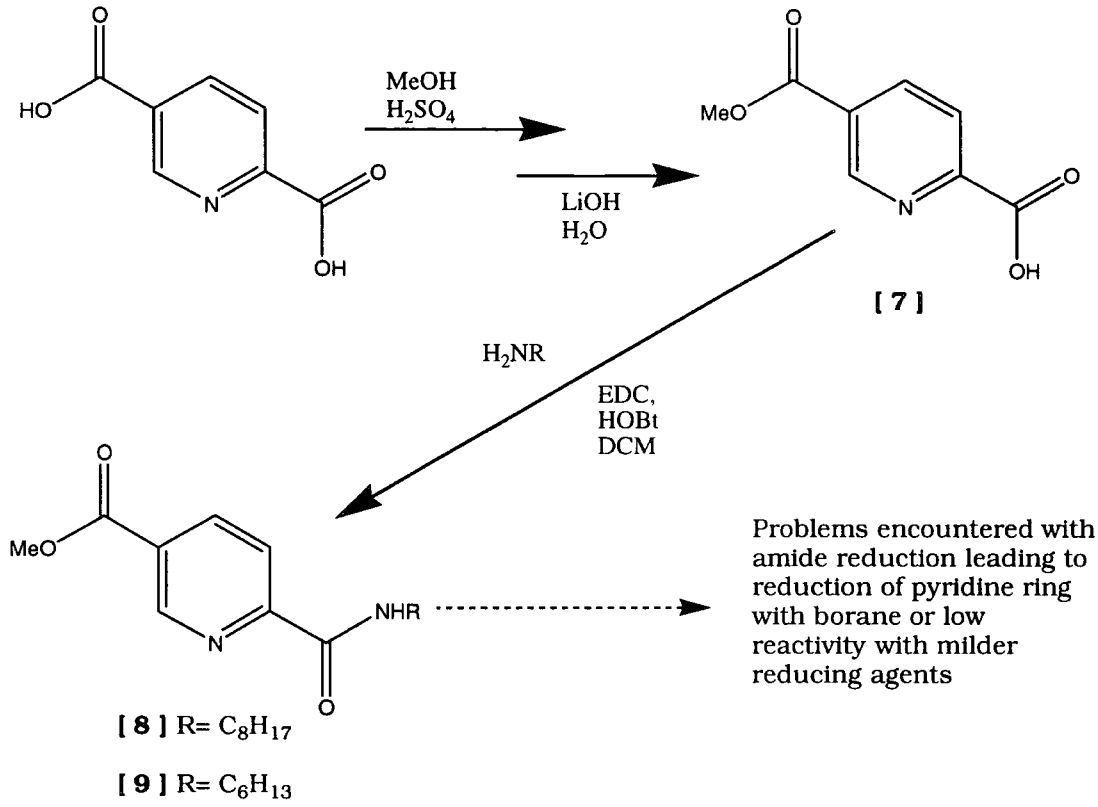

Figure 19 Initial steps in synthetic route from pyridine 2,5-dicarboxylic acid

In each of the above cases the routes were abandoned as work on other routes began to show greater promise of success. The route eventually successful, is less commonly used than the routes based on the modification of substituted pyridines. It relies upon the formation of a 6-membered ring *via* a [4+2] cycloaddition strategy. The key stage involves an aza-Diels-Alder reaction which was used to form a 2,5 disubstituted pyridine[71]. Following the application of this pyridine ring forming reaction, the steps found to be effective during earlier synthetic routes attempted were used to complete the synthesis of the desired cationic amphiphile. By using n-alkyl aldehydes of different length to carry out the reactions shown in Figure 20, it is possible to vary the alkyl chain length at the 5-position in the final pyridine.

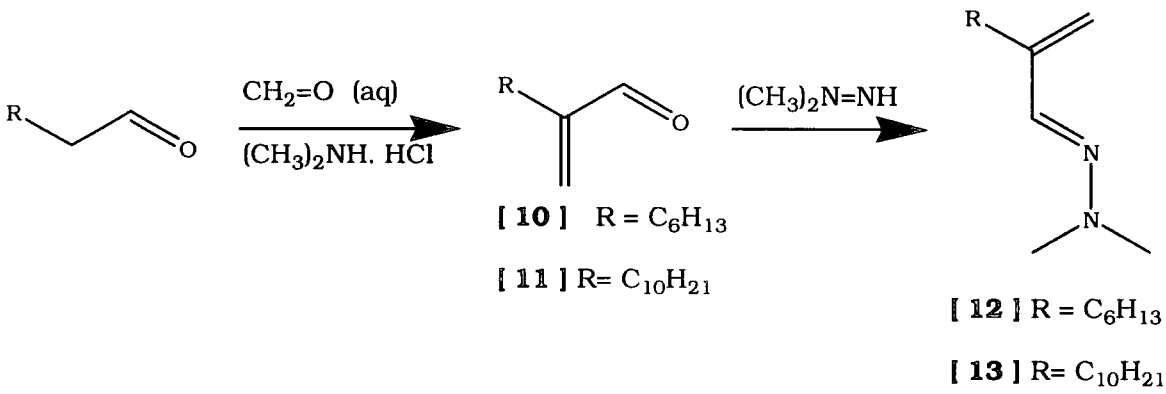

[10] R = C_6H_{13}

[11] R= $C_{10}H_{21}$

[12] R = C_6H_{13}

[13] R= $C_{10}H_{21}$

Figure 20 Formation of the aza-diene used in pyridine ring synthesis[71,125-127].

Two molecules were synthesised for this work, one beginning with dodecanal to give a decyl chain at the pyridine 5-position [11]and the other starting from octanal leading to a shorter hexyl chain [10]. The aza-Diels-Alder reaction of the hydrazone products [12] and [13] from Figure 20 with chloroacrylonitrile gives rise to 5-alkyl-2-cyanopyridines [14] and [15] in good yield.

Hydrolysis of [14] and [15], using potassium hydroxide in ethanol, gives rise to the 2-carboxylic acid compounds [16] and [17]. However, an early synthesis in which the hydrolysis was given insufficient reaction time, yielded the intermediate 5-hexylpyridine-2-carboxamide [22]. This product formed crystals of suitable quality to allow single crystal X-ray diffraction to be performed. The resulting structure is shown in Figure 22 and 23, with further details included in Appendix 1.

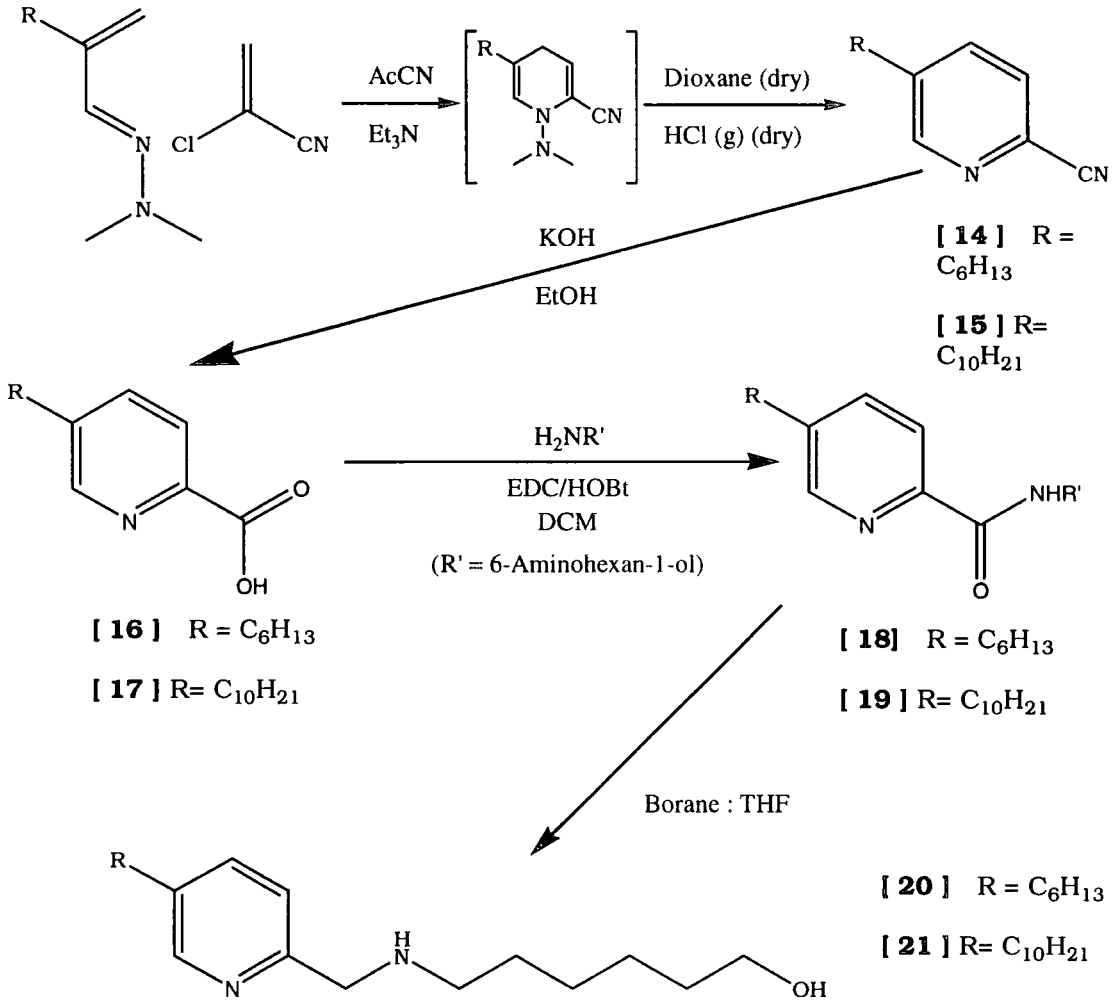

Figure 21 Reaction Scheme Showing Aza-Diels-Alder Pyridine Formation and the Amide Coupling Step (as in Figure 20, R = C_6H_{13} or $C_{10}H_{21}$.)[71,127]

The alkyl chain, adopts the expected extended linear conformation and it can be seen in the packing diagram (Figure 23), that these chains align themselves into organised rows. The packing diagram also shows intermolecular hydrogen-bonds (dotted lines) between the amide carbonyl oxygen and the acidic pyridine C-6 hydrogen.

Having formed [16] and [17], following complete hydrolysis of the [14] and [15], it was possible to make use of the amide coupling route used in previous syntheses (Figure 18 & Figure 19) to afford the desired aminomethyl compounds (Figure 21).

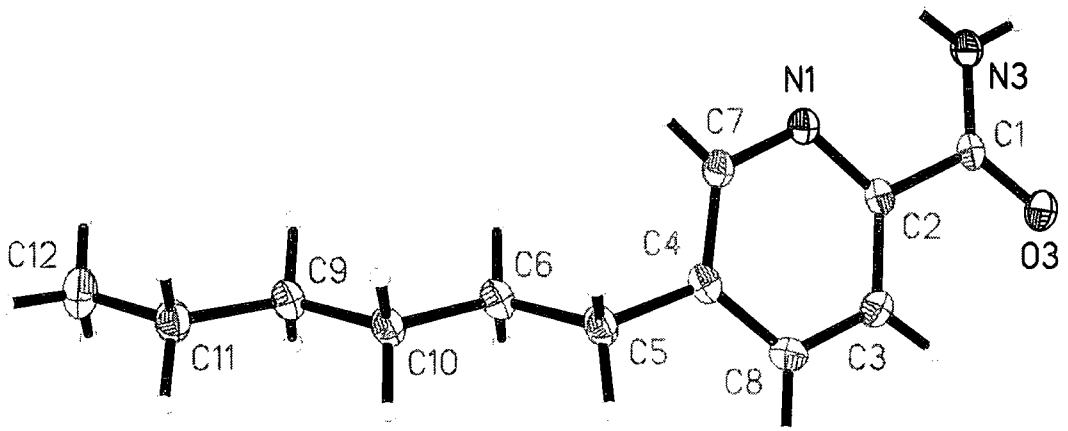

[22]

Figure 22 Crystal structure of 5-hexylpyridine-2-carboxamide **[22]** (for more detailed information see Appendix 1)

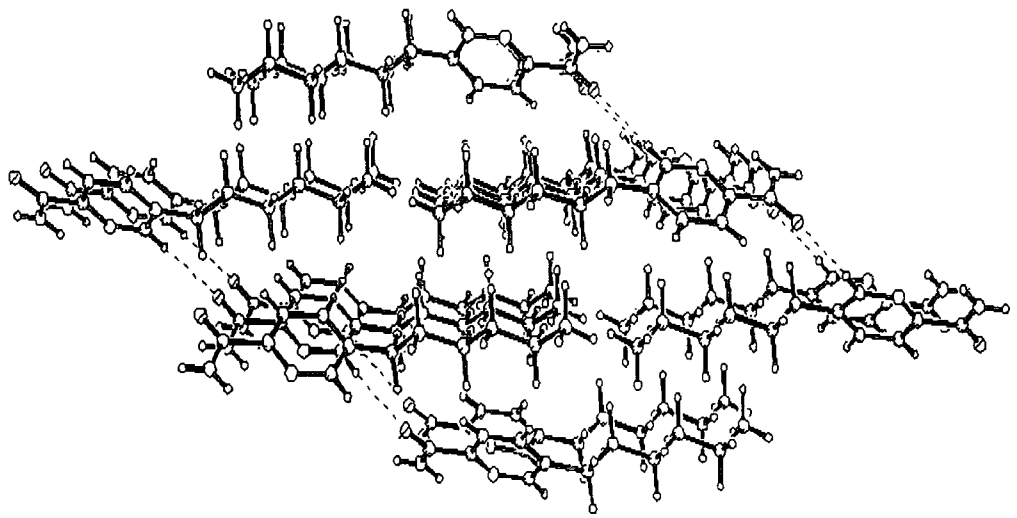

Figure 23 Crystal packing of 5-hexylpyridine-2-carboxamide (for more detailed information see Appendix 1).

To avoid complications in the early steps of the synthesis, it was decided to locate the head group on the 2-position substituent. Variations are possible in the length of the amine alkyl chain by

coupling with different n-alkyl amines. However, readily available 6-aminohexan-1-ol was used here first, as it gave a simple route to the inclusion of a charged head group (Figure 24). After BOC protection of the amine functionality, the alcohol compounds [23] and [24] were converted to the reactive mesylate compounds [25] and [26]. With its improved properties as a leaving group, the mesyl compounds were then treated with a solution of trimethylamine in ethanol to produce the cationic trimethylammonium compounds [27] and [28] with a methanesulphonate counter ion. The BOC protecting group was then removed in the conventional manner using TFA. At the end of this step, a counter ion system predominatly comprised of triflate, with the possibility of some remaining mesylate, was present. Using DOWEX® 1X8 (Cl) strong anion exchange resin, this mixed anion system was replaced to leave chloride as the sole counter ion. These chloride salts [29] and [30] were then characterised by NMR and accurate electrospray mass spectroscopy. Figure 25 shows the accurate ESMS spectra for the two pyridine surfactant compounds. The sodium iodide reference (m/z 172.884) can be clearly seen as a truncated peak in the spectrum for the hexyl compound (m/z 334.3191), as can a peak corresponding to the doubly charged species (m/z 167).

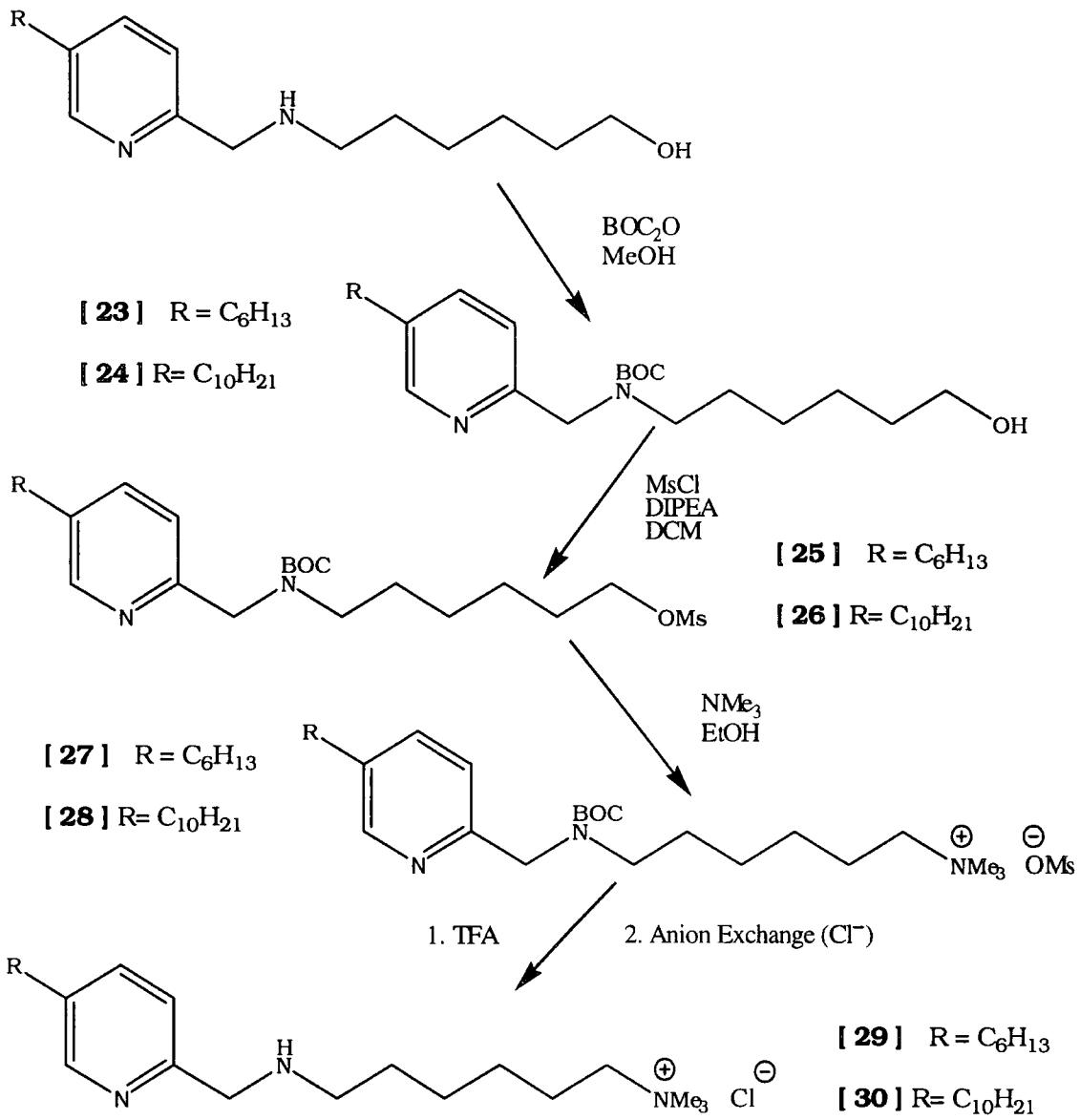

Figure 24 Scheme Showing Amino Alcohol Modification to Trimethyl Ammonium Head Group

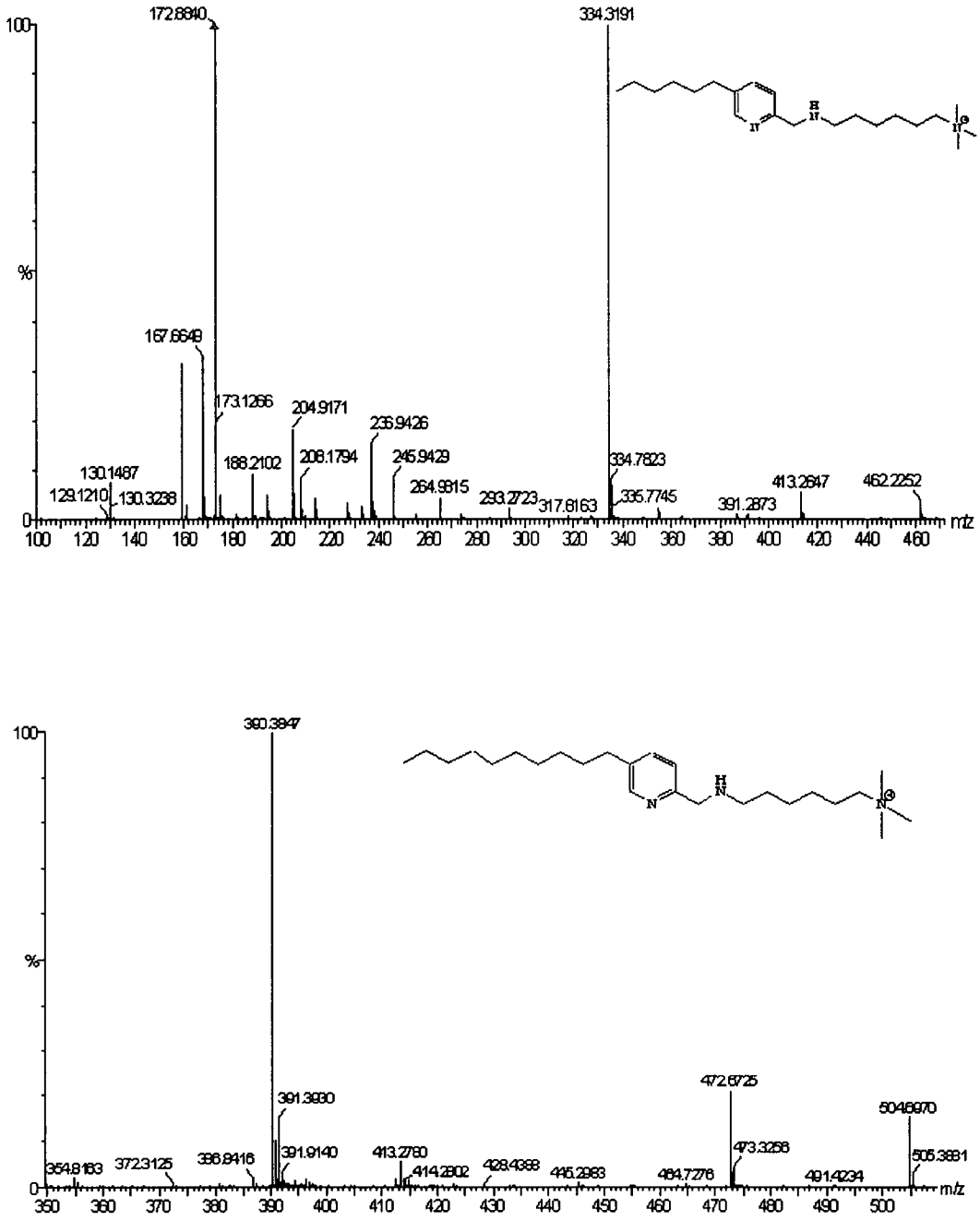

Figure 25 Accurate electrospray mass spectra for compounds **[29]**(m/z 334.3191) and **[30]**(m/z 390.3847).

2.3 Aggregation and Protonation Properties

In addition to the spectroscopic characterisation of the two target molecules produced, N,N,N-trimethyl-2-{[(5-hexylpyridin-2-yl)methyl]amino}hexan-1-aminium chloride [29] and N,N,N-trimethyl-2-{[(5-decylpyridin-2-yl)methyl]amino}hexan-1-aminium chloride [30], their CMC and pK_a values were determined. These values were then considered in the design of further experiments to assess their ability to cause aggregate disruption.

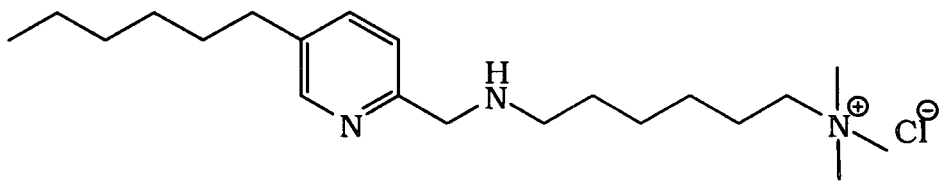

[29]

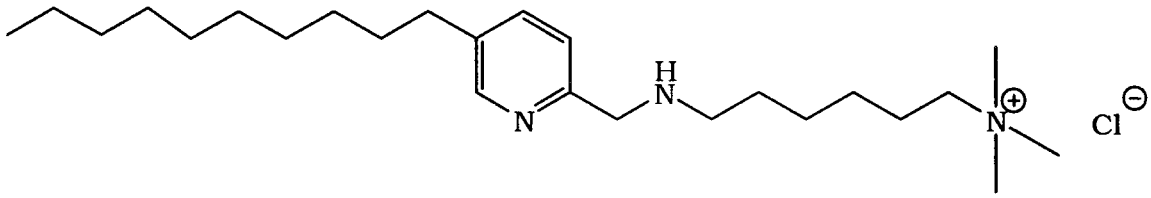

[30]

2.3.1 CMC Determination

The critical micelle concentration for each of these compounds was measured using two methods. Firstly, conductivity measurements were undertaken as a function of concentration and secondly the CMC was determined using pyrene as a fluorescent polarity probe. Each of these methods has been used frequently to measure CMC and should give rise to similar values[47,48,76].

As was mentioned in Chapter 1 (section 1.3.1), the CMC can be observed and measured by the change in the conductivity of a

solution. This is done by preparing solutions, of the surfactant molecule being analysed, in increasing concentration using high purity water (≤ 0.045 μScm^{-1}) to minimise background conductivity. The conductivity measurements were made using a Jenway 4010 conductivity meter and a pair of clean platinum electrodes positioned 1cm apart. The solutions of [29] and [30] were prepared using ELGA Ultra High Purity water; the initial pH of the solutions prepared was between 4 and 5. The addition of base needed to adjust these solutions to the required pH 7.2, increased the electrolyte content of the solution to such an extent as to mask the relatively small change in conductivity due to micellisation.

a) Pyrene Fluorescence Method for CMC Determination

Pyrene can be used as a fluorescent probe for CMC determination as the spectral form of the emission from the excited π-system varies depending on the micropolarity of its surroundings.[72,73,74] Combined with the fact that the planar organic pyrene molecules readily associate with the hydrophobic sections of surfactants as they aggregate in aqueous solution, this leads to the observed emission spectrum from pyrene in solution with surfactants below their CMC being different to that of pyrene in solution with surfactants at or above their CMC. Solutions of the pyridine surfactant to be measured were prepared over a range of concentrations, from 0.025mM to 2.5mM. The samples for measurement were prepared by taking 2.95ml portions of the aqueous surfactant and adding 50µl of pyrene solution in methanol (0.125mM). This gives rise to a pyrene concentration of 2×10^{-3}mM in the samples used for the fluorescence measurements. The small quantity of methanol should have little effect on the overall micropolarity of the aqueous solution or the aggregation properties of the surfactant. This assumption has been made in several earlier analyses using this approach[75,76,77]. The CMC

is evaluated from a plot of the ratio of two maxima of the pyrene emission spectra against concentration of [75-77] surfactant. The pyrene emission spectrum shows five local maxima across its emission range, the fourth (λ_{MAX} ~ 386-388nm) is usually only seen as a shoulder peak on the fifth (λ_{MAX} ~392-393nm) and may in many cases be difficult to discern (Figure 26). The relationship between several of these maxima changes with the micropolar environment. The I_1:I_3 ratio and the I_1:I_5 ratio have both been used to determine CMC[78]. However, more recent investigations have shown CMC values determined using the I_1:I_5 ratio match more closely with values determined using other methods[77]. This ratio was therefore used in this work.

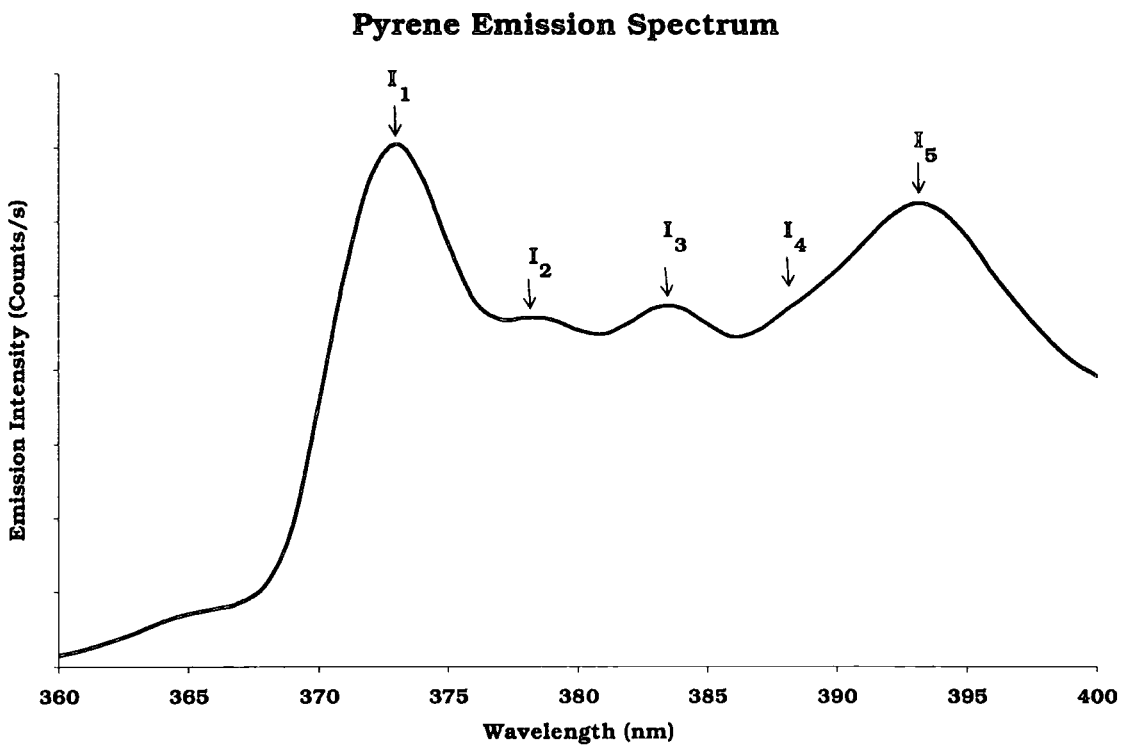

Figure 26 Typical aqueous pyrene emission spectrum showing five local maxima.

b) CMC Measurements for Pyridine Species

The pyrene emission ratio data was used to calculate the CMC values shown in Table 1. (The experimental data can be found in appendix 2)

Species	CMC Value determined at pH 7
[29]	1.45mM
[30]	0.52mM

Table 1 CMC values for [29] and [30] determined *via* pyrene fluorescence.

Figure 27 shows the plot obtained from a CMC determination experiment for species [30] using pyrene fluorescence. The CMC is defined as the concentration of surfactant at which any further reduction in concentration would lower the micelle population to zero. The CMC is usually determined from data plots as the first 'break' point, or where two sections of linear change within the data plot meet. Having determined CMC values for both [29] and [30] it was then possible to prepare an experiment to measure the pK_a of [29] and [30] in dilute solution and also to include them below their CMC in a co-aggregate with a well know cationic surfactant. The cationic surfactant chosen was CTAB[79,80] (CMC 0.85-0.92mM[77,81]). Experiments were carried out using mixtures of CTAB and [29] or [30] to assess the extent of pK_a suppression with aggregation.

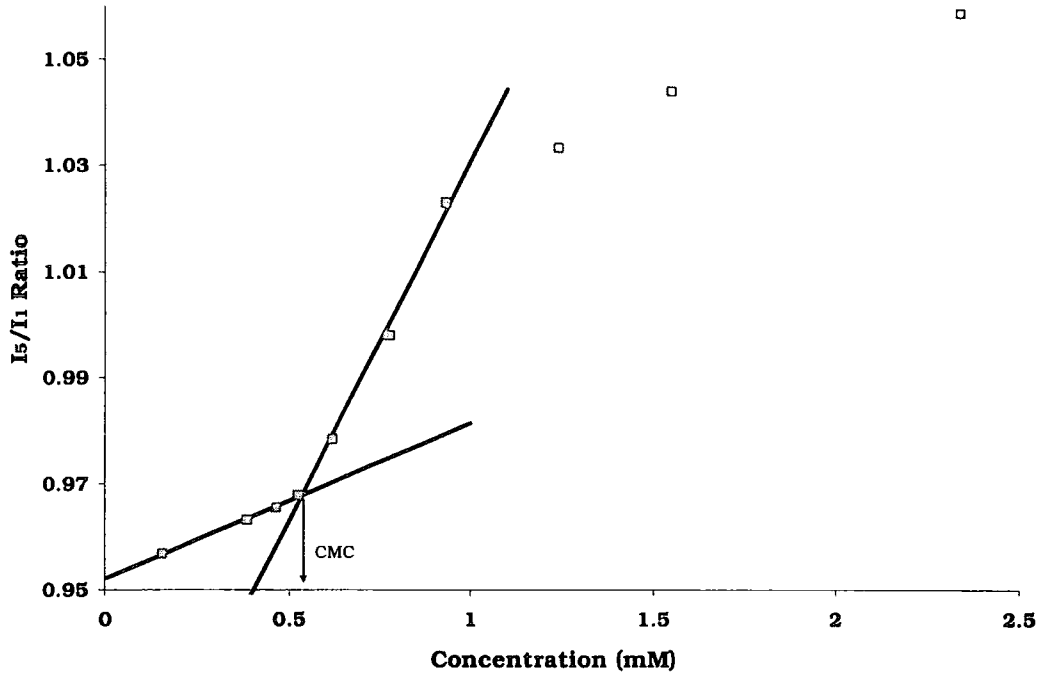

Figure 27 Pyrene method for cmc determination with [30] (pH 7 295K)

2.3.2 Measurement of pK_a

The pK_a of the pyridine species was measured by monitoring the change in UV absorbance as a function of pH. The proximity of the secondary amine group to the pyridine was expected to lead to a change in the polarisation of the C-C σ-bond in the 2 position, and hence the absorbance behaviour of the pyridine ring, following protonation of the amine. A more direct effect was also expected, at a point where the pyridine nitrogen itself was protonated. Initial experiments were performed to assess the possibility of using fluorescence emission as well as absorption spectroscopy. However, there was insufficient observable change in the pyridine emission spectrum with pH to use this method. The UV absorbance maximum was seen to shift from 264nm to 276nm in certain cases, as the pH

changed from 5 to 12. This change was used to assess the pK_a of the pyridine species both in free solution and as part of a mixed aggregate with CTAB. Solutions of both [29] and [30] (0.04mM, 22°C) were prepared as were solutions containing CTAB(1.2mM, 22°C) and ~1 mole percent [29] or [30] (0.013mM, 22°C) and solutions containing CTAB(1.2mM, 22°C) and ~5 mole percent [29] or [30] (0.062mM, 22°C). All solutions were prepared using Purite water (0.05 Scm^{-1}) and a duplicate set of solutions were prepared with 0.1M NaCl solution. In each case, the solution pH was varied from 3-12 using 0.1M aqueous solutions of NaOH or HCl; the pH was measured using a glass electrode and a Jenway 3320 pH meter calibrated (±0.02) using standard pH 4, 7 and 10 buffer solutions. UV absorption spectra were measured at intervals across the entire pH range using a UNICAM UV2 spectrometer (bandwidth 0.25nm). Figure 29 shows the raw data obtained for [30] in dilute solution and for the same compound as a 5 mole percent co-aggregate with CTAB. The change in maximum absorbance seen at low pH in each of the plots in Figure 29 is most likely to be due to the protonation of the pyridine nitrogen (Figure 28) and was a common feature in each of the experiments undertaken

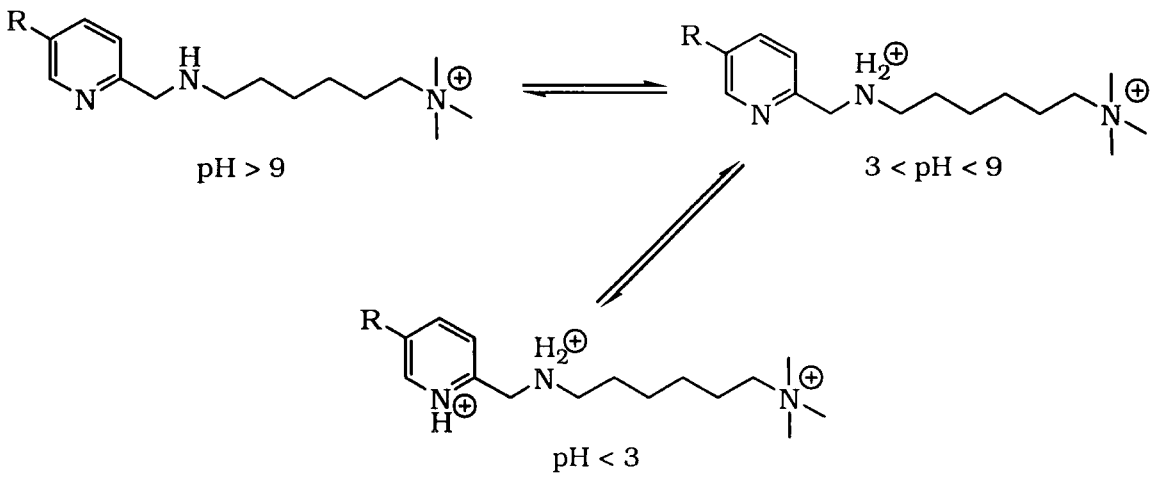

Figure 28 Protonation scheme for aminoalkylpyridines

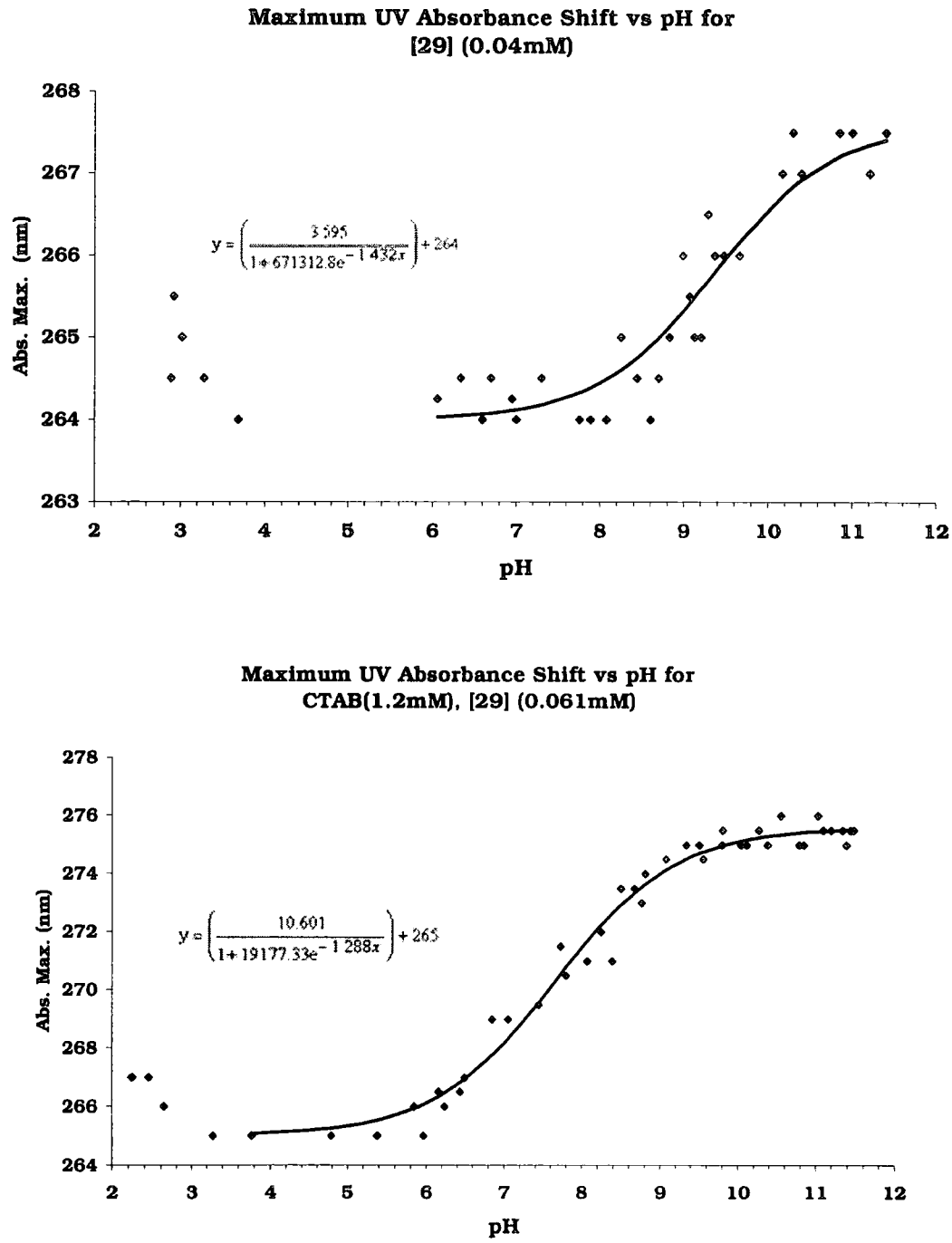

Figure 29 Data plots showing maximum absorbance change vs pH, For [30] In solution and in 5 Mol% ratio with CTAB.

Optimum curves were fitted to the selected sections of the experimental data by using CurveExpert v.1.37 curve fitting

software[82] and the resulting best fit equations used in the calculation of the pK_a values.

The pK_a values obtained for both compounds in dilute solution and as co-aggregates are shown in Table 2. The solutions containing 0.1M NaCl showed no observable difference in behaviour to those without the constant ionic background and so the data were combined. From these results the suppression of pK_a on aggregation can be seen. The greatest effect being observed in the longer chain product [30] at 5 mole percent, while compound [29] shows much smaller shifts in pK_a when included at the 1 and 5 mole percent levels used in this experiment.

Amphiphile Conc^n (mM)	**CTAB Conc^n (mM)**	**pKa (± 0.25)**
[29] ; 0.04	none	9.4
[30] ; 0.04	none	9.3
[29] ; 0.013	1.2mM	8.3
[30] ; 0.013	1.2mM	7.6
[29] ; 0.062	1.2mM	8.6
[30] ; 0.062	1.2mM	7.4

Table 2 pK_a Values for pyridine species [29]& [30], measured using UV-spectroscopy (1cm cell path, 295K)

Both of these compounds show protonation constants close to those expected and close to those of similar compounds found in the literature (Figure 15). The highest suppression seen for compound [30] only reduces the pKa by 1.9 units to 7.4 which is probably not sufficiently low for the proposed function.

In order to reduce the pK_a still further, either electron-withdrawing groups need to be introduced into the amine β-position (e.g. a CF_2 moiety) or longer chains should be incorporated at C-5 and/or C-2, in order to encourage greater hydrophobic interactions with the co-

aggregate and therefore, further suppress the apparent pK_a in the aggregated complex.

Chapter 3

3 EDTA/DTPA Diamide Based Twin Chain Amphiphile Systems

3.1 Twin Chain System Approach

Producing pH sensitive amphiphiles, with twin chain lipid-like structures, offers the potential for greater affinity with liposome and bilayer vesicles, along with a potentially enhanced level of disruption in these more rigid aggregate structures. The lipophilic EDTA/DTPA structures chosen also allow for the possibility of a response to the changing metal ion concentrations which are also found within the endosomal compartment.

Each of these systems was designed so as to produce twin chain surfactant molecules with the amino portion of the molecules forming the hydrophilic head group and the two amide alkyl chains aligning to form the hydrophobic tail section of the amphiphile. Amphiphilic DTPA dialkylamides have previously been synthesised and their lanthanide complexes used in the NMR study of liposomes and 'bicelles' (bilayer micelles.)[83,84]. Both DTPA and EDTA have strong metal binding properties and so both the rates and the equilibria defining metal ion complexation and dissociation are intrinsically sensitive to $\Delta[M^{n+}]$ as well as to changes in pH. Both EDTA and DTPA form dianhydrides and reaction with 2 equivalents of amine produces a diamide ligand forming charge neutral complexes with doubly and triply charged metal ions respectively. These diamides generally form metal complexes of lower thermodynamic stability and of reduced kinetic stability to acid catalysed dissociation. The sensitivity of EDTA and DTPA diamides, to pH changes within the pH 4 to pH 7 range required for response to endosomal acidification, is seen in the published pK_a data for the various protonation events involved in EDTA and DTPA diamide solutions. For EDTA species the protonation steps of most interest are those of the two tertiary amine nitrogens of

the ethylenediamine structure, with pK_a values of 3.5 - 4.5 and 6.6 - 7.3 respectively[85]. DTPA protonates in much the same way. The first site to protonate in this case is likely to be the central nitrogen in the structure, followed by the other tertiary amines. DTPA bisbutylamide has pK_a values of 9.36, 4.44 and 3.31 for these dissociation steps[86].

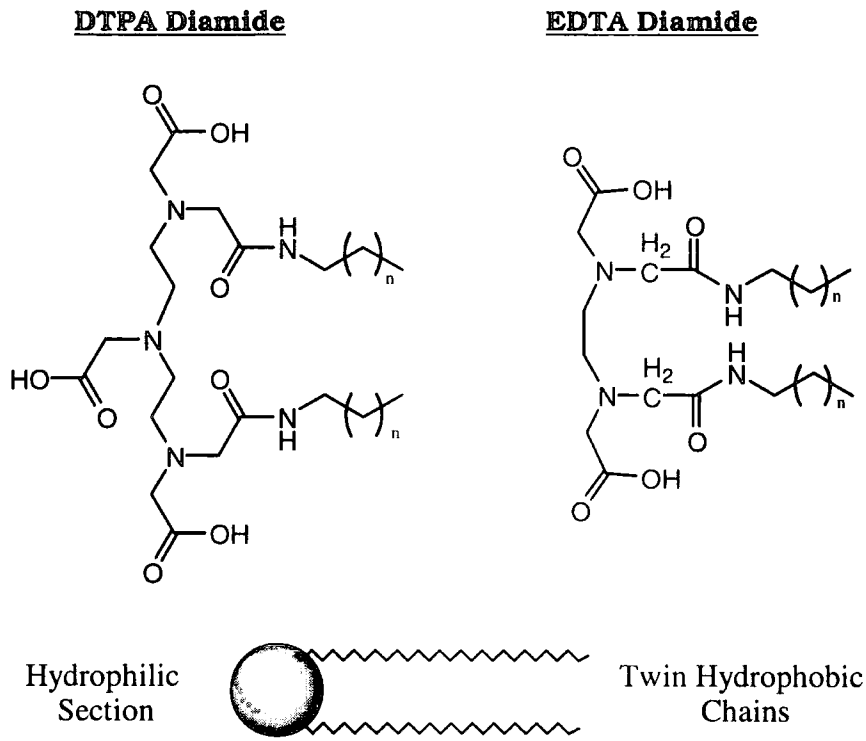

Figure 30 General structures of EDTA and DTPA diamide molecules and diagram representing twin chain amphiphile structure

The potential for the DTPA molecules to adopt a conformation where the amide groups align, was identified by an analysis of published X-ray structural data using the Cambridge Structural Database[87,88,89,90,91,92]. The yttrium dibenzyl amide complex shown as an example in Figure 31 has the amide groups aligned approximately parallel, with the oxygens of the two amide groups 3.16 Å apart and the amide nitrogens 6.95 Å apart. This solid state data is a strong indication that DTPA diamides will be able to adopt the required

conformation in solution, with the alkyl chains of the amide substituents forming the hydrophobic section of the amphiphile. EDTA diamide crystal structures exhibit a number of different conformations depending on the nature of the co-ordinating metal, the extent of any structural modifications of the ligands EDTA section and the nature of the substituent in the amide R group. However, no EDTA diamide structures were found to show cis-related amide groups or amide alignment in the solid phase.

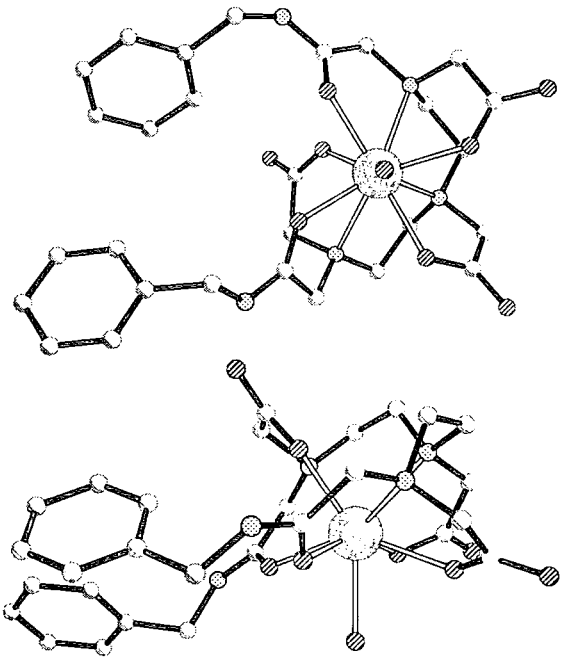

Figure 31 Images from X-ray structural data for Aqua-(N,N''-bis(benzylcarbamoylmethyl)diethylenetriamine-N,N',N''-triacetato)-yttrium trihydrate, showing amide group alignment[87].

The examples shown in Figure 32, Figure 33 and Figure 34 are representative of EDTA bisamide structures. The (+)-(N,N'-1,2-ethanediyl-bis(N-(carboxymethyl)glycyl-L-methionine)ethyl esterato)-copper(II) sesquihydrate structure (Figure 32)[93], shows the amide groups are trans-related. In the aqua-(N,N'-ethylenebis(N-carbamoylmethylglycinato))-copper(ii) dihydrate structure Figure 33[94], the amide groups are also trans-related, although the ligand is five

co-ordinate, leaving an amide group unbound. Figure 34 shows (N,N'-bis(acetato)-N,N'-bis(N''-uracil-5-ylacetamido)-1,2-ethylenediamine)-aqua-zinc tetrahydrate[95]. In this structure, the amide groups are also in a trans arrangement. However, the co-ordination to the metal through each of the amide oxygens in this case, has the effect of drawing the amide substituents towards the same axis, although not aligning them parallel with each other. The lack of cis-EDTA diamide structures in the solid state however, does not rule out the possibility of these conformations being adopted in solution by a simple pseudorotation. Such cis-EDTA diamides are potentially more favourable configurations, in terms of producing amphiphile molecules, as they bring the alkyl chain carrying amide R substituents into closer proximity.

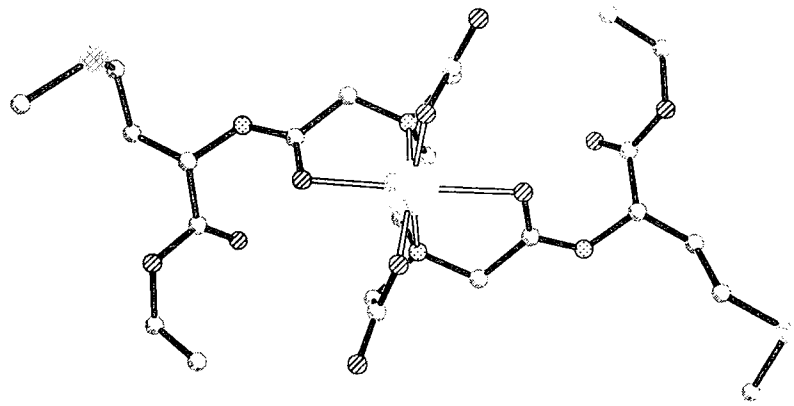

Figure 32 Image from X-ray structural data for (N,N'-1,2-ethanediyl-bis(N-(carboxymethyl)glycyl-L-methionine)ethyl esterato)-copper(II) sesquihydrate[93]

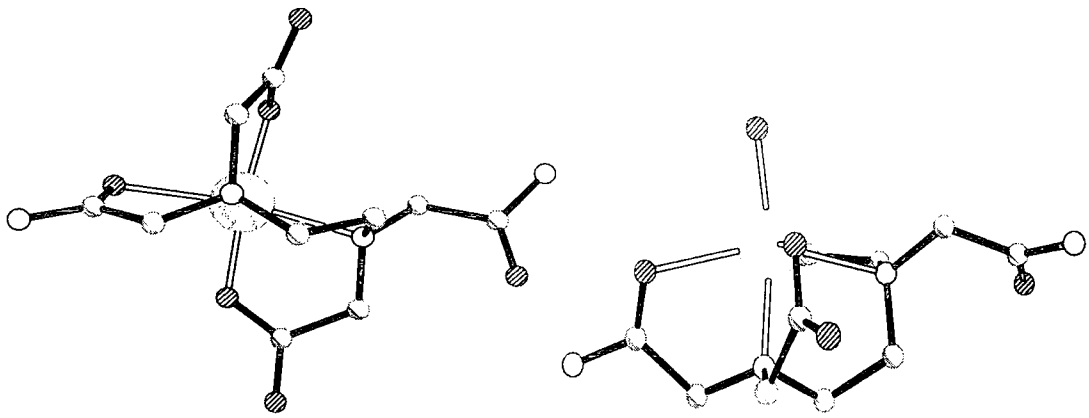

Figure 33 Images from X-ray structural data for aqua-(N,N'-ethylenebis(N-carbamoylmethylglycinato))-copper(II)[94]

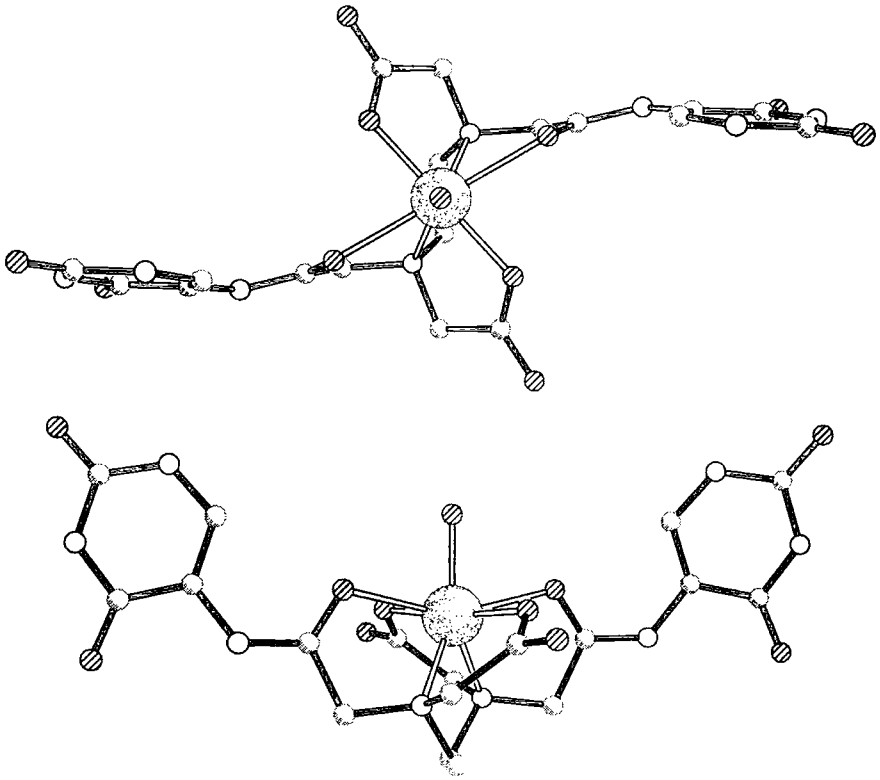

Figure 34 Images from X-ray structural data for (N,N'-bis(acetato)-N,N'-bis(N''-uracil-5-ylacetamido)-1,2-ethylenediamine)-aqua-zinc tetrahydrate[95]

The synthesis of both EDTA and DTPA diamide compounds (Figure 30) was achieved in high yield in a single step reaction. The dianhydride of either EDTA or DTPA was recrystallised and combined with 2.25 molar equivalents of the desired amine in dry THF, diethyl ether, pyridine or DMF (Figure 35). The resultant diamide products were purified simply by washing the white solid with several portions of the appropriate organic solvent, in order to remove any remaining amine.

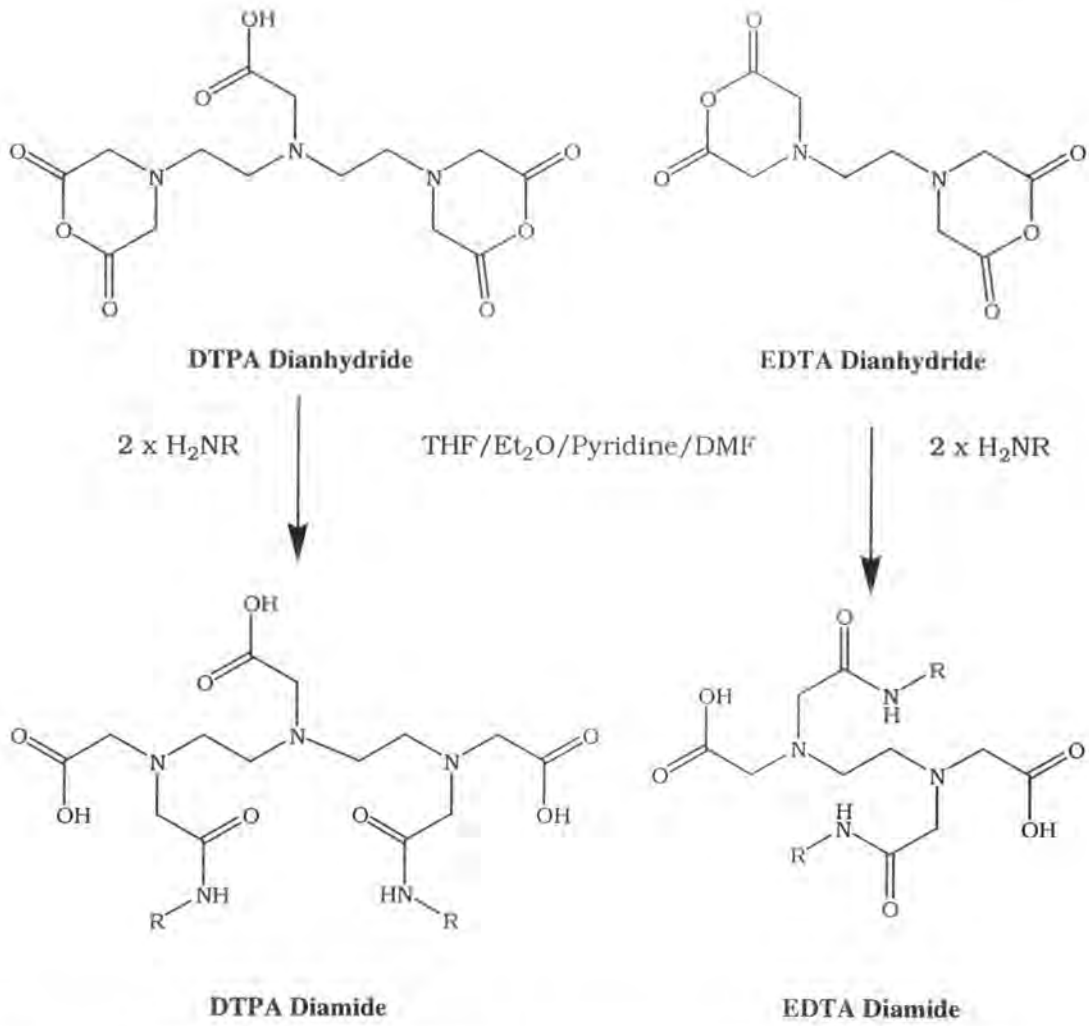

Figure 35 Reaction scheme showing the formation of DTPA and EDTA diamides.

The products were then characterised using elemental analysis and ^1H NMR. Elemental analysis often indicated the inclusion of water in the structure of the solids. This method was used to synthesise the DTPA and EDTA dinaphthyl substituted amides, [31] and [32] respectively, along with; EDTA dioctylamide [33], EDTA didodecylamide [34] and EDTA dihexadecylamide [35].

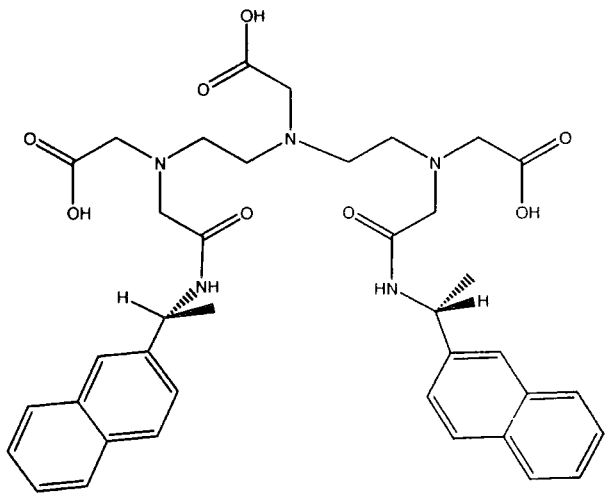

[31]

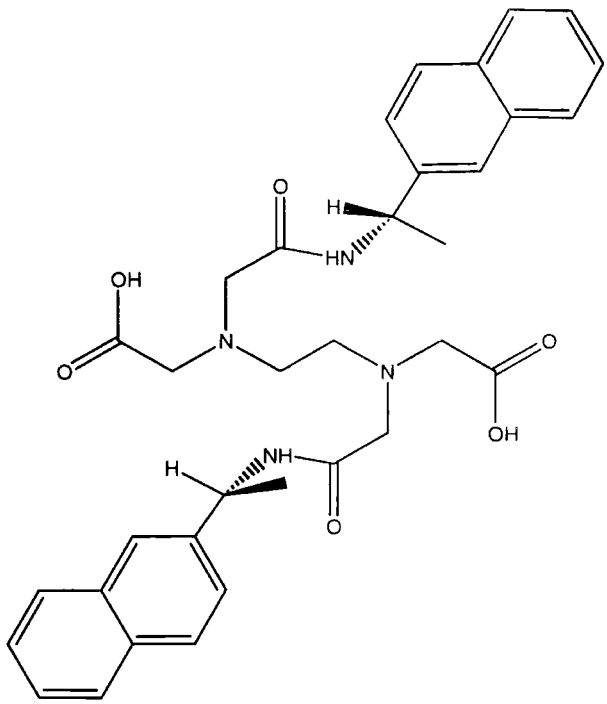

[32]

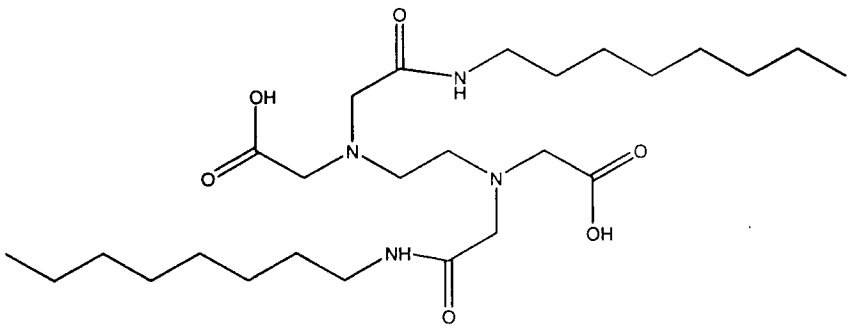

[33]

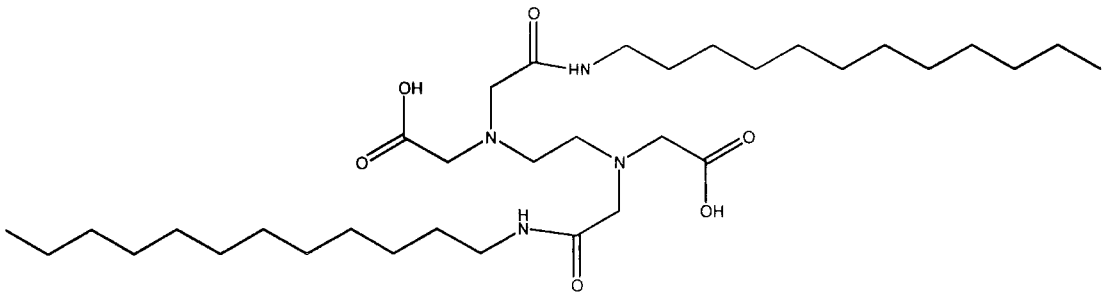

[34]

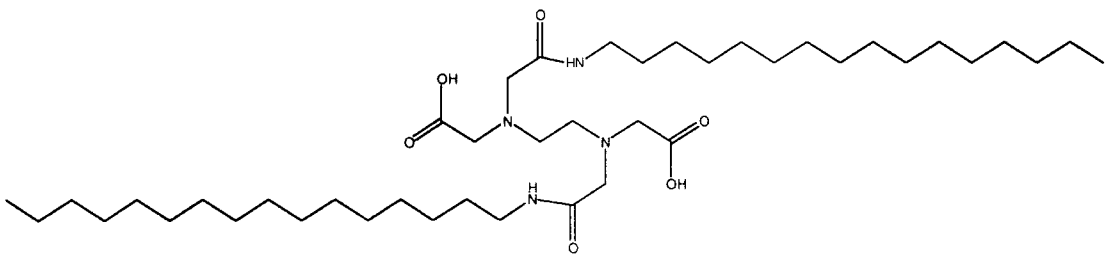

[35]

In addition to the ligands listed, Zn^{2+} complexes of the EDTA dialkylamides [33], [34] and [35] were synthesised by combining the ligand with 1.1 equivalents of zinc acetate in Purite™ water at reflux for three hours. The resulting white solid which precipitated on cooling was filtered and washed with copious amounts of cold Purite™ water. Again, characterisation by ^1H NMR and elemental analysis allowed the differences between the ligand and complex to be observed (Figure 36)

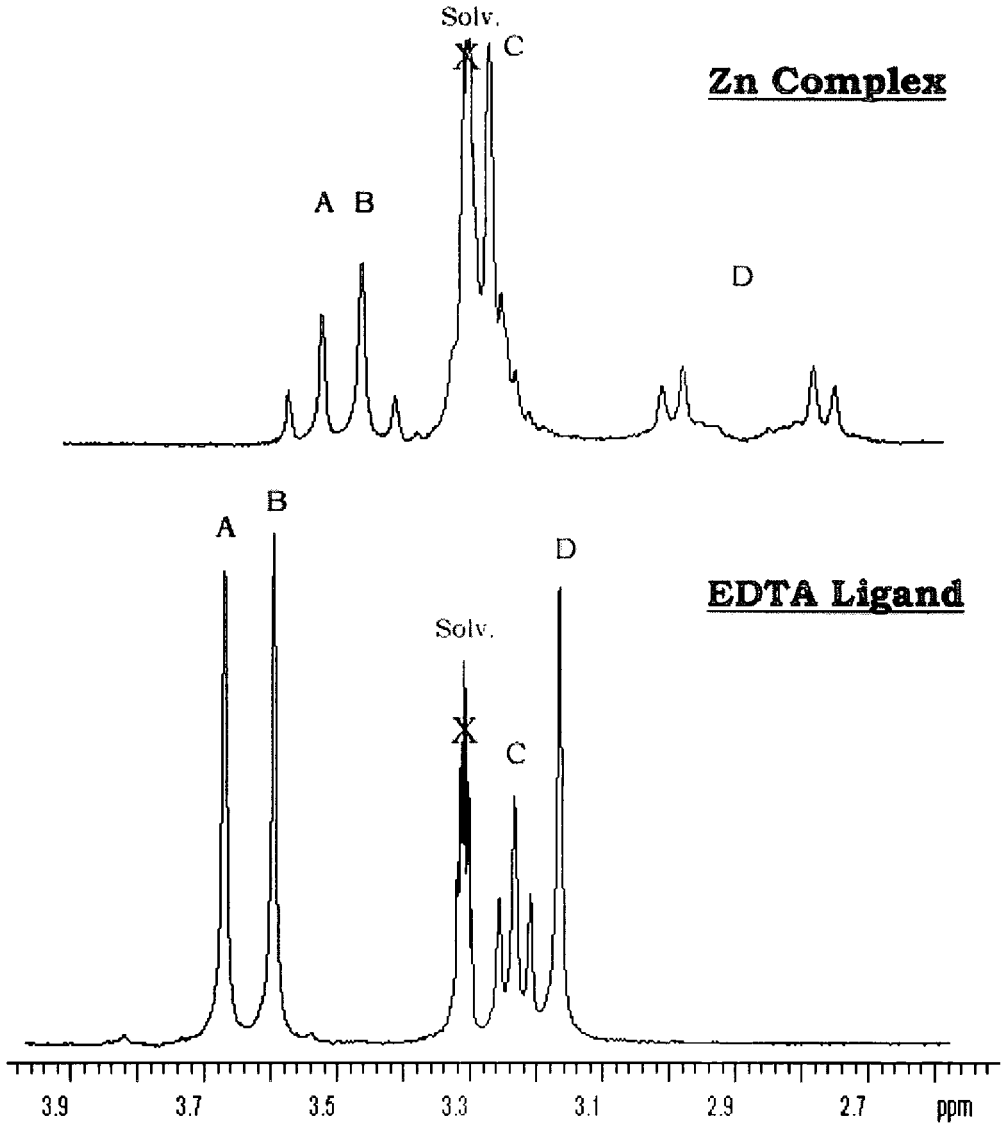

A: CH_2-CONH, **B**: CH_2-COOH, **C**: NH-CH_2-, **D**: N-(CH_2)$_2$-N.

Figure 36 ^{1}H NMR (CD_3OD 300MHz) spectra of a representative EDTA diamide ligand [33] and the corresponding zinc complex.

In the free ligand, the geminal CH_2N methylene groups appear as singlets (A, B, D.), except for the CONHCH_2 resonance which appears as a triplet through coupling to the adjacent CH_2 group. In the zinc complex, the NCH_2CH_2N protons resonate to lower frequency as a

major AA'BB' second order multiplet. The CH_2-CO resonances (A and B) also are rendered distereotopic by metal ion complexation, with geminal coupling constant of -16Hz.

3.2 Studies on the DTPA-Diamide System

3.3.1 Structure and Conformation

In addition to an examination of related solid state structural data, the conformation adopted by the DTPA diamide structures in solution was probed by examining the behaviour of a related dinaphthyl amide derivative. This structure allowed the proximity of the two amide groups to be detected *via* fluorescence, through the formation of an intramolecular excimer (excited dimer [Naph.....Naph.]*) between the proximate naphthyl groups. Excimers can be formed by most aromatic hydrocarbons, one molecule in an excited state and the other in the ground state. In this situation, the usual repulsion which would be experienced by two ground state molecules at close internuclear distances is replaced by weak stabilisation, leading to the formation of a weak dimer[96,97]. Emission from this excited dimer, gives rise to two molecules in the ground state and in close proximity. The ground state aromatic molecules experience the expected mutual repulsion and move apart following emission, leading to an absence of vibrational structure in the emission from the excimer. Excimer emission is characterised not only by the lack of vibrational structure seen in the monomer emission spectrum (Figure 37)[98], but, also by a wavelength shift. The potential energy curve diagram (Figure 38) shows clearly that the emission from an excited dimer should be of lower energy (longer wavelength) than that from isolated excited state monomers.

If the naphthyl groups in the DTPA compound synthesised are able to adopt a conformation where they are close and parallel, then

this excimer emission should be visible in the fluorescence emission spectrum for the compound.

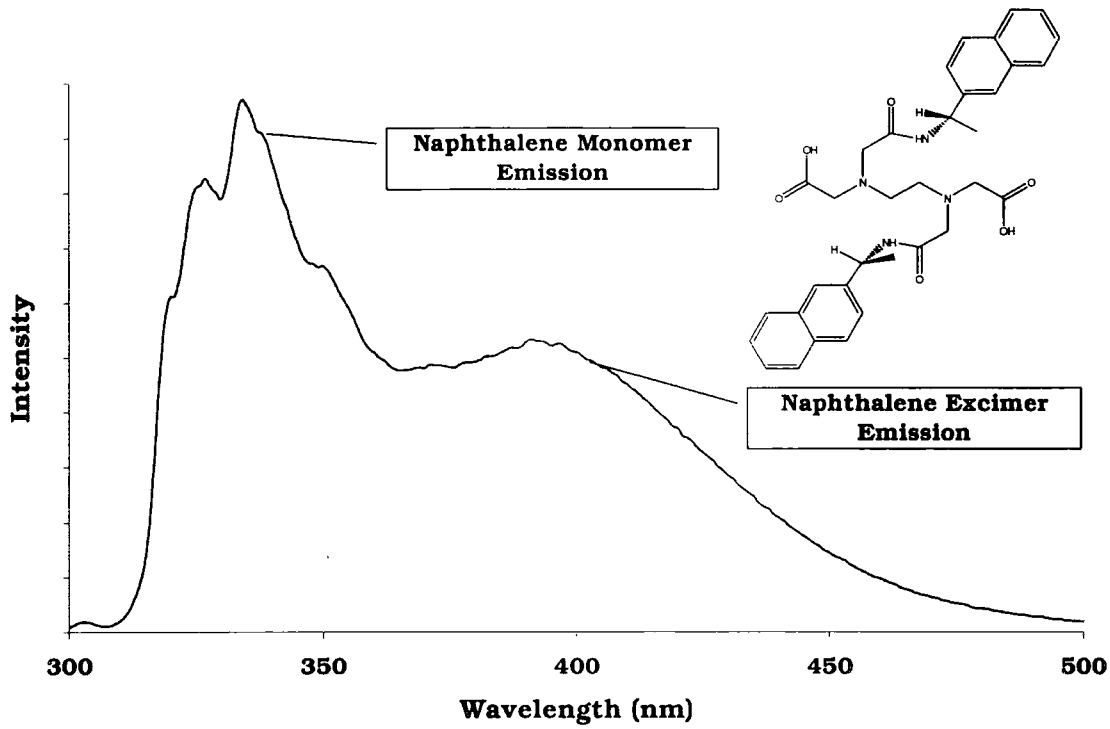

Figure 37. Example of naphthalene fluorescence emission spectrum showing monomer and excimer emission. (compound [32] 295K H_2O pH 5)

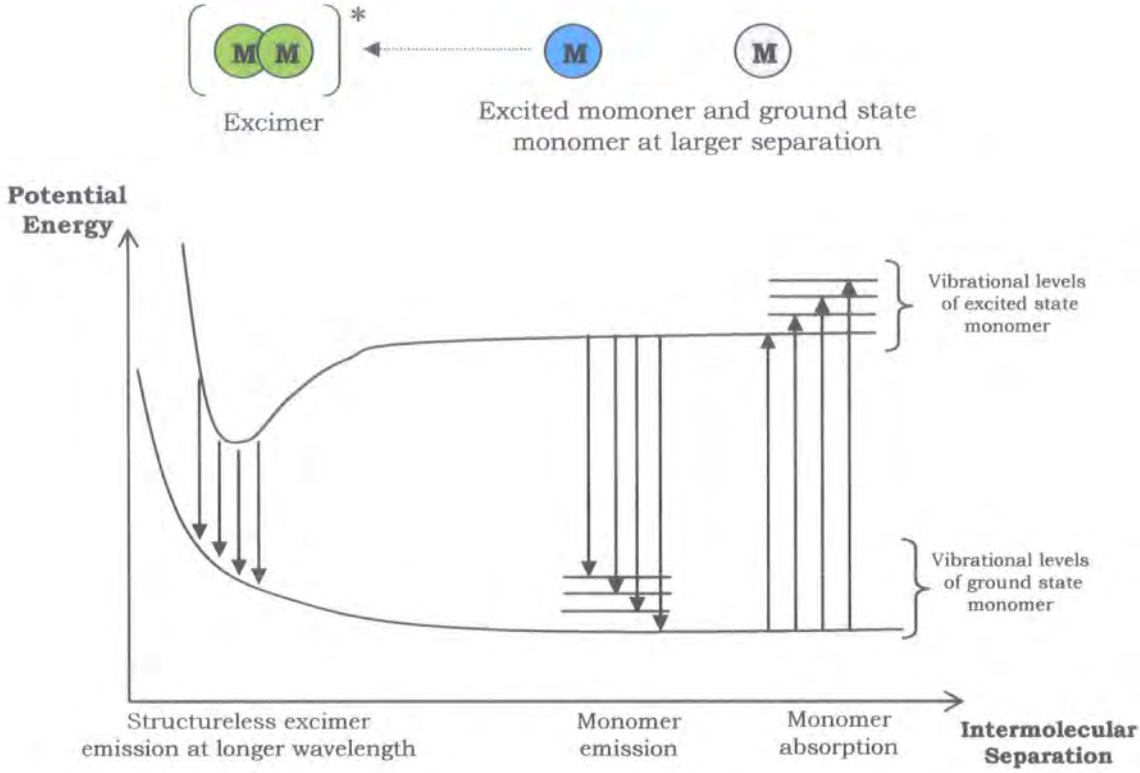

Figure 38 Schematic representation of excimer emission in terms of potential energy curves. The lower curve represents the ground state molecule and the upper curve that of a molecule in the first excited state.[99]

3.3.2 Solution Behaviour

Solutions of the dinaphthyl DTPA [31] compound were prepared and used in fluorescence experiments to determine solution conformation by monitoring the presence of the naphthalene excimer. Initial experiments were performed at pH 7.2 (HEPES Buffer) over a range of concentrations in order to determine if any excimer emission observed was due to intra- or intermolecular interactions. The relative intensity of the excimer emission compared to the monomer emission was calculated and was seen to remain constant at around 5-7%, independent of ligand concentration, indicating that an intramolecular excimer was being formed and therefore that the amide groups were able to align in parallel.

Further experiments were performed using the dinaphthyl substituted amide compound [31] to determine the effects of pH variation on the conformation of the molecule and therefore the degree of excimer emission. The data from these experiments showed that the relative excimer intensity varied with pH to give a bell shaped profile. Excimer formation was at a maximum between pH 3.5 and 8 remaining almost constant, while above and below these pH values its relative intensity fell sharply (Figure 39). This stable plateau of excimer intensity seems correspond to the pH range across which, the central amine of the DTPA moiety is protonated and one of the outer tertiary amines protonates (Figure 40).

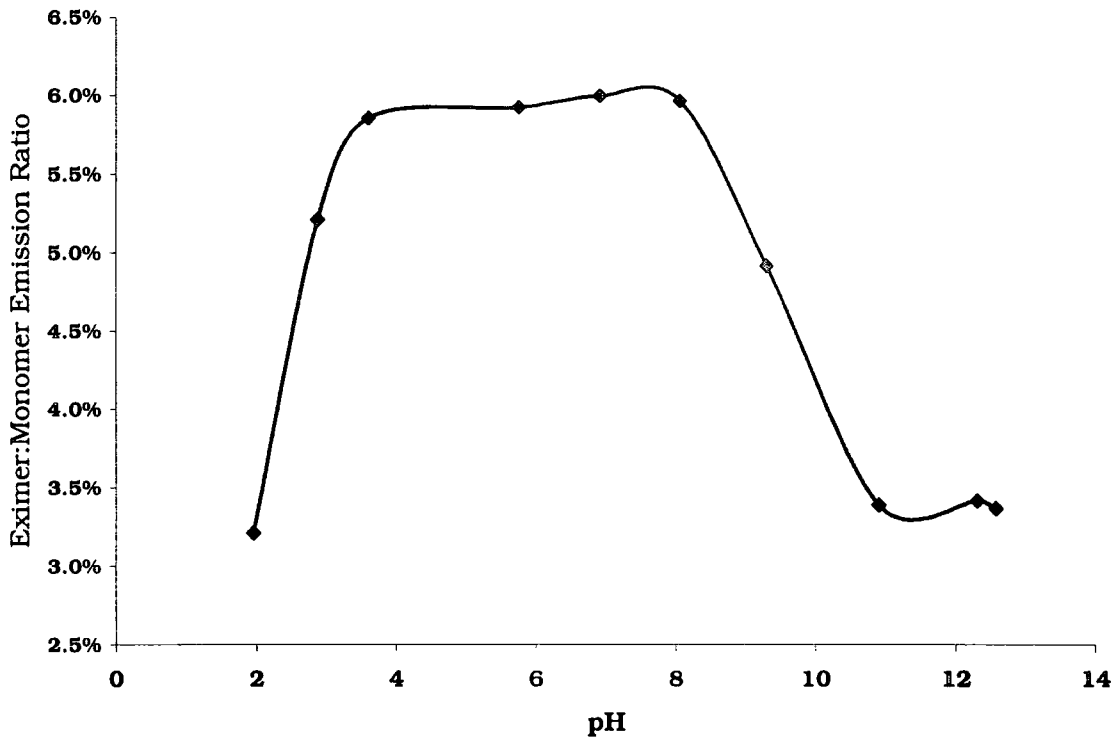

Figure 39 Plot of relative excimer emission vs pH for DTPA dinaphthyl substituted amide species [31]

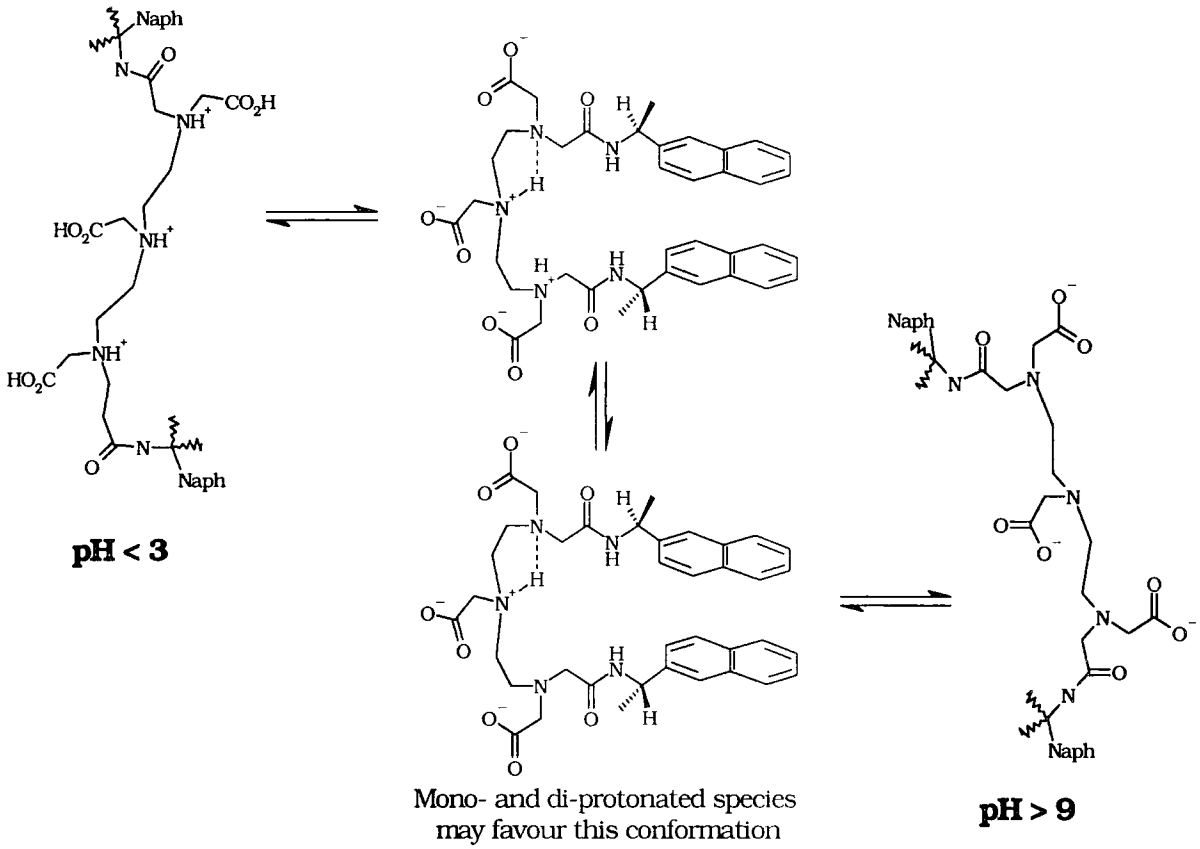

Figure 40 Diagram showing plausible protonation scheme for DTPA dinaphthyl substituted amide [31].

The decrease in intensity at pH 3.5 is most likely to be the consequence of electrostatic repulsion: as the third amine protonates the ion adopts a more extended conformation and the amide groups move apart. All these observations assume that the pK_a values for species [31] are similar to those of simpler DTPA bisamides.

Similar experiments were also carried out with a range of metal ions in solution, in a 1:1 molar ratio, to determine the effect metal binding would have on the solution conformation and how it would modify the response of the molecule and excimer emission to pH. The metals chosen were calcium, lanthanum, yttrium and zinc. Calcium and zinc are know to be present in biological media, the calcium concentration, in particular is known to vary greatly between the

extracellular background (ca 1-2mM) and intracellular fluids (sub micromolar).

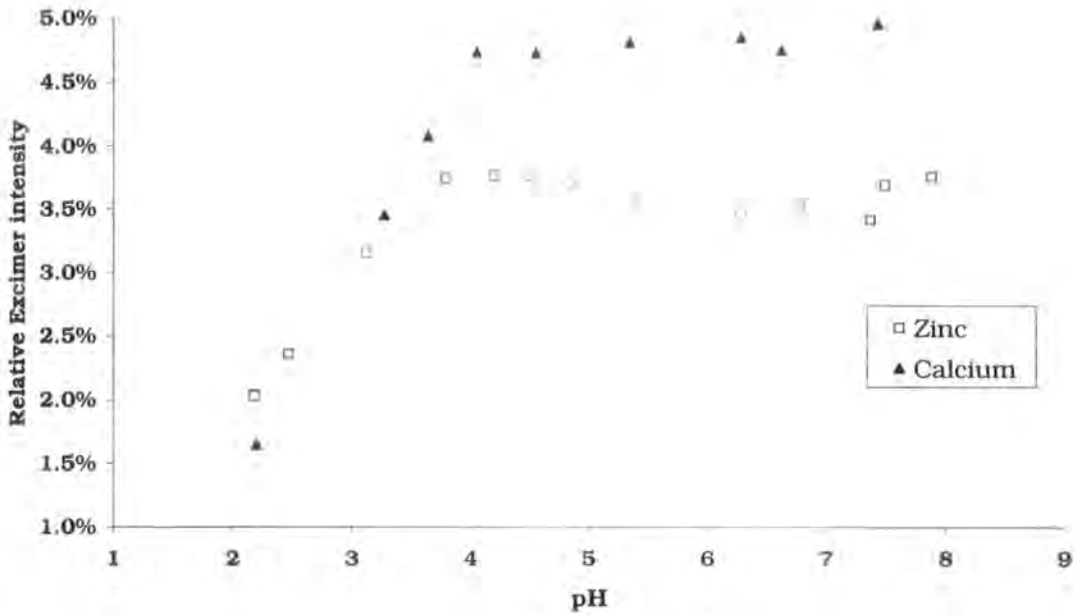

Figure 41 Plot of relative excimer intensity vs pH for the DTPA dinaphthyl substituted amide [31] showing response with metal ions in solution

The yttrium and lanthanum complexes form 9-co-ordinate structures with one water molecule and each of the ligand heteroatoms bound in a tricapped trigonal prismatic structure[87]. These metals were included to allow comparison of a wider range of co-ordination geometries. The inclusion of these metals in solution had little impact on the relative excimer intensity plots with the same features being present over the pH range from 2 to 8 (Figure 41). With each of the metal ions, the decrease in intensity from pH 8 to pH 11, observed in the free ligand was not seen. In the case of zinc, the precipitation of zinc hydroxide from the solution prevented useful measurements being taken above pH 8.5. It would appear from this experimental data that the stability of DTPA bisamides in binding these metal ions,

removes any response to pH above pH 4. That is, the 1:1 metal complex resists any protonation above pH 4, which is associated with a change in complex conformation. The response observed below pH 4 is consistent with that of the free ligand and is most likely caused by the decomplexation of the metal, leaving the ligand free in solution and able to protonate. This stability of the metal complexes of [31] reduces the suitability of these compounds for use in endosome triggered disruption systems. Complexation removes any response to the pH drop within the endosomal compartment, between pH 7.2 and pH 4. The observation that the complexed DTPA ligand [31] appears to favour a conformation in which the amide groups can align, which can be seen from the relative excimer intensity (Figure 39, Figure 40, Figure 41), is consistent with the solid state data. The DTPA dinaphthyl substituted amide [31] excimer experiments showed no response to either pH or metal ion concentration within the range required for action as an endosomal release trigger. It is possible that related amphiphillic DTPA diamides[83,84] may have the pK_a values of the key protonation steps suppressed when included as part of an aggregate. However, the location of the tertiary amine groups in the hydrophilic 'head' section of the molecule may significantly reduce any pK_a suppression which aggregation might cause.

3.3 Studies on the EDTA-Diamide Systems

3.3.1 Solution Conformation and Behaviour

In order to investigate the conformations adopted by EDTA diamide species in solution, the EDTA bisnaphthyl substituted amide [32] was synthesised by the method described in section 3.1.

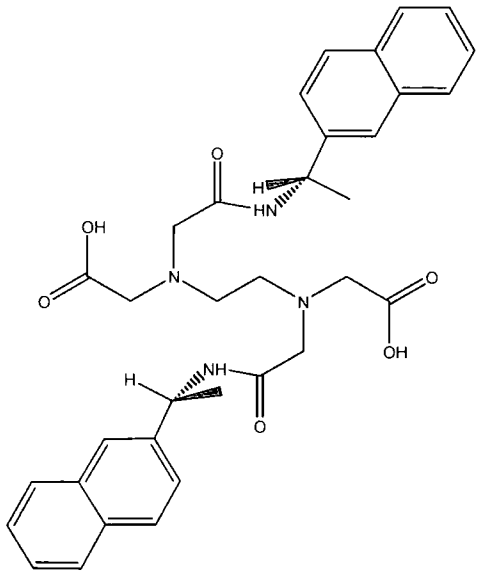

[32]

This compound was then used to perform experiments similar to those carried out with compound [31]. Firstly, concentration-dependent experiments were carried out at pH 7.2 to confirm that the excimer observed was associated with an intramolecular process. The ratio of excimer/monomer emission intensity remained constant at ~12% (pH 7), over the concentration range 0.1M to 0.5μM, consistent with intramolecular excimer formation. Further experiments were then performed to determine the response of compound [32] to changes in pH. The naphthalene excimer was observed for compound [32] with a relative excimer/monomer intensity ratio of between 10% and 70%. This is a significantly higher degree of excimer formation within the EDTA species [32] than was seen for the DTPA system [31], notwithstanding the X-ray structural data discussed above.

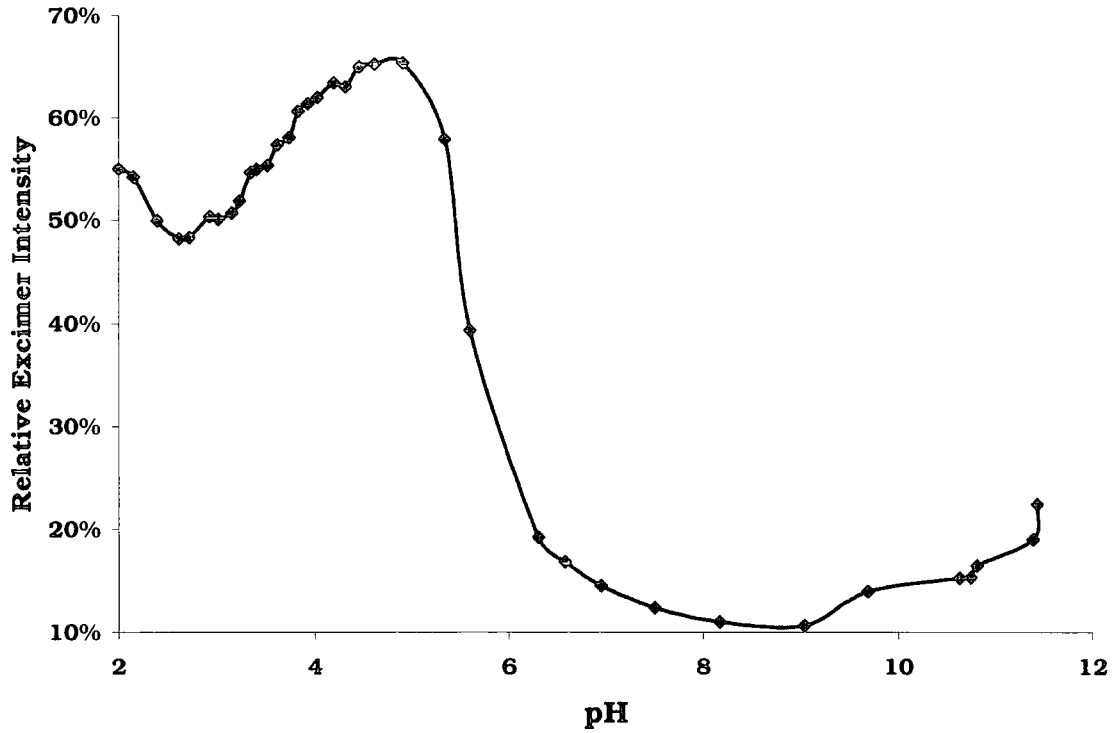

Figure 42 Plot of relative excimer intensity vs pH for the EDTA bisnaphthyl substituted amide [32]

The results of the compound [32] pH variation experiments are depicted in Figure 42. Changes in excimer intensity are observed within the desired pH range for endosomal triggering, i.e. between 4 and 7. The first change, an increase in relative excimer intensity, is seen between pH 3 and 5. A much bigger change, a decrease in the relative excimer emission, was observed between pH 5 and 7.

These changes appear to correspond to the protonation / deprotonation of the tertiary nitrogens in the EDTA structure. Similar EDTA diamide derivatives show pK_a values for these steps of between 3.5 and 4.5 for the first and between 6.6 and 7.3 for the second[85].

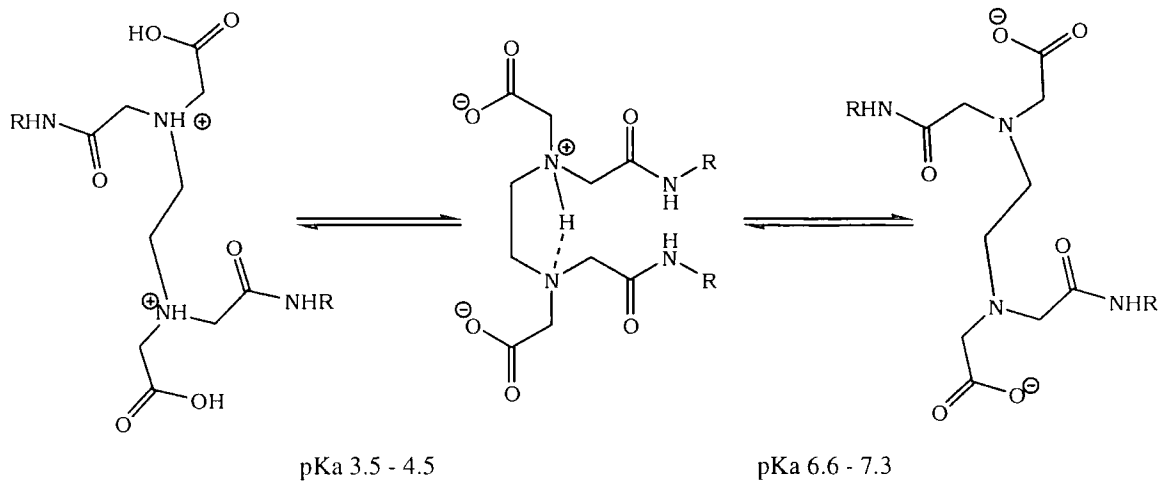

Figure 43 Diagram showing likely N-protonation scheme for EDTA diamides

This leads to the conclusion that, the singly protonated species allows conformations to be adopted with the amide groups oriented more closely and more readily than either the doubly charged or unprotonated forms (Figure 43). Experiments were carried out in the presence of $ZnCl_2$ and $CaCl_2$ at equal concentration to the EDTA dinaphthyl substituted amide species [32] in solution. These showed no excimer intensity change within the pH ranges seen for the free ligand. (Figure 44) In the experiments carried out using $ZnCl_2$, the initial change in excimer intensity was observed at much lower pH, which is consistent with the strongly bound metal only being displaced by protons at higher concentration. The intensity ratio then remained at a constant level of ~15% until precipitation of zinc hydroxide at higher pH prevented further useful measurements being taken. The experiments carried out $CaCl_2$ however, showed a similar response to the free ligand. The excimer intensity changes were shifted to lower pH, with the first occurring at pH 3-3.5 and the second around pH 4. Given that there is not likely to be much 'free' zinc (II) inside cellular systems[100], the observed behaviour with pH/Ca^{2+} variations offers some potential in the definition of the desired responsive system. In particular the significant changes around pH 4-

6, modulated by changes in Ca^{2+} concentration, fall close to the desired range.

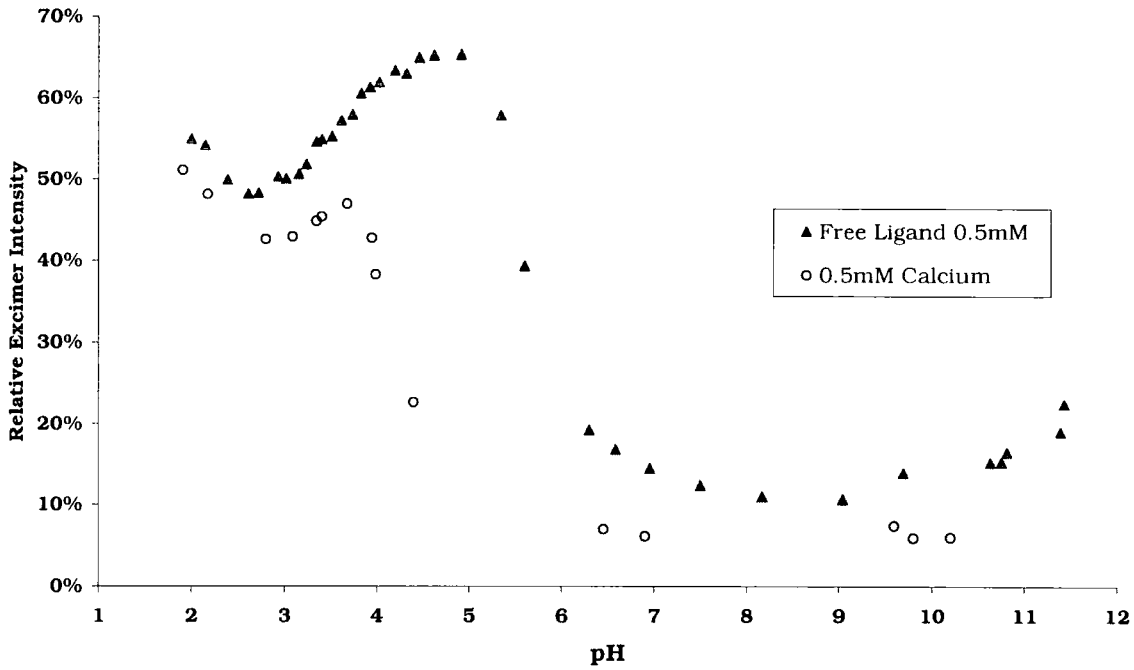

Figure 44 Plot of EDTA Dinaphthyl substituted amide [32] relative eximer intensity vs pH showing the effect of Ca^{2+} ions in solution

3.3.2 Straight Chain Amphiphilic EDTA Dialkyl Amides

The EDTA dialkylamides, [33], [34] and [35] were synthesised and characterised as described above. Compound [35], which has previously been synthesised by the same method, was studied in metal ion transport through organic solvents[101]. The critical aggregation properties of each ligand were investigated along with any pH dependent effects they might have on the stability of co-aggregate assemblies of which they were a part (sections 4.1a) and 4.2).

3.3.3 CAC Determination

Critical aggregation concentration determination for the C_8, C_{12} and C_{16} diamide compounds [33], [34] and [35] was undertaken using the conductivity method. The conductivity of each solution was measured and the molar conductivity measured as a function of the concentration of surfactant at 295K. The absolute values of the conductivity recorded are of lesser importance than the observation of the change in conductivity. This is all that is required to give a value for the CAC.

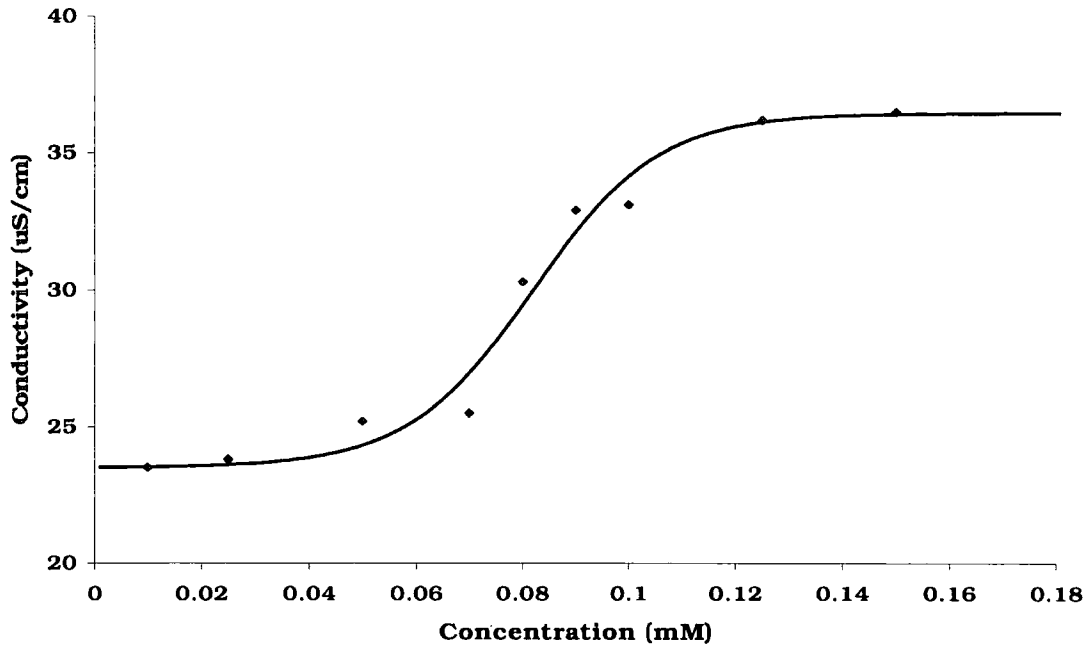

Figure 45 Variation of solution conductivity with concentration of [34] (295K), allowing determination of the critical aggregation concentration: the line shows the fit to the experimental datapoints.

Buffered solutions (pH 7.2 HEPES) of each of the three ligand species were prepared over a range of concentrations from ~1 μM to 400 μM, using the same low conductivity water used in the earlier conductivity measurements. The CAC values determined for the three

species are shown in Table 3. (Further experimental data can be found in appendix 2). These values are considerably lower than for the pyridine species indicating much lower concentration is required before the amphiphilic molecules reach a saturation point in solution and begin aggregating. (Figure 45).

The concentration/conductivity plots show further changes at higher concentration. These further critical aggregation events could be due to the changes in aggregate form (Figure 10). As the EDTA diamides are likely to adopt a twin chain amphiphile arrangement in solution, it is possible with this structural similarity to natural twin chain lipids, that these observed events are linked to the formation of bilayer structures. Again, the CAC values determined were utilised in the design of further experiments to determine co-aggregate properties and aggregate disruption effects.

EDTA Diamide	CAC Value determined at pH 7
[33] (C_8)	**0.12 (mM)**
[34](C_{12})	**0.068 (mM)**
[35](C_{16})	**0.0083 (mM)**

Table 3 CAC Values from conductivity experiments with EDTA diamides

Following the determination of the aggregation properties of [29], [30], [33], [34] and [35], each of these species was used to form co-aggregate micellar and liposomal systems in order to assess their ability to disrupt aggregate assemblies as a function of solution pH and metal ion concentration. While the EDTA based species have well known and strong metal binding properties, the presence of the amine at the pyridine 2-position in compounds [29] and [30] raises the possibility that these compound might also show some ion-

chelating behaviour which may affect their behaviour within a micelle or bilayer membrane.

Chapter 4

4 Aggregate Disruption

4.1 Micellar Models

4.3.1 CTAB Micelle Disruption

Cetyltrimethylammonium bromide (CTAB) is the archetypal cationic detergent, forming well-defined cationic micellar aggregates [102,103,104,105,106] with a CMC of 0.85-0.92mM[77]. To assess the disrupting effects of the trigger molecules on this model micellar system, the following experiments were carried out using CTAB as the major component in co-aggregates of varying composition. Co-aggregate solutions, containing 5 mole percent of the pyridine or EDTA amphiphiles, were prepared. In each case, the solutions were prepared with a concentration of CTAB of 1.2mM, significantly above its CMC. In preparation of the solutions, the concentration of the additive pyridine amphiphiles, [29] (CMC 1.45mM) and [30] (CMC 0.52mM) was maintained at 0.06mM (5 mol%), significantly below the CMC of either compound. However, to produce CTAB co-aggregate solutions, containing the EDTA based species at 5 mole percent, with CTAB above its CMC, the concentration of the longer chain EDTA diamides [34]and [35] required, was close to or above the CMC measured for these compounds (CMC [34] 0.065mM, CMC [35] 0.016mM). This situation is unavoidable, due to the relatively large difference in the CTAB CMC of 0.8mM and EDTA diamide CMC values below 0.08mM.

The solutions were made using 0.1M NaCl to maintain a constant ionic background during the pH variation. Small aliquots of 0.1M NaOH and HCl aqueous solutions were used to vary the pH. The fluorescence of pyrene was again used as a probe signal to determine the presence of the different micropolar environments expected following the onset of micellisation. As micelles are dynamic species

in constant equilibrium with the bulk surfactant in solution, it was not clear at the outset if the experiments proposed would be able to detect any change due to the effects of pH on the trigger molecules in the co-aggregate. Disruption of the aggregate by the trigger, would be relatively rapid if it occurred and the surfactant molecules released by this disruption, could readily form another micelle and reincorporate the pyrene molecules. This process could easily occur after the addition and measurement of solution pH and before the emission observation could be undertaken. The average pyrene emission being observed would therefore show little or no difference to that of the stable co-aggregate. Pyrene emission would also remain unchanged if the protonation of trigger molecules simply caused them to leave the dynamic micelle structure, as their aggregation properties changed, without causing any disruption of the micelle.

a) EDTA Diamide Experiments

The pyrene fluorescence experiments for the co-aggregates of the EDTA diamides [33] and [34], showed no significant change in the I_1/I_5 emission ratio as a function of pH. Compound [35] however, showed a clear change between pH 4.5 and pH 7.5 which can be seen in Figure 46. This change corresponds quite well to the changes seen in the pH variation of naphthyl excimer emission (section 3.3.1). However, due to the fact that this EDTA diamide species is above its self-aggregation concentration, it is possible that the effect on the pyrene emission ratio is, at least in part, caused by the pH dependent disruption of the self-aggregate of compound [35], with little effect being related to the CTAB co-micelle system. It is difficult to be certain whether this is the case, without further experimental substantiation.

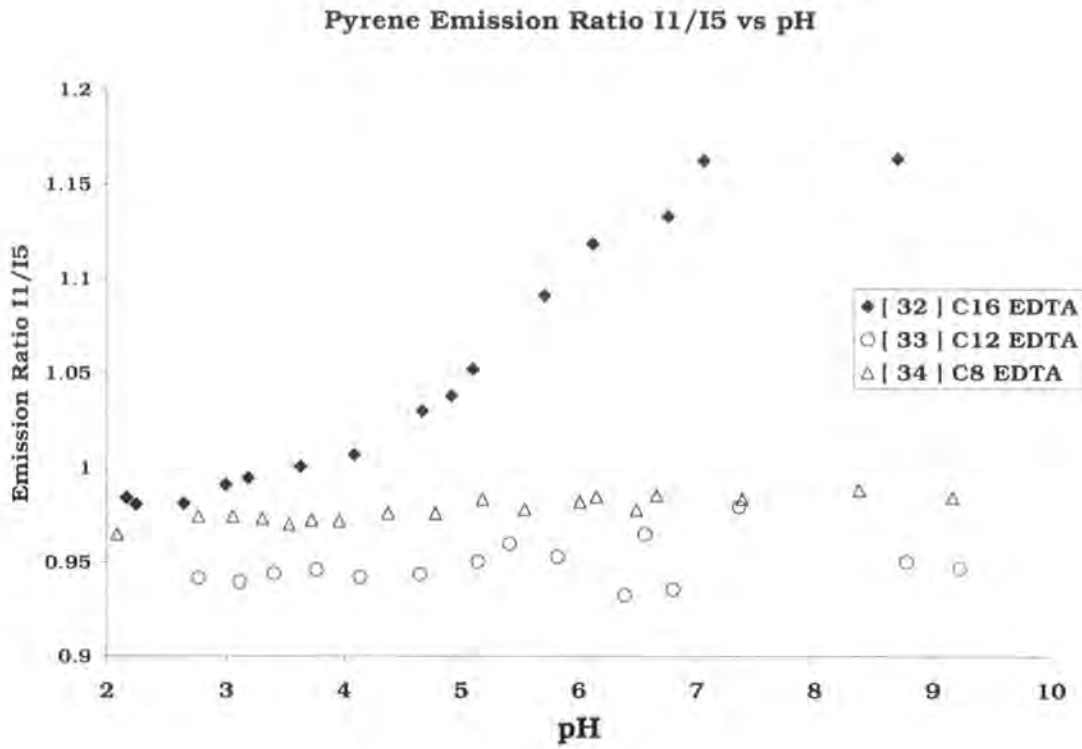

Figure 46 Variation of pyrene I_1/I_5 ratio vs pH for EDTA dialkyl amides [33], [34] and [35]

b) Pyridine Experiments

The pyridine experiments were carried out, as discussed above, and the pyrene I_1/I_5 emission for the CTAB pyridine co-aggregates remained virtually constant across the entire pH range observed. The data and results were very similar to those obtained for the shorter EDTA diamides.

4.2 Liposome Models for Aggregate Disruption Measurements

In addition to the micelle experiments, the EDTA and pyridine based surfactant products were used as additives in liposome preparations. Liposome aggregates are bilayer structures which wholly enclose a volume of solvent and are considerably more stable than micellar systems. Amphiphiles, which form liposomes, are usually insoluble in aqueous solution, or at least not truly soluble in the traditional sense. They disperse only by forming bilayer aggregates and in this way they differ from micelle-forming amphiphiles. There is no solvated amphiphile population in solution and therefore no equilibrium exchange between the aggregate and this solvated population. Liposomes are similar in their gross structural features to biological cell membranes and are frequently made using the same amphiphilic components, in order to model the cell membrane. Liposome membranes, like cell membranes, allow some small molecules and ions to diffuse across the bilayer, however larger molecules cannot cross the membrane. The lipid used for the experiments carried out, was dimyristoylphosphatidylcholine (DMPC). This is a well known lipid molecule that forms stable unilamellar vesicles and has well characterised gel and liquid crystal phases (Figure 47). Unilamellar vesicles are those which have a single bilayer membrane enclosing the contents, in much the same way as a biological cell. Multilamellar vesicles can be thought of as having an "onion skin" structure of nested bilayers. These structures can be formed by simple solutions of lipid molecules but, in many cases treatment with ultrasound or extrusion of the initial solution through a membrane of a fixed pore size, will disperse these larger multilamellar systems in favour of the desired single membrane structures[49]. Liposomes can be co-aggregate structures in the same way as micelles, they can also incorporate organic molecules

'dissolved' within the bilayer, or large molecules such as proteins which bridge the membrane.

Figure 47 SEM image, of a cryogenically frozen DMPC unilamellar liposome dispersion showing a range of vesicle sizes[107]

4.3.1 Fluorescence Probes For Liposomal Membrane Disruption

In order to detect any disruption caused by the inclusion of the trigger molecules, fluorescence assays used to detect liposome leakage, bursting or membrane pore formation were employed. The most common of these assays employs carboxyfluorescein (CF); CF is a fluorescent probe, which undergoes self-quenching above a critical concentration. By forming liposomes containing CF above this critical concentration, removing the liposomes from the CF solution in which they formed and then collecting emission spectra, it is possible to detect any leakage from the liposomes by monitoring the emission wavelength of dilute (unquenched) CF.[108] However, carboxyfluorescein fluorescence is affected significantly by pH. Indeed, it has been used

to monitor pH within cell environments[109]. The use of this analysis method, for detecting liposome leakage is therefore only useful over a very narrow pH range, around pH 7. The alternative assay chosen, involves a quencher pair 8-aminonaphthalene-1,3,6-trisulfonic acid (ANTS) and *p*-xylene-bis-pyridinium bromide (DPX). This system works in a similar way to the CF system, using liposomes containing both components. The DPX quenches the ANTS fluorescence and so, intact liposomes show no emission. On liposome disruption, both ANTS and DPX are released into the external solution environment. The relative concentrations of ANTS and DPX change and the ANTS fluorescence is no longer quenched. By observing the change in ANTS fluorescence intensity, the level of liposome disruption can be determined (Figure 48)[110,111]. This quencher pair method has been shown to be effective over the whole of the desired pH range for the experiments, from pH 7.5 to 4.5[111].

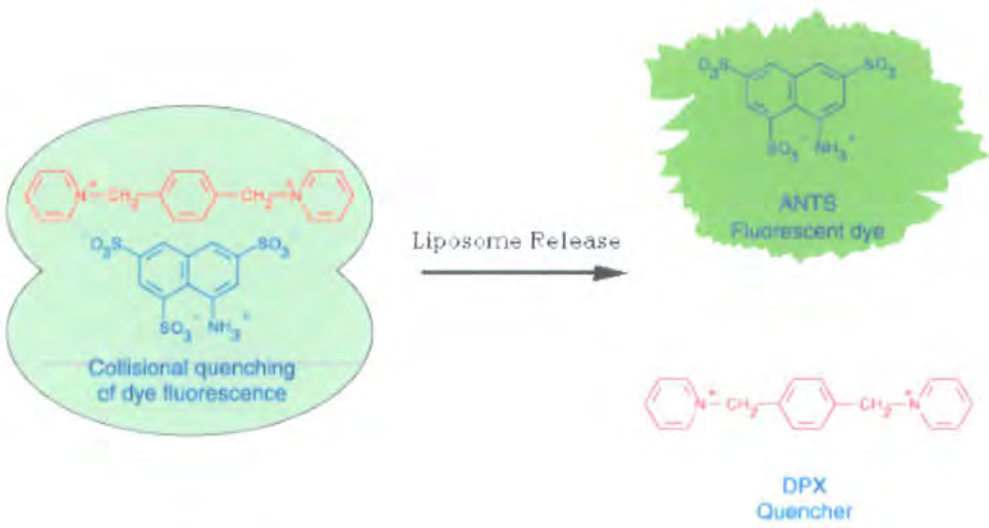

Figure 48 Diagram representing the detection of liposome disruption, using ANTS/DPX[112]

4.3.2 Liposome Preparations and Disruption Experiments

Liposomes were prepared, using known quantities of pure synthetic DMPC and the required trigger amphiphile, at 5 mole percent concentration. The mixed amphiphiles were coated onto the surface of a flask from solution in chloroform and dried under high vacuum. A solution, containing ANTS (12 mM) and DPX (45mM) HEPES buffer (5mM) and KCl (20mM), was added and the amphiphile mixture dissolved with agitation. The resulting very pale, opaque lipid solution (pH 7.5), was then subjected to a series of freeze/thaw steps before being extruded 3 times through a 100nm polycarbonate membrane. After these extrusions, the more transparent resulting solution, was passed down a Sephadex™ PD-10 column, using a solution of Hepes (5mM) and KCl (100 mM) as eluent. Small (50μl) samples of the resulting clear, slightly blue, liposome solution, were diluted into one of the pH buffered solutions listed in Table 4. All solutions were prepared, such that the osmotic potential across the liposome membrane was as low as possible, to prevent liposome bursting.

Buffer & Concentration	KCl Concentration	Solution pH
HEPES (5mM)	100mM	7.2
MES (5mM)	100mM	6.1
Acetate (5mM)	100mM	4.8

Table 4. experimental buffer solution details for ANTS/DPX liposome disruption experiments.

Experiments monitoring the intensity of ANTS fluorescence were carried out using the above solutions at 295K. The ANTS fluorescence intensity of each solution was measured (I_i), firstly, before a small amount of Triton-X100, a non-ionic surfactant, was added (0.25ml 10

wt% (aq)) and subsequently, following addition and agitation ($\mathbb{I}_{tri}$). The non-ionic surfactant has the effect of completely disrupting the cationic liposomes in solution. The ANTS fluorescence emission intensity of the measurements, taken after the addition of Triton, $\mathbb{I}_{tri}$, were considered to represent the emission from 100 percent 'dequenched' ANTS, as all the liposomes containing the quenched system are believed to be disrupted under these conditions. The values of $\mathbb{I}_i$ and $\mathbb{I}_{tri}$ were used to calculate the percentage difference $\Delta\%$ between the fluorescence, before and after addition.

$$\Delta\% = 100 - I\% \qquad I\% = {}^{I_i}\!/\!_{I_{tri}} \times 100$$

$$I_{tri} = 100\% \text{ dequenched emission}$$

Figure 49 Equations used to calculate Δ% values shown in Table 5 and Table 6

By comparing the results for the additive-containing liposomes, with values for a control of pure DMPC, a comparison of the effect of each additive on liposome stability as a function of pH,could be made. The initial experiments, with additive levels of 5 mole percent showed little variation across the three pH values (Table 5). Solutions of liposomes were then prepared, with the additive levels set at 25 mole percent.

Additive (5mol%)	pH	ANTS Emission Change (Δ%) (± 6%)
None	7.2	10 %
None	6.1	12 %
None	4.8	12 %
[35]	7.2	24 %
[35]	6.1	27 %
[35]	4.8	26 %
[30]	7.2	14 %
[30]	6.1	14 %
[30]	4.8	14 %

Table 5 Showing percentage ANTS emission intensity change, on addition of non-ionic surfactant, to solutions of different liposomes at pH 7.2, 6.2, 4.8 at 295K

With the additive levels at 25 mole percent, the effects on the membranes with pH became more apparent. The shorter chain, C_8 and C_{12}, EDTA derived surfactant molecules [33] and [34] along with, the C_6 pyridine molecule [29], still gave rise to little observable change. However, both the hexadecyl EDTA diamide [35] and the pyridine species with the decyl chain, [30], showed a significant effect on the membrane. With the additive levels at 25 percent, experimental measurements were also taken at 308K so as to reflect more closely an *in vivo* temperature.

Additive	pH	Temp. (K)	ANTS Emission Change (Δ%) (± 6%)
None	7.2	308	12 %
None	6.1	308	12 %
None	4.8	308	12 %
[35](25%)	7.2	295	44 %
[35] (25%)	6.1	295	40 %
[35](25%)	4.8	295	31 %
[30] (25%)	7.2	295	-4 %
[30] (25%)	6.1	295	-6 %
[30] (25%)	4.8	295	-3 %
[35] (25%)	7.2	308	12 %
[35] (25%)	6.1	308	12 %
[35] (25%)	4.8	308	8 %
[30] (25%)	7.2	308	21 %
[30] (25%)	6.1	308	5 %
[30] (25%)	4.8	308	6 %

Table 6. Showing percentage ANTS emission intensity change, on addition of non-ionic surfactant, to solutions of different liposomes at different temperature and percentage composition.

DMPC is known to have a gel to liquid crystal thermal transition at 297K[113], so the action of raising the temperature crosses this transition, allowing such effects attributed to the different bilayer phase to be observed (Table 6).

Changes with pH were evident for liposomes prepared with the C_{16} EDTA diamide (25% at 295K). It can be seen from the data that the EDTA based systems appear to have an initially stabilising effect on the liposomes at pH 7.2, as the percentage change observed on Triton addition, is much greater than for the pure DMPC liposomes. Long

chain DTPA diamide compounds have been used previously to align lipid membranes in NMR experiments. The EDTA diamides synthesised here could presumably have similar effects on liposomes, which could account for more stable liposomes being formed by the EDTA/DMPC mixed membranes. The pyridine species [30] however, showed no pH dependent disruption. When the percentage change values for this species are compared with those for the pure DMPC, it can be seen that the presence of the pyridine species is having a destabilising effect on the liposome membrane, at each of the pH points used in the experiments at 295K. At the higher temperature, the stabilising effect of the EDTA compound [35] is less apparent, the more dynamic lipid leading to greater overall freedom of movement. At 308K, the pyridine species [30]is seen to cause disruption, this time related to the solution pH. It is possible that the more dynamic lipid phase, is able to form more stable co-aggregates with the pyridine species at pH 7 and above, with the protonation of the additive causing the desired destabilisation of this co- aggretate at the lower pH points examined.

Chapter 5

5 Conclusions and Future Work

The experimental work, carried out and described in chapters 2, 3 and 4 has given rise to 5 amphiphile species, which respond to changes in pH, and some ([33], [34] and [35]) which respond, to a lesser degree, to changes in $[M^{2+}]$. Their efficacy as aggregate disruption species appears, from the analytical results obtained, to be rather limited. The EDTA diamide species [35] has been shown to possess pH induced disruption effects, when included at 25 mole percent in a DMPC liposome membrane model, using the ANTS/DPX membrane leakage assay. However, this level of inclusion is at the upper limit of that which is desirable. The pyridine species were eventually synthesised cleanly using a versatile and effective route. The pyridine-amine targets were specifically chosen to have pK_a values above the desired range for endosomal triggering, of between 4.5 and 7, in order that on the suppression of pK_a, previously observed with aggregation, the pyridine amine pK_a would be suppressed into the desired range. However, even after suppression within a CTAB micellar co-aggregate, the measured pK_a was still above the desired range. The pyridine species [30], on inclusion in a simple DMPC liposome model, showed some pH dependant response at levels of 25 mole percent at 35°C, above a critical phase transition for the lipid model used. However, due to the quantities of lipid available and the time constraints placed on this work, by both funding and liposome lifetimes, only a small number of experiments were carried out at this elevated temperature. The other species of shorter length appeared to have much less, or no, observable impact on aggregates in which they were included.

In order to confirm the effects observed for compounds [30] and [35], further liposome experiments are needed. In addition to the collection of more data points, other lipid molecules or mixtures of lipids, could be used in the formation of liposomes for future

experiments. The effects of the inclusion of cholesterol and other molecules into the membrane could also be investigated.

In terms of producing other, potentially more effective, pH sensitive disruption species to undergo similar testing, an alternative strategy to mid-chain sites of protonation might be a tail terminus site as this type of system has been investigated and found to be effective with photo-triggered systems. This possibility could be investigated with a modification of the route to the N-[(5-methylpyridin-2-yl)methyl]-N-alkylamine molecules synthesised in this work. The flexibility of the pyridine synthesis used to form [29] and [30], also allows the possibility of including the electron-withdrawing substituents mentioned earlier, β- to the amine group (Figure 50). This could be achieved by a using a modified amine in the coupling step.

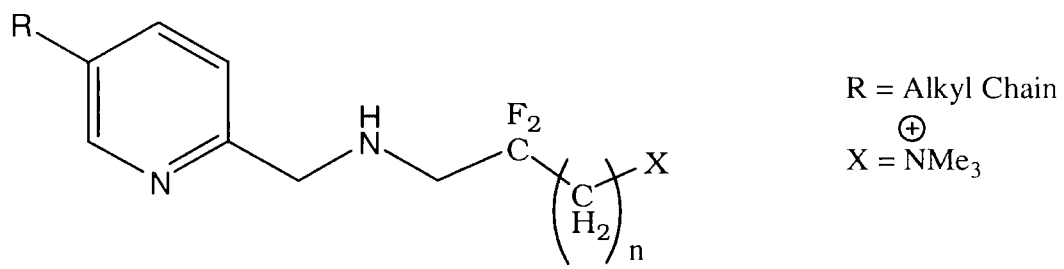

Figure 50 Structure of modified 5-alkyl pyridine-2methyl amine with electron with-drawing β-CF_3 group.

An alternative amine based functionality might be the morpholine group (pK_a ~8.5). This functionality's lower solution pK_a could lead to suppression on aggregation into the desired range. Synthesis of trans-2,5- or trans-2,6-disubstituted morpholines could produce suitable systems for analysis (Figure 51).

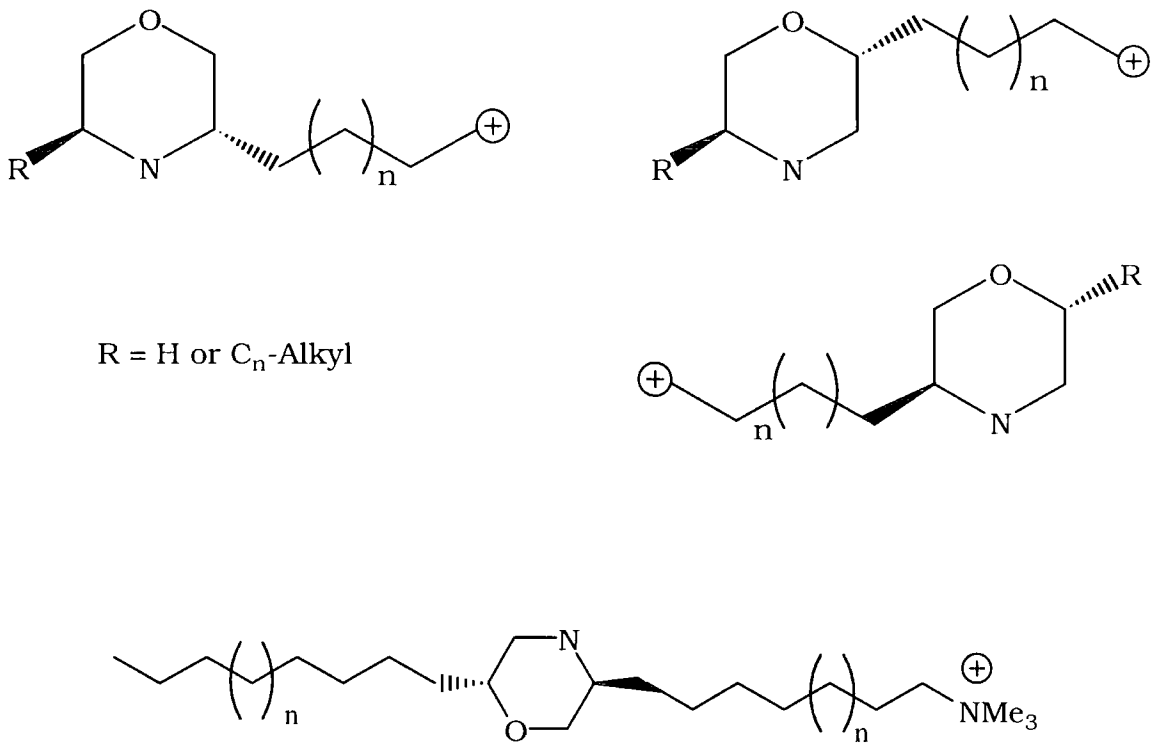

Figure 51 Possible structures of morpholine, based terminal and mid-chain protonating pH sensitive disruption surfactants

As well as modifying the protonatable functionality, further modification of the alkyl chain sections of both the pyridine and EDTA molecules with branched chains, twin chains or simply synthesis of a greater array of chain lengths, could lead to better aggregation properties and more effective disruption effects.

Chapter 6

6 Experimental Procedures

6.1 General

a) Reagents and solvents

Reagents were supplied by the Aldrich Chemical company or the Lancaster Chemical company, with some common solvents being sourced from Fisher Scientific. Solvents were purified and dried, with the appropriate drying agents using standard procedures (e.g. THF was dried over sodium with benzophenone as an indicator). N,N'-dimethyl formamide (DMF), pyridine and 1,4-dioxan were used directly as supplied from Aldrich 'Sure-Seal' bottles. Other reagents were used as supplied, unless further purification is specified in the synthetic details.

b) Chromatography

Column chromatography was carried out using "flash column" silica gel 60 (0.04-0.063mm)(Merck) and thin layer chromatography was carried out on silica gel 60, with F_{254} fluorescent indicator (Merck), on aluminium plates.

c) Spectroscopy

^{1}H NMR spectra were recorded, using a Varian Unity Inova-500 spectrometer at 499.97 MHz; a VarianVXR-400 at 399.96 MHz; a Varian Unity-300 spectrometer at 299.91 MHz and a Varian Mercury-200 spectrometer at 199.99 MHz. ^{13}C NMR spectra were recorded on the Varian Unity Inova-500 at 125.6 MHz; on the VarianVXR-400 at100.58 MHz; on the Varian Unity-300 at 75.4 MHz and on the

Varian Mercury-200 at 50.2 MHz. Mass spectra were recorded, using a VG Platform II electrospray mass spectrometer, with methanol as the carrier solvent and accurate masses were measured by the EPSRC National Mass Spectroscopy Service at the University of Swansea or by the Durham University mass spectroscopy service using a Micromass LCT electrospray mass spectrometer. Elemental analyses were determined using an Exeter Analytical Carlo ERBA 1106 instrument. Anion chromatography was carried out using a Dionex chromatograph.

d) pH and Conductivity Measuerments

Conductivity measurements were carried out using clean platinum electodes mounted 1cm apart and connected to a Jasco 4090 conductivity meter. pH measurements were made using a Coring semi-micro glass electrode, operated through a Jenway 3320 pH meter, which was calibrated using standard buffer solutions of pH 4, 7 and 10 at 25°C.

e) Absorbance and luminescence

UV absorption and transmission spectra were recorded using a UNICAM (UV2) spectrometer. Fluorescence measurements were obtained using a Fluorolog 3-11 fluorimeter. Fluorescence emission spectra were acquired following excitation at the given wavelength and were corrected for the wavelength dependence of the photomultiplier tube. Experiments were carried out using 3ml aliquots in standard quartz cuvettes with 1cm path length. In certain cases 700µl aliquots and low volume quartz cuvettes with 1cm path length were used.

f) Determination of pK_a values

Solutions contained 0.1M NaCl to maintain an approximately constant ionic strength during the titrations. Titrations were run from alkaline to acid pH, and in each case, were shown to be reversible with respect to the UV wavelength shift. In a typical pH titration study, a known mass of 2,5-pyridine compound was dissolved in 0.1M aqueous NaCl (10 ml) to make a solution of approximately 0.04mM pyridine concentration. This solution was adjusted to pH 11.0, using 1M NaOH stock solution. A constant volume (5 µl) from 1M, 0.5M or 0.1M HCl stock was added sequentially and the pH measured before and after the absorbance was recorded. A plot was made of the pyridine absorbance maximum as a function of pH. These curves were fitted using a simple iterative method under the CurveExpert 1.3 software and the pK values derived from the fitted curve.

6.3.1 Determination of CMC

Solutions for the determination of CMC were prepared, by dilution of a stock solution, to produce a range of solutions of the surfactant to be assessed at increasingly dilute concentrations. The stock solution was prepared, using a known mass of the required surfactant, and the concentration of that stock was chosen so as to be above the range expected for the CMC of the surfactant in question. The sections below describe the treatment and measurement of these solutions, in the determination of CMC, using conductivity measurements and the fluorescent pyrene micropolarity probe.

a) Conductivity Method

Solutions were prepared by the method above (using ELGA Ultra High Quality water) and the conductivity of a 10 ml aliquot of each solution was then measured using the apparatus described earlier. Between each measurement, the platinum electrodes were rinsed with high purity water (4 x 25 ml) and a clean sample container used for each solution to prevent contamination and an increase in background conductivity.

b) Pyrene Micropolarity Probe Method

The preparation of the solutions was carried out as mentioned above using Purite water. A set of dilutions were also prepared, using 0.1M NaCl in order to maintain an approximately constant ionic strength and to allow a comparison between the CMC values determined in each case. 50µl of 0.125mM pyrene solution in methanol was added to 2.95ml aliquots of each solution before fluorescence emission spectra were recorded for each solution (excitation 365nm). The first and fifth emission maxima were then used, as described, and plotted as a function of surfactant concentration.

c) Micelle Disruption Experiments Using Pyrene Probe

In a typical experiment, stock solutions of pyridine compound [29] or [30] (0.5mM in 0.1M NaCl(aq)), CTAB (1.45mM in 0.1M NaCl(aq)) and 0.1M NaCl were used to make a solution (4.9ml) of approximately 0.013mM pyridine concentration, 1.2mM CTAB concentration with an approximately constant NaCl background of 0.1M. Pyrene solution in methanol (100µl of 0.125mM) was then added, before the solution pH was adjusted to pH 10.0 using 1M

NaOH stock solution. A constant volume (5 µl) from 1M, 0.5M or 0.1M HCl stock was added sequentially and the pH measured before and after the pyrene emission spectrum (excitation 365nm) was recorded. The first and fifth emission maxima were then used to produce an intensity ratio and this was plotted as a function of pH for each species.

6.3.2 Liposome Preparation

DMPC liposomes were prepared, as described in the main text, by deposition 0.0125 mMol quantities (100µl 0.125M $CHCl_3$ solution) of the lipid molecules onto the surface of a glassware flask from chloroform solution. The mixed liposome systems were prepared by depositing DMPC (0.0125 mMol) and the appropriate additive in the desired molar ratio, onto the surface of the flask from chloroform solution. The deposited thin film of lipid molecules was then desolved from the glass surface with the buffered (pH 7.2) ANTS/DPX quencher pair solution (1 ml). This solution was made by dissolving ANTS (133.5mg), DPX (474.9 mg), HEPES (29.8mg) and KCl (37.3mg) in 25ml of water, adjusting the pH to 7.2 using a small quantity of the appropriate stock acid or base (0.1M NaOH or HCl). The crude liposome solution was subjected to a series of five freeze-thaw cycles, before being extruded through a polycarbonate membrane with a pore size of 100nm. The resulting solution was then passed through a Sephadex PD-10 pre-packed column and eluted with a pH 7.2 buffer solution, containing 5mM HEPES and 100mM KCl. The liposome solution (~2.5ml) collected from the column was then used in the ANTS/DPX liposome leakage assay measurements.

6.3.3 ANTS/DPX Liposome Fluorescence Assay

In a typical experiment, quencher pair filled liposome solution [20μl pH7.2 (see section 6.3.2 above)] was added to a buffer solution (2.48ml), (pH 7.2 HEPES 5mM KCl 100mM, pH 6.1 MES 5mM KCl 100mM, or pH 4.8 acetate 5mM KCl 100mM) in a standard 3ml quartz fluorescence cuvette. The fluorescence emission spectrum of this solution was then recorded (excitation 353 nm). Following the collection of the emission spectrum, 0.5 ml of Triton X-100 (0.1M) solution was added and the cuvette agitated. The emission spectrum was then recorded again and the maximum fluorescence intensity, at 515nm, for the two spectra compared. The experiments were repeated and mean values for the percentage difference are shown in the Tables.

6.2 Synthetic Procedures

6.3.1 Pyridine Syntheses, Precursors and Modifications

5-Methylpyridine-2-carboxylic acid[114].

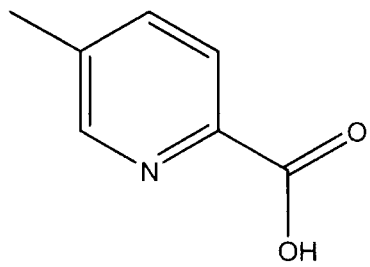

[2]

2,5-Lutidine (5g, 46.65 mmol), was combined with selenium dioxide (9.3g 83.8mmol), in pyridine (20ml). The reaction mixture was heated to reflux for 4h. During this time, the solution turned from colourless, through red to black. The black solution/suspension was

filtered through celite® filter agent and the residue was thoroughly washed, with pyridine (50ml) and water (75ml). The filtrate was charged to a 250ml two-neck round bottom flask fitted for steam distillation. Around 1l of water was used in the steam distillation, and after removal of the steam line, the mixture was distilled to dryness under reduced pressure. The dry residue, was treated with ethyl acetate (75ml) and refluxed with activated carbon (2g) before being filtered hot, through a small celite® plug. This plug was washed, with more hot ethyl acetate (50ml), the solvent was then removed under reduced pressure, and the solid residue recrystallised from water yielding an orange crystalline solid. (3.2g, 50%)

m.p. 168-170°C. (Lit. 168-169°C[114])

δ_H ppm ($CDCl_3$): 2.48 (3H, s, CH_3), 7.78 (1H, d, J = 8 Hz, H 4), 8.16 (1H, d, H 3), 8.48 (1H, s, H 6).

δ_C ppm (CD_3OD): 17.38 (CH_3), 124.99 (C 4), 138.8 (C 5), 139.95 (C 3), 145.19 (C 2), 147.87 (C 6) 165.76 (CO_2H).

MS (ES^+) m/z 138 (*MH^+*), 160 *(MNa+)*.

Anal. $C_7H_7NO_2.{}^1/_8H_2O$ calculated C, 60.32%, H, 5.24%, N, 10.05%, Found C, 60.56%, H, 5.34%, N, 10.08%.

General procedure for formation of 5-bromomethyl pyridines *via* N-bromosuccinimide (NBS) bromination[115-118].

The 5-methylpyridine (11.6mmol), was added along with NBS (11.6 mmol for predominantly monobromomethyl pyridine], or 34.8 mmol for predominantly dibromomethyl pyridine), in carbon tetrachloride (20 ml). The contents of the flask were heated to reflux, before 2,2'-azobis (2-methylpropionitrile) (AIBN) (~5mg) was added to initiate the reaction. Reaction progress, was monitored by ^1H NMR, from which levels of both bromination products, and the relative amount of remaining starting material was determined. This was determined by integration of the CH_3, CH_2Br and $CHBr_2$ proton NMR

resonances at 2.4 ppm, 4.4 ppm and 6.6ppm respectively. After stirring under reflux, for 14-18h, the reaction mixture was filtered, and washed with carbon tetrachloride before being cooled. The cooled solution was washed with aqueous sodium hydrogencarbonate solution (2x25ml), in order to remove any remaining succinimide. The organic layer was dried, using magnesium sulphate and the solvent removed under reduced pressure, to leave the crude product. This crude mixture was purified using flash column chromatography on silica. The solvent system used was 10% methanol in DCM.

2-Bromo 5-bromomethyl pyridine [119].

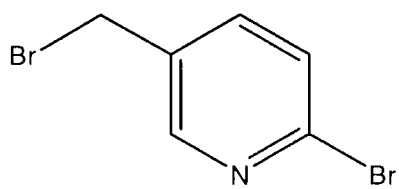

Lit. m.p. 62°-63°C[119]

m.p. 61°-63°C

Rf. 0.53 (5% MeOH in DCM)

δ_H ppm ($CDCl_3$):4.36, (2H, s, CH_2Br), 7.4 (1H, d, J = 8 Hz, H 3), 7.55 (1H, dd, J = 8 Hz, J = 3 Hz, H 4), 8.3 (1H, d, J = 3 Hz, H 6).

MS (ES+): m/z 249.9 (*MH+*), 272 *(MNa+)*

2-Bromo 5-dibromomethyl pyridine[120].

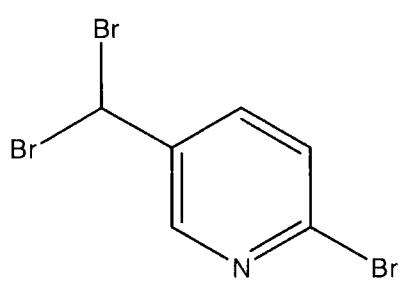

Lit. m.p. 91°C

m.p. 89°-92°C[120]

Rf. 0.61 (5% MeOH in DCM)

δ_H ppm ($CDCl_3$): 6.55 (1H, s, $CHBr_2$). 7.49 (1H, d, J = 8 Hz. H 3), 7.83 (1H, d, H 4), 8.39 (1H, s, H 6).

MS (ES+): m/z 328 (*MH*+).

5-Methylpyridine-2-carbonitrile[121,122].

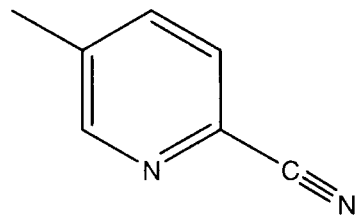

[1]

2-Bromo-5-methylpyridine (2g, 11.6 mmol), copper (I) cyanide (4.157g, 46.4mmol) and tetraethylammonium cyanide (1.81g 11.6mmol), were charged to a round bottom flask with dry 1,4 dioxane (30ml) and degassed by a freeze/pump/thaw method, before tris(dibenzylideneacetone)-dipalladium [$Pd_2(dba)_3$] (0.26g, 0.465 mmol) and diphenyl-phosphinoferrocene (DPPF) (1.025g, 1.85mmol), were added. The reaction mixture was heated to reflux under an inert atmosphere for 12h. After this time, the mixture was diluted with ethyl acetate (50ml), and filtered through celite®. The filtered solution was washed with saturated, aqueous sodium bicarbonate solution (50ml), separated and dried over magnesium sulphate. The solvent was removed under reduced pressure. The resulting crude product, (deep brown oil and crystals) was recrystallised from petroleum ether to leave a yellow crystalline solid.

Lit. m.p. 76°-77°C(petroleum ether) [123]; 73°-75°C (hexane) [124].

m.p. 74.2°-76.4°C

δ_H ppm ($CDCl_3$): 2.45 (3H, s, CH_3), 7.62 (2H, s, H 3&4), 8.56 (1H, s, H 6).

General procedure for the synthesis of 2-alkylacrylaldehydes (acroleins)[125,126].

The required, n-alkyl aldehyde (0.02mol), N,N-dimethylmethyleneammonium Chloride (0.02mol) and water were combined in a 100ml round bottom flask. The mixture was stirred and heated to 75°C for 24h. After this time, the two phases were separated, and the aqueous layer extracted with hexane (3x50ml). The organic phases were combined, and the solvent evaporated. The remaining light yellow organic oil was fractionally distilled under reduced pressure, yielding the product as a clear colourless oil. Previously synthesised and reported compounds were characterised by comparison of b.p.[126] All products were additionally characterised by ^1H and ^{13}C NMR and ESMS

2-Hexylacrylaldehyde[125].

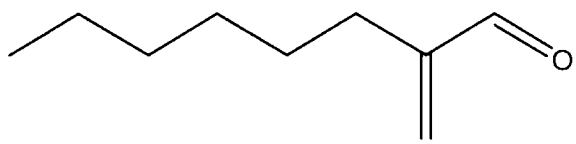

[10]

Lit. b.p.: 76°C/20mm Hg. [125]

b.p.: 38°C/ 2mm Hg

δ_H ppm ($CDCl_3$): 0.81 (3H, t, J = 6.6Hz, CH_3), 1.20 (8H, m, $-(CH_2)_4-CH_3$), 2.16 (2H, t, J = 7.6Hz, $-CH_2-C(COH)=CH_2$), 5.91 (1H, s, $C=CH_2$ trans), 6.17 (1H, s, $C=CH_2$ cis), 9.46 (1H, s, CHO).

δ_C ppm ($CDCl_3$): 14.21 (CH_3), 22.75 (CH_2), 27.89 (CH_2), 27.95 (CH_2), 29.15 (CH_2), 31.78 (CH_2), 134.02 (C=CH_2), 150.68 (C=CH_2), 194.94 (CHO).

MS (ES^+) m/z 140.2 (*MH+*), 163.5 *(MNa+)*

2-Decylacrylaldehyde[126].

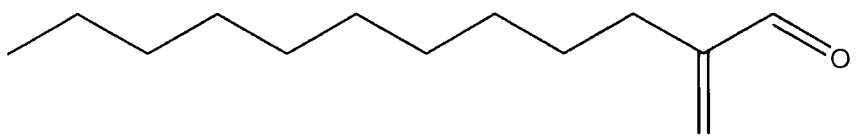

[11]

Lit. b.p.: 70°-75°C/1mm Hg. [126]

b.p.: 89°C/2.5mm Hg

δ_H ppm ($CDCl_3$): 0.80 (3H, t, J = 6.7Hz, CH_3), 1.18 (14H, m, –(CH_2)$_7$-CH_2-CH_3), 1.37 (2H, m, CH_2-CH_3), 2.16 (2H, t, J = 7.5Hz, CH_2-C(COH)=CH_2), 5.91 (1H, s, C=CH_2 trans), 6.17 (1H, s, C=CH_2 cis), 9.46 (1H, s, CHO)

δ_C ppm ($CDCl_3$): 14.34 (CH_3), 22.91 (CH_2), 24.93 (CH_2), 27.99 (CH_2), 29.30 (CH_2), 29.55 (CH_2), 29.63 (CH_2), 29.8 (CH_2), 29.82(CH_2), 32.13 (CH_2), 134.15 (C=CH_2), 150.68 (C=CH_2), 195.06 (CHO).

MS (ES^+) m/z 196.4 (*MH+*)

General procedure for the formation of (1E)-2-alkylacrylaldehyde dimethylhydrazones[127].

The required, 2-alkyl propenal (0.025 mol), N,N-dimethyl hydrazine (0.05mol) and a catalytic amount of glacial acetic acid (~100-250 µl) were combined under an inert atmosphere, in diethyl ether (30ml) and the mixture was boiled under reflux, for 45min. The solution was cooled, and washed in turn, with water (50ml) and saturated sodium chloride solution (50ml). The ethereal solution was

dried over anhydrous $MgSO_4$ and the solvent removed under reduced pressure. The resultant product was typically a yellow oil, which was used directly without further purification.

(1E)-2-Hexylacrylaldehyde dimethylhydrazone.

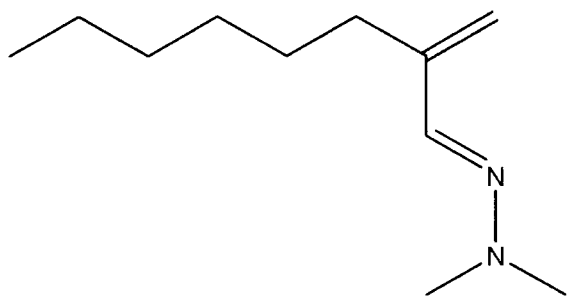

[12]

δ_H ppm ($CDCl_3$): 0.81 (3H, m, CH_2-*CH_3*), 1.22 (6H, m, -$(CH_2)_3$-), 1.42 (2H, m, *CH_2*-CH_3), 2.24 (2H, t, -*CH_2*-C=CH_2), 2.77 (6H, s, N-$(CH_3)_2$), 4.97 (1H, d, J = 1.5Hz, C=CH_2), 5.02 (1H, d, J = 1.5Hz, C=CH_2), 6.93 (1H, s, CH=N).

δ_C ppm ($CDCl_3$): 14.3 (CH_3), 22.85 (CH_2), 28.49 (CH_2), 29.45 (CH_2), 31.24 (CH_2), 31.97 (CH_2), 42.95 (N-$(CH_3)_2$), 114.56 (=CH_2),136.78(C=), 147.20(C=N),

MS (ES^+) m/z 182.1 (*MH+*), 205.9 *(MNa+)*

(1E)-2-Decylacrylaldehyde dimethylhydrazone.

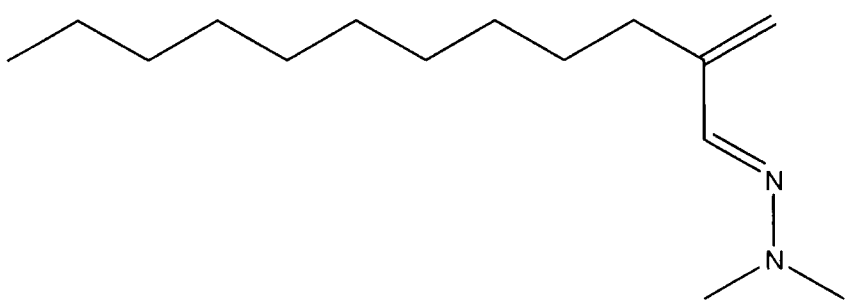

[13]

δ_H ppm ($CDCl_3$): 0.81 (3H, t, J = 6.6Hz, CH_2-*CH_3*), 1.21 (14H, m, -$(CH_2)_7$-), 1.42 (2H, m, -*CH_2*-CH_3), 2.24 (2H, t, J = 7.2Hz, -*CH_2*-C=CH_2), 2.76 (6H, s, N-$(CH_3)_2$), 4.97 (1H, d, J = 1.5Hz, C=CH_2), 5.02 (1H, d, J = 1.5Hz, C=CH_2), 6.93 (1H, s, CH=N).

δ_C ppm ($CDCl_3$): 13.1 (CH_3), 21.68 (CH_2), 27.28 (CH_2), 28.29 (CH_2), 28.36 (CH_2), 28.46 (CH_2), 28.60 (CH_2), 28.64 (CH_2), 29.99 (CH_2), 30.92 (CH_2), 41.78 (N-$(CH_3)_2$), 113.46 (=CH_2), 135.82(C=), 145.93(C=N).

MS (ES^+) m/z 238.7 (*MH+*), 262.1 *(MNa+)*

General procedure for the formation of 2-cyano,5-alkylpyridines[71,127]

(1E)-2-Alkylacrylaldehyde dimethylhydrazone (0.06 mol) was combined with trimethylamine (17.5g, 0.12 mol), and acetonitrile (50ml) under an inert atmosphere. Chloroacrylonitrile (0.07 mol), was added to the solution and this mixture was heated to 75°C with stirring for 8-12 h. At the end of this period, a colour change from the initial light yellow to dark brown was observed, along with a small amount of a pale precipitate. The solution was filtered to remove the precipitate, and concentrated by evaporation. The viscous residue was dissolved in dry 1,4-dioxane (100ml) and a stream of dry HCl gas was bubbled through this solution until the dioxane was acidic. The acidified solution, was stirred for 30min, the dioxane evaporated, and the residue dissolved in chloroform (50ml). This chloroform solution, was washed in turn, with saturated aqueous $NaHCO_3$ solution, (2x50ml). Distilled water (2x50ml) and saturated aqueous NaCl solution (50ml). The organic phase, was separated and dried over $MgSO_4$, before the solvent was removed under reduced pressure. The product in each case was a pale brown waxy solid.

5-Hexylpyridine-2-carbonitrile.

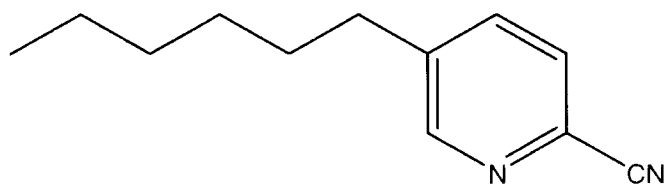

[14]

δ_H ppm ($CDCl_3$): 0.79 (3H, m, CH_3), 1.22 (6H, m, $-(CH_2)_3-$), 1.56 (2H, m, CH_2-CH_3), 2.58 (2H, t, J = 8.5 Hz, $-CH_2$-py), 7.56 (2H, m, H3, H 4), 8.45 (1H, s, H 6).

δ_C ppm (CD_3OD): 14.21 (CH_3), 22.89 (CH_2), 30.81 (CH_2), 31.64 (CH_2), 31.67 (CH_2), 33.27 (CH_2), 117.66 (CN), 128.34 (C 4), 131.21 (C 5), 136.82 (C 3), 142.73 (C 2), 151.54 (C 6).

MS (ES^+) m/z 188.4 (*MH*$^+$), 211.2 *(MNa+)*

5-Decylpyridine-2-carbonitrile.

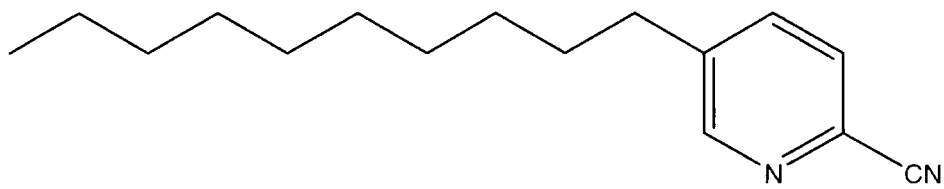

[15]

δ_H ppm ($CDCl_3$): 0.78 (3H, m, CH_3), 1.18 (14H, m, $-(CH_2)_7-$), 1.57 (2H, m, CH_2-CH_3), 2.68 (2H, t, J = 7.5 Hz, $-CH_2$-py), 8.30 (2H, m, H3, H 4), 8.87 (1H, s, H 6).

δ_C ppm (CD_3OD): 14.30 (CH_3), 22.85 (CH_2), 29.33 (CH_2), 29.43 (CH_2), 39.52 (CH_2), 29.70 (CH_2), 29.76 (CH_2), 30.52 (CH_2), 32.07 (CH_2), 33.24 (CH_2), 119.86 (CN), 128.66 (C 4), 136.89 (C 5), 142.73 (C 3), 147.78 (C 2), 159.51 (C 6).

MS (ES^+) m/z 244.2 (*MH*+), 267.5 *(MNa+)*

5-Hexylpyridine-2-carboxamide.

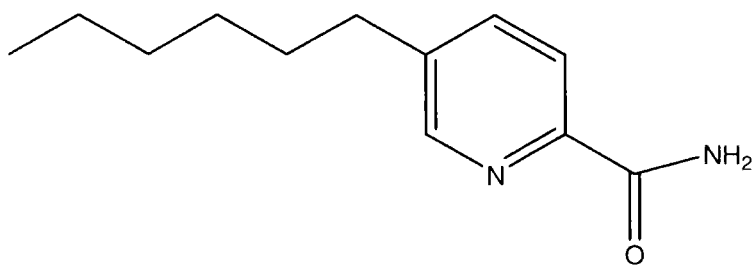

[22]

A solution of 5-hexylpyridine-2-carbonitrile (3g ~16 mMol) in ethanolic potassium hydroxide, (~15wt%) was boiled under reflux for 8-10 h. The solution was then concentrated, acidified with hydrochloric acid solution (1M) and extracted with diethyl ether (3x50ml). The ethereal solution, was dried over $MgSO_4$ and the solvent removed under reduced pressure to give an orange crystalline soild. The crystals were of such size and quality as to allow single crystal, X-ray structural analysis to be carried out. (see Appendix 1 for X-ray diffraction data).

m.p. 134°-136°C

δ_H ppm ($CDCl_3$): 0.79 (3H, m, CH_3), 1.22 (6H, m, $-(CH_2)_3-$), 1.56 (2H, m, CH_2-CH_3), 2.58 (2H, t, J = 8.5 Hz, $-CH_2$-py), 7.69 (1H, s, H3), 7.72 (1H, s, H 4), 8.25 (2H, s br, NH_2), 8.45 (1H, s, H 6).

δ_C ppm (CD_3OD): 14.21 (CH_3), 22.89 (CH_2), 30.81 (CH_2), 31.64 (CH_2), 31.67 (CH_2), 33.27 (CH_2), 124.97 (C 4), 136.82 (C 3), 143.58 (C 2), 145.37 (C 5), 148.95 (C 6), 166.02 ($CONH_2$).

MS (ES^+) m/z 206.3 (*MH+*)

5-Hexylpyridine-2-carboxylic acid[71,127].

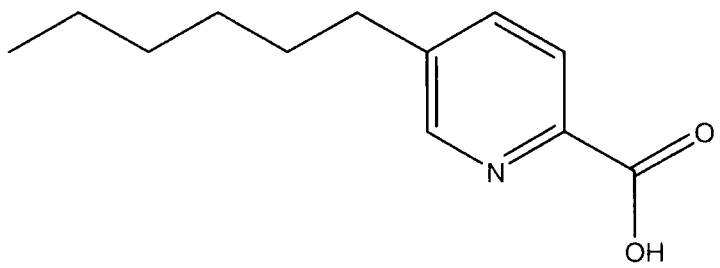

[16]

A solution of 5-hexylpyridine-2-carbonitrile in ethanolic potassium hydroxide, (~20wt%) was boiled under reflux for 24 h. The solution was then concentrated, acidified with hydrochloric acid solution (1M) and extracted with diethyl ether (3x50ml). The ethereal solution was dried over $MgSO_4$ and the solvent removed under reduced pressure to give a waxy solid.

m.p. 128°-131°C

δ_H ppm ($CDCl_3$): 0.79 (3H, m, CH_3), 1.22 (6H, m, $-(CH_2)_3-$), 1.56 (2H, m, CH_2-CH_3), 2.58 (2H, t, J = 8.5 Hz, $-CH_2$-py), 7.56 (2H, m, H3, H 4), 8.45 (1H, s, H 6).

δ_C ppm (CD_3OD): 14.21 (CH_3), 22.89 (CH_2), 30.81 (CH_2), 31.64 (CH_2), 31.67 (CH_2), 33.27 (CH_2), 128.34 (C 4), 131.21 (C 5), 136.82 (C 3), 142.73 (C 2), 151.54 (C 6) 176.26 (COOH).

5-Decylpyridine-2-carboxylic acid.

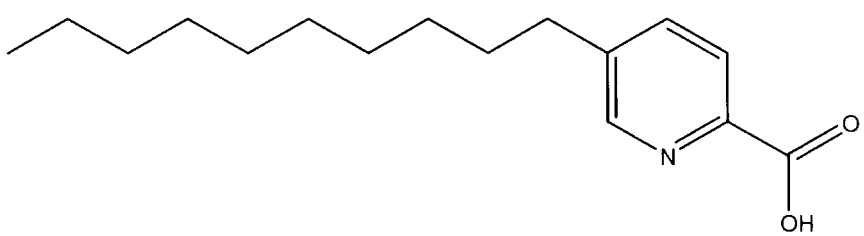

[17]

This product was formed by the hydrolysis of 5-decylpyridine-2-carbonitrile, using the same reaction conditions as above.

δ_H ppm ($CDCl_3$): 0.78 (3H, m, CH_3), 1.18 (14H, m, $-(CH_2)_7-$), 1.57 (2H, m, CH_2-CH_3), 2.68 (2H, t, J = 7.5 Hz, $-CH_2$-py), 8.30 (2H, m, H3, H 4), 8.87 (1H, s, H 6).

δ_C ppm (CD_3OD): 14.30 (CH_3), 22.85 (CH_2), 29.33 (CH_2), 29.43 (CH_2), 39.52 (CH_2), 29.70 (CH_2), 29.76 (CH_2), 30.52 (CH_2), 32.07 (CH_2), 33.24 (CH_2), 128.66 (C 4), 136.89 (C 5), 142.73 (C 3), 147.78 (C 2), 159.51 (C 6), 173.48 (COOH)

Typical procedure to 5-alkyl-N-alkylpyridine-2-carboxamides

5-Alkylpyridine 2-carboxylic acid (10mmol), was combined with 1-(3-dimethylaminopropyl)-3-ethylcarbodiimide (EDCI) (10mmol) and hydroxybenzotriazole, (~ 0.06mmol), in dry dichloromethane (20 ml), under an inert atmosphere. The appropriate amine, (11mmol, 1.1 equivalents), was added to this mixture. The mixture was then stirred for 12h., when the solution was washed successively with, water (50ml) aqueous hydrochloric acid solution (0.1M, 50ml), and finally aqueous sodium bicarbonate solution (0.1M, 50ml). After this, the organic layer was dried over calcium chloride, and the solvent removed under reduced pressure. The residue in each case, was a light orange oil or waxy solid.

5-Methyl-N-octylpyridine-2-carboxamide.

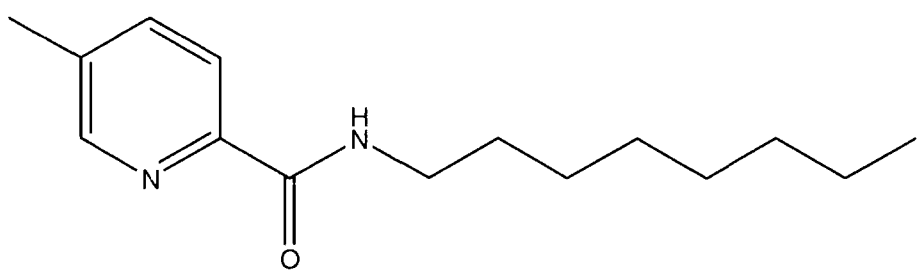

[3]

δ_H ppm ($CDCl_3$): 0.81 (3H, t, J = 7 Hz, CH_2CH_3), 1.20 (10H, m, $[CH_2]_5$), 1.56 (2H, m, CH_2CH_3), 2.33 (3H, s, 5-CH_3), 3.39 (2H, q, J = 6 Hz, $NHCH_2$), 7.55 (1H, d, J = 8 Hz, H 4), 8.02 (1H, d, H3), 8.29 (1H, s, H 6).

δ_C ppm ($CDCl_3$): 17.93(CH_3), 22.34 (CH_3), 26.49 (CH_2), 30.87 (CH_2), 33.05 (CH_2), 33.14 (CH_2), 33.53(CH_2), 35.64(CH_2), 43.26 (CH_2NH), 125.60 (C 3), 139.95 (C 5), 141.47 (C 4), 151.49 (C 2), 152.29 (C 6), 168.24 (CO),

MS (ES^+) m/z 249 (*MH+*), 271 *(MNa+)* 519 ((2M)Na^+).

Acc.MS (ES^+) Found: m/z 249.1974 (*MH+*). $C_{15}H_{25}N_2O$ requires: 249.1967 (*MH+*)

5-Methyl-N-hexylpyridine-2-carboxamide.

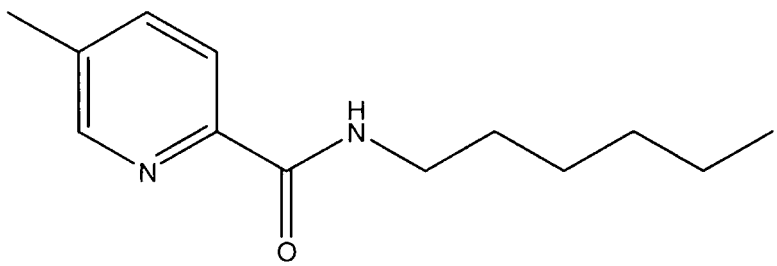

[4]

δ_H ppm ($CDCl_3$): 0.55 (3H, t, J = 6.5 Hz, CH_2CH_3), 0.95 (6H, m, $[CH_2]_3$), 1.29 (2H, m, $CH_2CH_2CH_3$), 2.03 (3H, s, 5-CH_3), 3.15 (2H, q, J = 6.5 Hz, CH_2NH), 7.28 (1H, d, J = 8 Hz, H4), 7.78 (1H, d, H3), 7.87 (1H, t, broad NH), 8.01 (1H, s, H6).

δ_C ppm ($CDCl_3$): 13.96 (CH_3), 18.32 (CH_3), 22.52 (CH_2), 26.66 (CH_2), 29.69 (CH_2), 31.49 (CH_2), 39.32 (CH_2NH), 121.59 (C 3), 135.94 (C 5), 137.42 (C 4), 147.74 (C 2), 148.38 (C 6), 164.26 (CO),

MS (ES^+) m/z 221(*MH+*), 243 *(MNa+)*.

Acc.MS (ES+) Found: m/z 221.1653 (*MH*+) $C_{13}H_{21}N_2O$ requires: 221.1654 (*MH*+).

5-Hexyl-N-(6-hydroxyhexyl)pyridine-2-carboxamide.

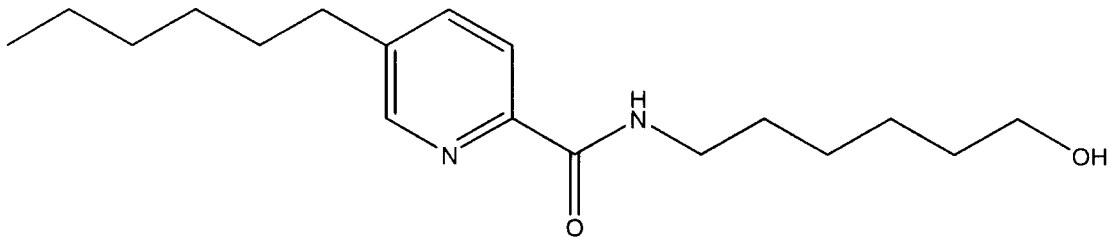

[18]

δ_H ppm ($CDCl_3$): 0.81 (3H, m, CH_2CH_3), 1.24 (14H, m, $[CH_2]_7$), 1.55 (2H, m, $CH_2CH_2CH_3$), 2.59 (2H, t, J = 8 Hz, CH_2-py), 3.38 (2H, q, J = 5 Hz, CH_2NH), 3.56 (2H, t, J = 4 Hz, CH_2-OH), 7.58 (1H, dd, J = 8 Hz, J = 2 Hz, H 4), 8.02 (1H, d, J = 8 Hz, H 3), 7.95 (1H, br t, NH), 8.27 (1H, d, J = 2 Hz, H 6).

MS (ES+) m/z 307(*MH*+),

5-Decyl-N-(6-hydroxyhexyl)pyridine-2-carboxamide.

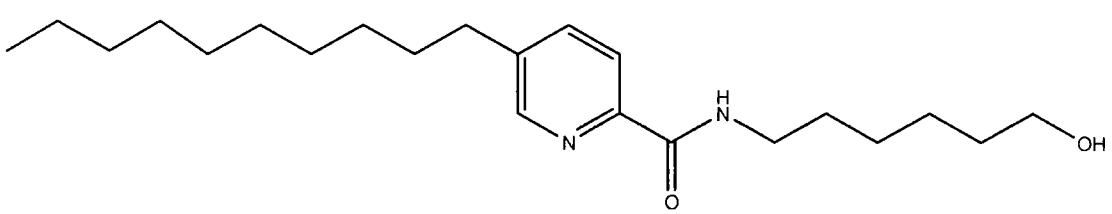

[19]

δ_H ppm ($CDCl_3$): 0.80 (3H, m, CH_2CH_3), 1.18 (22H, m, $[CH_2]_{11}$), 1.45 (2H, m, $CH_2CH_2CH_3$), 2.53(2H, t, J = 8 Hz, CH_2-py), 3.38 (2H m, CH_2NH), 3.56 (2H, m, CH_2-OH), 7.15 (1H, br d, J H4), 7.39 (1H, br d, H3), 8.27 (1H, s, H6).

MS (ES+) m/z 363(*MH*+), 385 *(MNa+)*.

Typical Procedure for Borane Reduction of amides

Between 0.2mmol and 1mmol, of the amide to be reduced was charged to a clean, dry, round bottom flask under an argon atmosphere. To the amide, was added borane THF complex (20-50ml of a 1M solution in THF). The solution was heated to a gentle reflux, with stirring for 36-48h. After this time, the reaction was quenched with methanol (50-100ml) and the solvent removed. The residue was treated with methanol (4x10ml), being dried under vacuum between each treatment. At this point, preliminary analysis using TLC, ^{1}H and ^{13}C NMR was undertaken. It was found that in almost all circumstances, a further treatment of this crude product with borane THF, was required for complete amide reduction. Therefore, further borane THF complex was added (1M, 50ml), and the solution heated to reflux under an argon atmosphere, for a further 12-24 h. The reaction mixture was treated with methanol as before and analysis carried out to detect any trace of amide. The residue, was then boiled under reflux in aqueous hydrochloric acid solution (3M, 75ml), for 4-6h. The acidic solution was neutralised with aqueous potassium hydroxide solution (3M), saturated with K_2CO_3 and extracted with diethyl ether (3x50ml). The extract, was dried over magnesium sulphate, filtered, and the solvent removed under reduced pressure to yield an oily product.

N-[(5-Methylpyridin-2-yl)methyl]-N-octylamine.

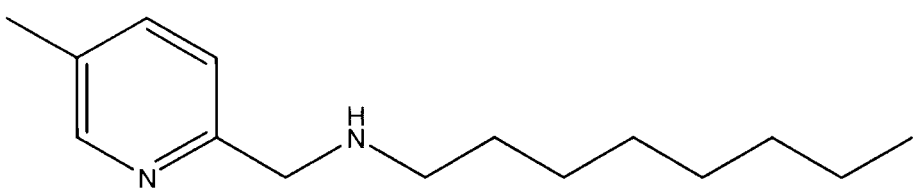

[5]

Reduction of 2-octylamido 5-methyl pyridine (0.25g, 1mmol) yielded a pale orange oil, (0.15g, 64%).

δ_H ppm ($CDCl_3$): 0.77 (3H, t, J = 7 Hz, CH_2CH_3), 1.19 (10H, m, $[CH_2]_5$), 1.42 (2H, m, J = 7 Hz, CH_2CH_3), 2.23 (3H, s, 5-CH_3), 2.55 (2H, t, J = 7 Hz, $NHCH_2$), 3.78 (3H, s, CH_2 2), 7.10 (1H, d, J = 8 Hz, H 4), 7.37 (1H, d, J = 8 Hz, H 3), 8.29 (1H, s, H 6).

δ_C ppm ($CDCl_3$): 17.14 (CH_3), 21.14 (CH_3), 25.70 (CH_2), 30.42 (CH_2), 32.30 (CH_2), 32.74 (CH_2), 33.22 (CH_2), 34.88 (CH_2), 52.75 (CH_2NH), 58.12 (CH_2NH), 124.84 (C 3), 134.17 (C 5), 139.98 (C 4), 152.64 (C 6), 160.03 (C 2),

MS (ES^+) m/z 235 (*MH+*), 257 *(MNa+).*

Acc.MS (ES^+) Found: m/z 235.2177 (*MH+*) $C_{15}H_{26}N_2$ requires: 235.2174 (*MH+*)

N-[(5-Methylpyridin-2-yl)methyl]-N-hexylamine.

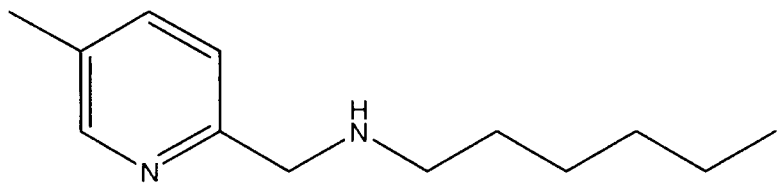

[6]

The general reduction procedure was again employed to reduce (0.22g, 1mmol) of 2-hexylamido 5-methyl pyridine and yielded a pale orange oil, (0.12g, 58%.)

δ_H ppm ($CDCl_3$): 0.79 (3H, t, J = 7 Hz, CH_2CH_3), 1.19 (6H, m, $[CH_2]_3$), 1.44 (2H, m, $CH_2CH_2CH_3$), 2.22 (3H, s, 5-CH_3), 2.56 (2H, q, J = 7 Hz, CH_2CH_2NH), 3.78 (2H, s, CH_2NH) 7.13 (1H, d, J = 7.5 Hz, H 4), 7.38 (1H, d, H 3), 8.29 (1H, s, H 6).

δ_C ppm ($CDCl_3$): 14.21 (CH_3), 18.25 (CH_3), 22.78 (CH_2), 27.23 (CH_2), 30.34 (CH_2), 31.96 (CH_2), 49.9 (CH_2NH), 55.29(CH_2NH), 121.94 (C 3), 131.28 (C 5), 137.09 (C 4), 149.8 (C 2), 157.26 (C 6),

MS (ES+) m/z 207 (*MH*+).

6-{[(5-Hexylpyridin-2-yl)methyl]amino}hexan-1-ol.

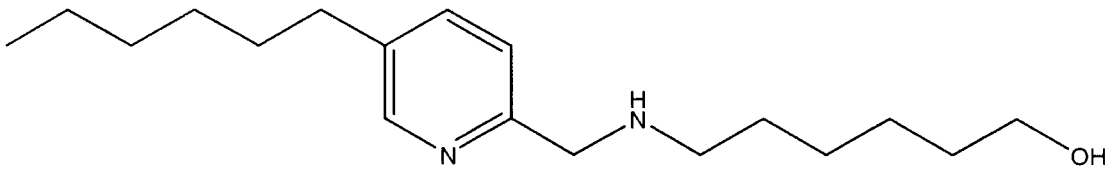

[20]

δ_H ppm ($CDCl_3$): 0.79 (3H, m, CH_2CH_3), 1.25 (14H, m, $[CH_2]_7$), 1.55 (2H, m, $CH_2CH_2CH_3$), 2.59 (4H, m, -CH_2-py, N-CH_2-py), 3.38 (2H, q, J = 5 Hz, CH_2NH), 3.56 (2H, t, J = 4 Hz, CH_2-OH), 7.57 (1H, dd, J = 8 Hz, J = 2 Hz, H 4), 8.12 (1H, d, J = 8 Hz, H 3), 8.26 (1H, d, J = 2 Hz, H 6).

δ_C ppm (CD_3OD): 14.30 (CH_3), 22.85 (CH_2), 25.43 (CH_2), 29.33 (CH_2), 29.70 (CH_2), 29.76 (CH_2), 30.52 (CH_2), 32.07 (CH_2), 33.24 (CH_2), 36.44 (CH_2), 48.67 (CH_2NH), 53.32 (CH_2NH), 61.01 (CH_2-OH), 128.66 (C 4), 136.89 (C 5), 140.73 (C 3), 147.78 (C 2), 149.53 (C 6),
MS (ES+) m/z 293(*MH*+),

6-{[(5-decylpyridin-2-yl)methyl]amino}hexan-1-ol.

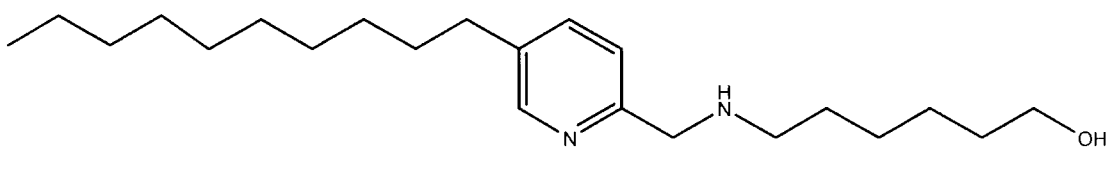

[21]

δ_H ppm ($CDCl_3$): 0.80 (3H, m, CH_2CH_3), 1.18 (22H, m, $[CH_2]_{11}$), 1.45 (2H, m, $CH_2CH_2CH_3$), 2.53(4H, m, -CH_2-py, N-CH_2-py), 3.38 (2H m, CH_2NH), 3.56 (2H, m, CH_2-OH), 7.15 (1H, br d, H 4), 7.39 (1H, br d, H 3), 8.27 (1H, s, H 6).

δ_C ppm (CD_3OD): 14.30 (CH_3), 22.85 (CH_2), 25.43 (CH_2), 25.83 (CH_2), 27.63 (CH_2), 29.12 (CH_2), 29.33 (CH_2), 29.70 (CH_2), 29.76 (CH_2), 30.52 (CH_2), 31.76 (CH_2), 32.07 (CH_2), 33.24 (CH_2), 36.44 (CH_2), 47.97 (CH_2NH), 52.82 (CH_2NH), 59.51 (CH_2-OH), 126.16 (C 4), 138.59 (C 5), 140.20 (C 3), 145.58 (C 2), 147.33 (C 6).
MS (ES^+) m/z 372*(MNa+)*

General Procedure for the Synthesis of N,N,N-trimethyl-2-{[(5-alkylpyridin-2-yl)methyl]amino}hexan-1-aminium chloride Surfactants.

The synthesis of these products, from the pyridine amino alcohols was carried out in several steps. However, as the intermediate products were not separated, and some stages were routine protection / deprotection reactions, only the final product was characterised fully. However, some characterisation of the intermediates was carried out (usually ^1H NMR), and representative examples, for each stage of the reaction process are given. The first step of the synthesis, was the BOC protection of the amine. The 6-{[(5-alkylpyridin-2-yl)methyl]amino}hexan-1-ol (0.1mmol), was combined with BOC anhydride (0.15mmol), in methanol (20ml) at room temperature for 6-8 hr. or until complete conversion of starting material was indicated by TLC. The solvent was removed, and the residue dried under reduced pressure, before the next step of the reaction was carried out. The mesylation of the alcohol, was performed by dissolving the BOC protected intermediate (0.1mmol), in DCM (35ml), under an inert atmosphere and cooling the solution to 0°C using an ice/salt bath, before adding disopropylethylamine (DIPEA) (3.5 mmol), and methanesulphonyl chloride (1.5mmol). The reaction mixture, was maintained at 0°C during addition, and for a further 4hr. Before being allowed to return to room temperature, the reaction was quenched with aqueous $NaHCO_3$ (25ml 0.1M). The organic layer was

separated and washed with aqueous citric acid solution (10 % 3 x 25ml), then dried over $MgSO_4$. Ethanolic trimethylamine solution (25ml 1M), was then added to this residue, and the mixture stirred for 3hr before the solvent was removed. The BOC protection group, was removed from the amine in the usual way, by treatment with TFA. Crude characterisation was then carried out (^1H, ^{13}C NMR and ESMS). The product was then dissolved in water, mixed with DOWEX® 1X8 strong chloride exchange resin (3.5meq/g [dry]). This mixture was stirred, filtered to remove the resin and washed with water. The aqueous solution obtained, was freeze-dried to yield the yellow-brown waxy product. These products [29] and [30] were characterised by ^1H, ^{13}C NMR, accurate ESMS and anion chromatography, which indicated the presence of chloride as the only anion.

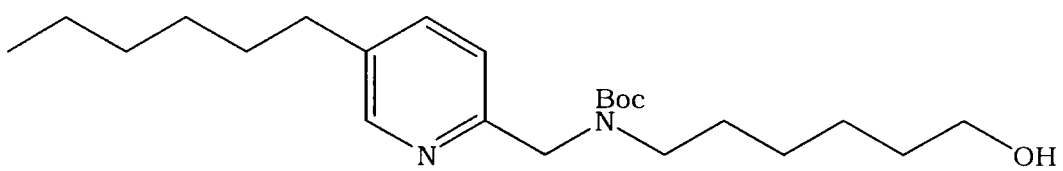

[23]

δ_H ppm ($CDCl_3$): 0.79 (3H, m, CH_2CH_3), 1.22 (14H, m, $[CH_2]_7$), 1.39 (18H, s, t-Bu x 2) 1.54 (2H, m, $CH_2CH_2CH_3$), 2.54 (2H, m, -CH_2-py), 3.19 (2H, m, NBoc-CH_2-py), 3.61 (2H, m, CH_2-OH), 3.97 (2H, m, CH_2NBoc), 7.07 (1H, m, H 3), 8.12 (1H, m, H 4), 8.24(1H, m, H 6).

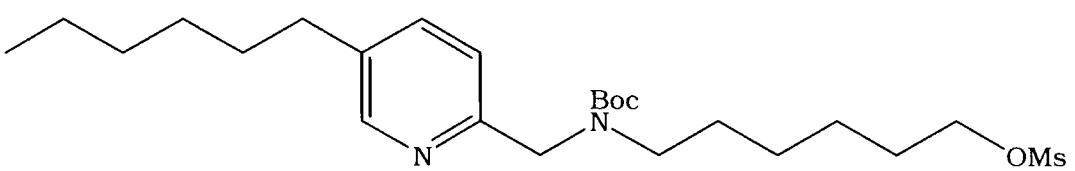

[25]

δ_H ppm ($CDCl_3$): 0.79 (3H, m, CH_2CH_3), 1.22 (14H, m, $[CH_2]_7$), 1.41 (9H, s, t-Bu) 1.54 (2H, m, $CH_2CH_2CH_3$), 2.54 (2H, m, -CH_2-py), 2.92

(3H, s, CH_3-S), 3.08 (2H, m, NBoc-CH_2-py), 4.12 (2H, m, CH_2NBoc), 7.07 (1H, m, H 3), 8.12 (1H, m, H 4), 8.24(1H, m, H 6).
MS (ES^+) m/z 470.3 (*MH*+)

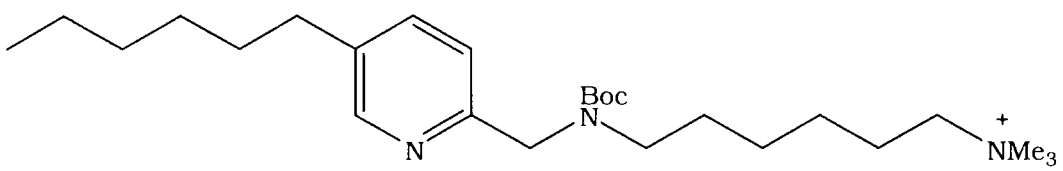

[27]

δ_H ppm (D_2O): 0.68 (3H, m, CH_2CH_3), 1.12 (14H, m, $[CH_2]_7$), 1.27 (2H, m, $CH_2CH_2CH_3$), 1.38 (9H, s, t-Bu) 2.65 (2H, m, -CH_2-py,), , 2.94 (9H, s, $(CH_3)_3$-N^+), 3.10 (2H, m, NBoc-CH_2-py,), 3.77 (2H m, CH_2NBoc), 4.39 (2H s, CH_2-N^+-Me_3),7.78 (1H, br d, H 4), 8.21 (1H, br d, H 3), 8.58 (1H, s, H 6).
MS (ES^+) m/z 434.7 (*MH*+)

N,N,N-Trimethyl-2-{[(5-hexylpyridin-2-yl)methyl]amino}hexan-1-aminium chloride.

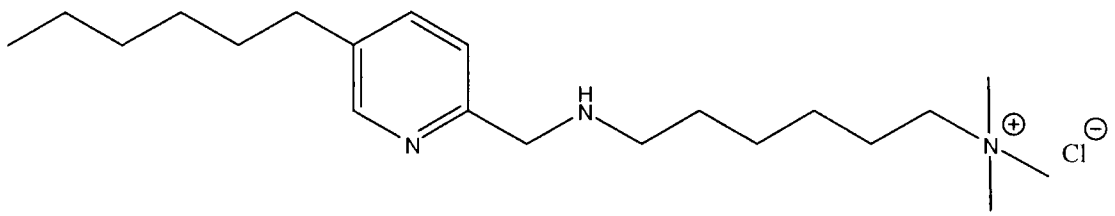

[29]

δ_H ppm (D_2O): 0.68 (3H, m, CH_2CH_3), 1.12 (14H, m, $[CH_2]_7$), 1.27 (2H, m, $CH_2CH_2CH_3$), 2.65 (2H, m, -CH_2-py,), , 2.94 (9H, s, $(CH_3)_3$-N^+), 3.01 (2H, m, HN-CH_2-py,), 3.17 (2H m, CH_2NH), 4.39 (2H s, CH_2-N^+-Me_3),7.78 (1H, br d, H 4), 8.21 (1H, br d, H 3), 8.58 (1H, s, H 6).
δ_C ppm (CD_3OD): 13.47 (CH_3), 22.00 (CH_2), 22.69 (CH_2), 25.12 (CH_2), 25.38 (CH_2), 25.43 (CH_2), 27.85 (CH_2), 29.64 (CH_2), 30.86 (CH_2), 31.96 (CH_2), 47.22 (CH_2NH), 48.32 (CH_2NH), 52.92 (CH_3N^+-),52.95 (CH_3N^+-

),52.98 (CH_3N^+-), 66.58 (-CH_2-N^+-), 127.86 (C 4), 130.37 (C 5), 133.25 (C 3), 143.00 (C 2), 147.17 (C 6).

Acc.MS (ES^+) Found: m/z 334.3190 (M^+) $C_{21}H_{40}N_3$ requires: 334.3222 (M^+).

N,N,N-Trimethyl-2-{[(5-decylpyridin-2-yl)methyl]amino}hexan-1-aminium chloride.

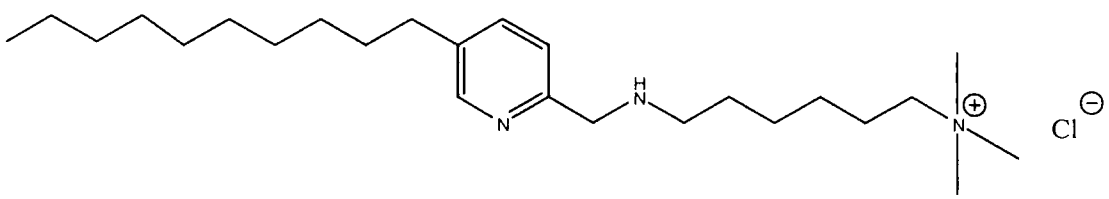

[30]

δ_H ppm (D_2O): 0.71 (3H, m, CH_2CH_3), 1.16 (22H, m, $[CH_2]_{11}$), 1.32 (2H, m, $CH_2CH_2CH_3$), 2.53 (2H, m, -CH_2-py,), , 2.87 (9H, s, $(CH_3)_3$-N^+), 2.99 (2H, m, HN-CH_2-py,), 3.20 (2H m, CH_2NH), 4.35 (2H s, CH_2-N^+-Me_3),7.71 (1H, br d, H 4), 8.11 (1H, br d, H 3), 8.46 (1H, s, H 6).

δ_C ppm (CD_3OD): 13.32 (CH_3), 18.18 (CH_2), 22.72 (CH_2), 22.85 (CH_2), 25.49 (CH_2), 25.63 (CH_2), 25.78 (CH_2), 29.02 (CH_2), 29.28 (CH_2), 29.54 (CH_2), 31.15 (CH_2), 31.89 (CH_2), 32.36 (CH_2), 38.40 (CH_2), 50.65 (CH_2NH), 51.72 (CH_2NH), 52.47 (CH_3N^+-),52.49 (CH_3N^+-),52.50 (CH_3N^+-), 66.42 (-CH_2-N^+-), 127.86 (C 4), 130.37 (C 5), 133.25 (C 3), 143.15 (C 2), 147.28 (C 6).

Acc.MS (ES^+) Found: m/z 390.3847 (M^+) $C_{25}H_{48}N_3$ requires: 390.3848 (M^+).

6.3.2 EDTA and DTPA Ligands and Complexes

2-[Carboxy(2-{carboxy[((R)-(+)-1-(2-naphthyl)ethylamino)carbonyl]amino}ethyl)amino]ethyl[((R)-(+)-1-(2-naphthyl)ethylamino)carbonyl]carbamic acid.

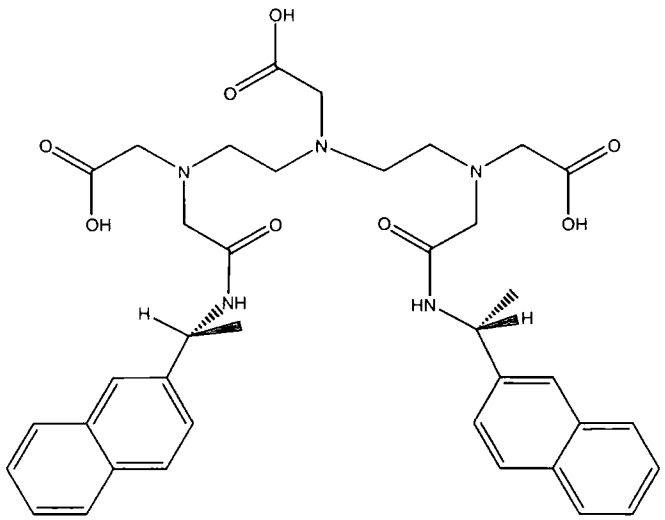

[31]

N,N"-bis[2-(2,6-dioxomorpholino)ethyl]glycine (DTPA dianhydride) 0.357g (1mmol), was combined with 5ml of dry DMF, under an argon atmosphere. (R)-(+)-2-Naphthyl ethyl amine solution 0.513g (3mmol) in $CHCl_3$ (2ml), was then added, dropwise, over 15 min. This mixture was stirred for 30min, until the initially observed precipitate dissolved. The solution was then heated to 50°C under reflux for 14h. After this time, the solvent was removed under reduced pressure. The solid white residue, was washed with water (3x20ml) and ether (3x50ml). The product, a white crystalline solid, was then dried under reduced pressure and characterised by elemental analysis and ^1H and ^{13}C NMR.

m.p. in excess of 250°C

δ_H ppm (CD_3OD): 1.74 (6H, d, J = 7 Hz, CH_3), 3.28 (4H, m, -N-CH_2 -), 3.33(4H, m, -N-CH_2-), 3.69 (6H, s, CH_2-COOH), 3.56 (4H, s, CH_2-

CONH) 4.62 (2H, m, -*CH*-Ar.), 7.50 (2H, m, Ar), 7.54 (2H, m, Ar), 7.93 (6H, m, Ar), 8.10 (4H, m, Ar).

δ_C ppm (CD_3OD): 24.25 (CH_3), 48.93 (CH_2NH), 53.34 (-N-*CH_2*-COOH), 53.36 (-N-*CH_2*-COOH), 59.32 (-N-*CH_2*-CONH), 60.04 (Naph-*CH*-NH), 123.78 (C 6), 124.41 (C 7), 125.45 (C 1), 125.91 (C 4), 127.42 (C 5), 127.68 (C 3), 128.07 (C 8),.132.92 (C 9), 133.80 (C 10),.144.58 (C 2), 157.98 (CONH), 179.11 (COOH), 179.40 (COOH)

MS (ES+): m/z 722.2 *(MNa+)*

{(2-{(Carboxymethyl)[2-(alkylamino)-2-oxoethyl]amino}ethyl)[2-(alkylamino)-2-oxoethyl]amino}acetic acid.

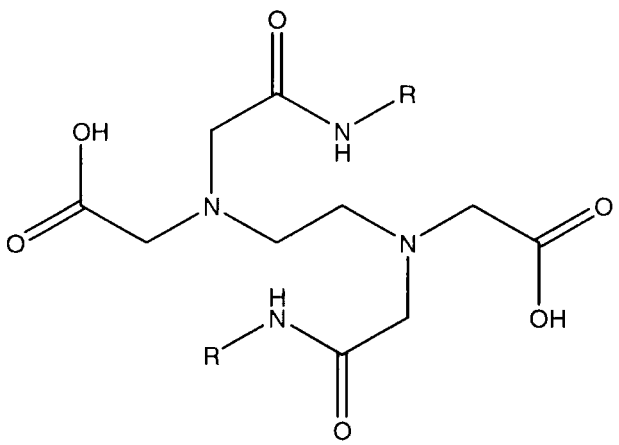

4-[2-(2,6-Dioxomorpholin-4-yl)ethyl]morpholin-2,6-dione (EDTA dianhydride) (10 mmol), was combined with dry THF (20ml), under an inert atmosphere. Addition of amine (22 mmol), to this suspension was carried out over a 15 min period. Liquid amines were added dropwise, directly to the stirred solution. Solid amines, were dissolved in the minimum volume of dry THF before addition. The suspension was stirred for 6-8h. The solvent was then removed under reduced pressure, and the solid white residue was washed with water (3x20ml) and ether (3x50ml). The solid white product, was then dried under reduced pressure and characterised by elemental analysis and NMR.

{(2-{(Carboxymethyl)[2-((R)-(+)-1-(2-naphthyl)ethylamino)-2-oxoethyl]amino}ethyl)[2-((R)-(+)-1-(2-naphthyl)ethylamino)-2-oxoethyl]amino}acetic acid.

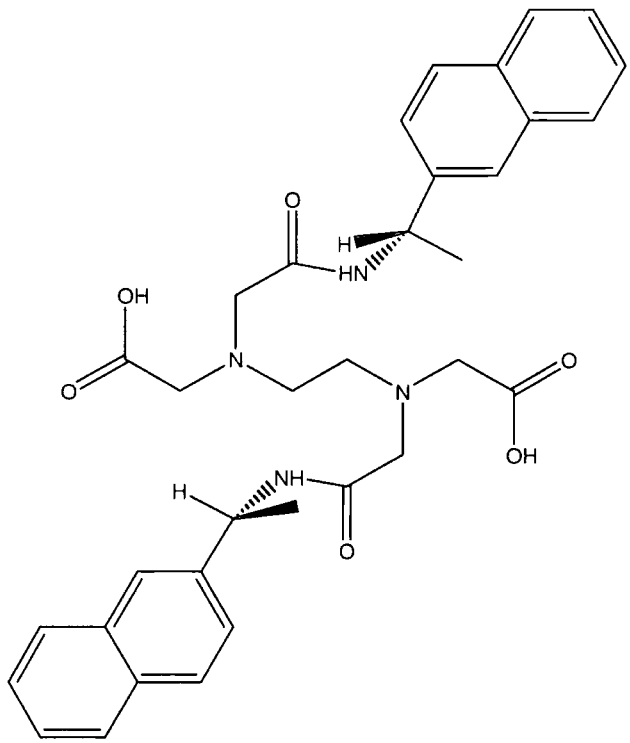

[32]

m.p. in excess of 250°C

Anal. $C_{34}H_{38}N_4O_6.Na.\ ^1/_2\ H_2O$ calculated C, 64.8% H, 6.18% N, 8.88%. Found C, 65.06%, H, 6.18%, N, 8.95%.

δ_C ppm (CD_3OD): 22.93 (CH_3), 49.05 (CH_2NH), 52.86 (-N-*CH_2*-COOH), 59.45 (-N-*CH_2*-CONH), 60.27 (Naph-*CH*-NH), 124.02 (C 6), 124.43 (C 7), 125.50 (C 1), 126.01 (C 4), 127.30 (C 5), 127.65 (C 3), 127.99 (C 8),.131.91 (C 9), 134.21 (C 10),.144.53 (C 2), 159.57 (CONH), 179.24 (COOH).

{(2-{(Carboxymethyl)[2-(octylamino)-2-oxoethyl]amino}ethyl)[2-(octylamino)-2-oxoethyl]amino}acetic acid.

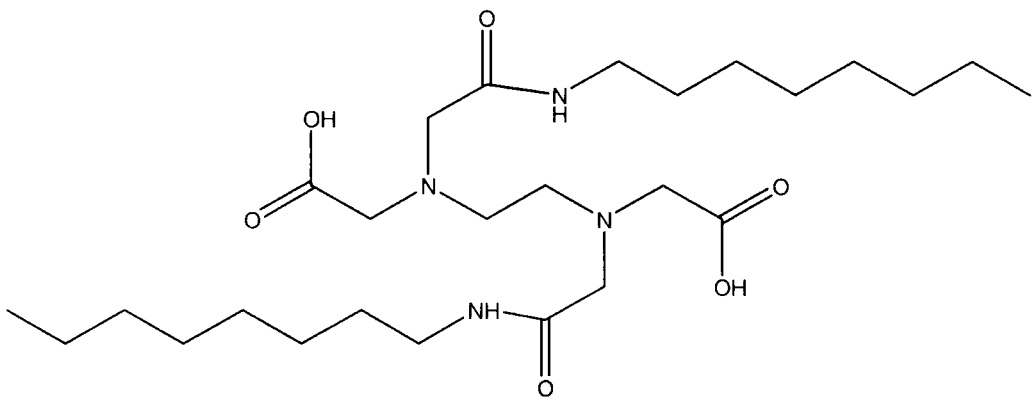

[33]

m.p. in excess of 250°C

δ_H ppm (CD_3OD): 0.86 (6H, m, CH_3), 1.27 (20H, m, $-(CH_2)_5-$), 1.5 (4H, m, CH_2-CH_3), 3.07 (4H, s, -HN-$(CH_2)_2$-NH-), 3.23 (4H, t, J = 6 Hz, HN-CH_2-), 3.52 (4H, s, -N-CH_2-COOH), 3.56 (4H, s, -N-CH_2-CONHR)

MS (ES+): m/z 537.2 *(MNa+)*

Anal. $C_{26}H_{50}N_4O_6$.Na Calc. C, 58.08%, H, 9.37%, N, 10.42%,

Found C, 58.93% H, 9.27% N, 10.56%

{(2-{(Carboxymethyl)[2-(dodecylamino)-2-oxoethyl]amino}ethyl)[2-(dodecylamino)-2-oxoethyl]amino}acetic acid.

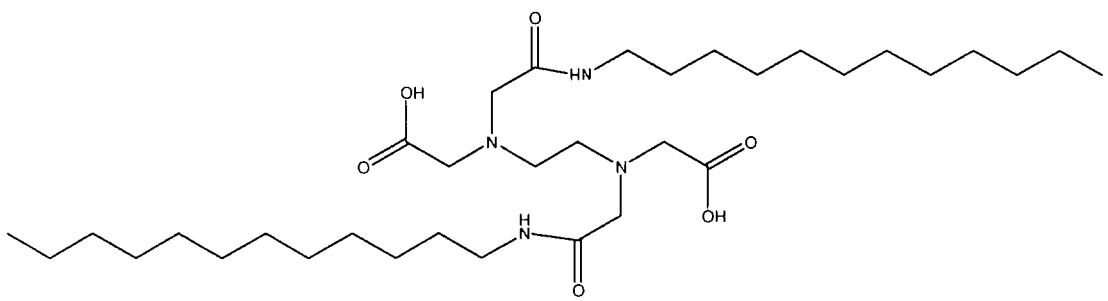

[34]

m.p. in excess of 250°C

δ_H ppm (CD_3OD): 0.89 (6H, m, CH_3), 1.32 (36H, m, $-(CH_2)_9-$), 1.53 (4H, m, CH_2-CH_3), 3.11 (4H, s, -HN-$(CH_2)_2$-NH-), 3.24 (4H, t, J = 6 Hz, HN-CH_2-), 3.54 (4H, s, -N-CH_2-COOH), 3.61 (4H, s, -N-CH_2-CONHR)

MS (ES+): m/z 649.5 *(MNa+)*

Anal. $C_{34}H_{66}N_4O_6$ calculated C, 65.14% H, 10.61% N, 8.94% Found C, 65.27% H, 10.95% N, 8.92%

{(2-{(Carboxymethyl)[2-(hexadecylamino)-2-oxoethyl]amino}ethyl)[2-(hexadecylamino)-2-oxoethyl]amino}acetic acid.

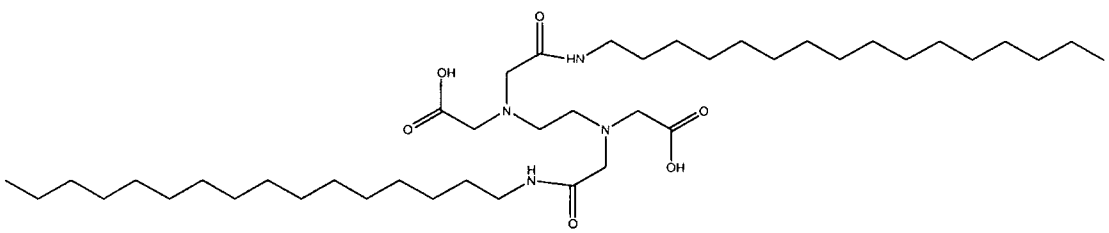

[35]

m.p. in excess of 250°C

δ_H ppm (CD_3OD): 0.87 (6H, m, CH_3), 1.34 (52H, m, $-(CH_2)_{13}-$), 1.51 (4H, m, CH_2-CH_3), 3.13 (4H, s, -HN-$(CH_2)_2$-NH-), 3.32 (4H, t, J = 6 Hz, HN-CH_2-), 3.60 (4H, s, -N-CH_2-COOH), 3.63 (4H, s, -N-CH_2-CONHR)

Anal. $C_{42}H_{82}N_4O_6$ calculated C, 68.25% H, 11.18% N, 7.58%. Found C, 68.32% H, 11.34% N, 7.44%

Zinc {(2-{(carboxymethyl)[2-(octylamino)-2-oxoethyl]amino}ethyl)[2-(octylamino)-2-oxoethyl]amino}acetate.

{(2-{(Carboxymethyl)[2-(octylamino)-2-oxoethyl]amino}ethyl)[2-(octylamino)-2-oxoethyl]amino}acetic acid (0.1mmol), was combined with zinc (II) acetate (0.11 mmol), in purite water (50ml) and boiled under reflux for 6-8 h. The mixture was then cooled and filtered, the

filtrate was washed with water (3 x 30ml) and then dried under reduced pressure. The complex was characterised using ^{1}H NMR to observe changes from the free ligand.

δ_H ppm (D_2O): 0.86 (6H, m, CH_3), 1.27 (20H, m, $-(CH_2)_5-$), 1.5 (4H, m, CH_2-CH_3), 2.65 (2H, d, J = 10 Hz, -HN-CH_2-CH_2-NH), 2.86 (2H, d, J = 10 Hz, -HN-CH_2-CH_2-NH) 3.17 (4H, m, HN-CH_2-), 3.38 (4H, d, J = -16 Hz, -N-CH_2-COOH), 3.44 (4H, d, J= -16 Hz, -N-CH_2-CONHR)

MS (ES+): m/z 578.4(*MH+*)

Anal $C_{26}H_{50}N_4O_6Zn.½H_2O$ calculated C, 53.01%, H, 8.73%, N, 9.51%, Found C, 53.41%, H, 9.02%, N, 9.67%,

Zinc {(2-{(carboxymethyl)[2-(dodecylamino)-2-oxoethyl]amino}ethyl)[2-(dodecylamino)-2-oxoethyl]amino}acetate.

δ_H ppm (CD_3OD): 0.89 (6H, m, CH_3), 1.32 (36H, m, $-(CH_2)_9-$), 1.53 (4H, m, CH_2-CH_3), 2.81 (2H, d, J = 9.5 Hz, -HN-CH_2-CH_2-NH), 3.05 (2H, d, J = 10 Hz, -HN-CH_2-CH_2-NH), 3.34 (*H, m, HN-CH_2-), 3.50 (4H, d, J = -15Hz, -N-CH_2-COOH), 3.64 (4H, d, J= -15 Hz, -N-CH_2-CONHR).

MS (ES+): m/z 691.9 *(MNa+)*

Zinc {(2-{(carboxymethyl)[2-(hexadecylamino)-2-oxoethyl]amino}ethyl)[2-(hexadecylamino)-2-oxoethyl]amino}acetate.

δ_H ppm (CD_3OD): 0.80 (6H, m, CH_3), 1.21 (20H, m, $-(CH_2)_5-$), 1.43 (4H, m, CH_2-CH_3), 2.68 (2H, d, J = 10 Hz, -HN-CH_2-CH_2-NH), 2.89 (2H, d, J = 10 Hz, -HN-CH_2-CH_2-NH) 3.29 (*H m, HN-CH_2-), 3.38 (4H, d, J = -16 Hz, -N-CH_2-COOH), 3.44 (4H, d, J= -16 Hz, -N-CH_2-CONHR)

(* = peaks overlap with residual solvent signal preventing accurate integration.)

References

1 Macilwain, C. *Nature* **2000**, *405*, 983-984.

2 Bottcher, C.; Endisch, C.; Fuhrhop, J. H.; Catterall, C.; Eaton, M. *Journal of the American Chemical Society* **1998**, *120*, 12-17.

3 Geall, A. J.; Taylor, R. J.; Earll, M. E.; Eaton, M. A. W.; Blagbrough, I. S. *Bioconjugate Chemistry* **2000**, *11*, 314-326.

4 Lambert, O.; Letellier, L.; Gelbart, W. M.; Rigaud, J. L. Proceedings of the National Academy of Sciences of the United States of America **2000**, 97, 7248-7253.

5 Anderson, W. F. *Nature* **1998**, *392*, 25-30.

6 Brown, M. D.; Schatzlein, A. G.; Uchegbu, I. F. *International Journal of Pharmaceutics* **2001**, *229*, 1-21.

7 Pouton, C. W.; Seymour, L. W. *Advanced Drug Delivery Reviews* **1998**, *34*, 3-19.

8 Choy, J. H.; Kwak, S. Y.; Jeong, Y. J.; Park, J. S. *Angewandte Chemie-International Edition* **2000**, *39*, 4042-4045.

9 Campbell, N. A. *Biology*, 3rd Edition, The Benjamin/Cummings Publishing Company Inc Redwood City, California, **1993**.

10 Lakhani S. R.; Dilly S. A.; Findlayson C. J. *Basic Pathology (An Introduction to the Mechanisms of Disease)*, 2nd Edition, Arnold Publishing, London, **1998**.

11 The big picture book of viruses, http://www.virology.net/Big_Virology/BVHomePage.html

12 Klasse, P. J.; Bron, R.; Marsh, M. *Advanced Drug Delivery Reviews* **1998**, *34*, 65-91.

13 Morin, K. W.; Atrazheva, E. D.; Knaus, E. E.; Wiebe, L. I. *Journal of Medicinal Chemistry* **1997**, *40*, 2184-2190.

14 Gerin, P. A.; Searle, P. F.; Al-Rubeai, M. *Biotechnology Progress* **1999**, *15*, 941-948.

15 Smith, J. M.; Torres, J. V. *Viral Immunology* **2001**, *14*, 339-348.

16 Wang, Y. M.; Mukherjee, S.; Fraefel, C.; Breakefield, X. O.; Allen,

P. D. *Human Gene Therapy* **2002**, *13*, 261-273.

17 Kircheis, R.; Wightman, L.; Wagner, E. *Advanced Drug Delivery Reviews* **2001**, *53*, 341-358.

18 Dekie, L.; Toncheva, V.; Dubruel, P.; Schacht, E. H.; Barrett, L.; Seymour, L. W. *Journal of Controlled Release* **2000**, *65*, 187-202.

19 Kwoh, D. Y.; Coffin, C. C.; Lollo, C. P.; Jovenal, J.; Banaszczyk, M. G.; Mullen, P.; Phillips, A.; Amini, A.; Fabrycki, J.; Bartholomew, R. M.; Brostoff, S. W.; Carlo, D. J. *Biochimica Et Biophysica Acta-Gene Structure and Expression* **1999**, *1444*, 171-190.

20 Franceschi, S.; Bordeau, O.; Millerioux, C.; Perez, E.; Vicendo, P.; Rico-Lattes, I.; Moisand, A. *Langmuir* **2002**, *18*, 1743-1747.

21 Meier, H.; Lehmann, M.; Kolb, U. *Chemistry-a European Journal* **2000**, *6*, 2462-2469.

22 Petersen, H.; Kunath, K.; Martin, A. L.; Stolnik, S.; Roberts, C. J.; Davies, M. C.; Kissel, T. *Biomacromolecules* **2002**, *3*, 926-936.

23 Benns, J. M.; Choi, J. S.; Mahato, R. I.; Park, J. S.; Kim, S. W. *Bioconjugate Chemistry* **2000**, *11*, 637-645.

24 Wadhwa, M. S.; Collard, W. T.; Adami, R. C.; McKenzie, D. L.; Rice, K. G. *Bioconjugate Chemistry* **1997**, *8*, 81-88.

25 Franceschi, S.; Bordeau, O.; Millerioux, C.; Perez, E.; Vicendo, P.; Rico-Lattes, I.; Moisand, A. *Langmuir* **2002**, *18*, 1743-1747.

26 Agier, C.; Bury, M.; Farinotti, R.; Viel, C. Bulletin De La Societe Botanique De France-Lettres Botaniques **1991**, 138, 39-45.

27 Ward, C. M.; Read, M. L.; Seymour, L. W. *Blood* **2001**, *97*, 2221-2229.

28 Yamazaki, Y.; Nango, M.; Matsuura, M.; Hasegawa, Y.; Hasegawa, M.; Oku, N. *Gene Therapy* **2000**, *7*, 1148-1155.

29 Godbey, W. T.; Wu, K. K.; Mikos, A. G. *Journal of Controlled Release* **1999**, *60*, 149-160.

30 Lim, Y. B.; Han, S. O.; Kong, H. U.; Lee, Y.; Park, J. S.; Jeong, B.; Kim, S. W. *Pharmaceutical Research* **2000**, *17*, 811-816

31 Lim, Y. B.; H., K. C.; K., K.; Kim, S. W.; Park, J. S. *Journal of the American Chemical Society* **2000**, *122*, 6524-6525

32 Kircheis, R.; Wightman, L.; Wagner, E. *Advanced Drug Delivery Reviews* **2001**, *53*, 341-358.

33 Lee, H.; Williams, S. K. R.; Allison, S. D.; Anchordoquy, T. J. *Analytical Chemistry* **2001**, *73*, 837-843.

34 Buijnsters, P.; Rodriguez, C. L. G.; Willighagen, E. L.; Sommerdijk, N.; Kremer, A.; Camilleri, P.; Feiters, M. C.; Nolte, R. J. M.; Zwanenburg, B. *European Journal of Organic Chemistry* **2002**, 1397-1406.

35 Woodle, M. C.; Scaria, P. *Current Opinion in Colloid & Interface Science* **2001**, *6*, 78-84.

36 Allison, S. D.; Molina, M. D. C.; Anchordoquy, T. J. *Biochimica Et Biophysica Acta-Biomembranes* **2000**, *1468*, 127-138.

37 Eaton, M. A. W.; Baker, T. S.; Catterall, C. F.; Crook, K.; Macaulay, G. S.; Mason, B.; Norman, T. J.; Parker, D.; Perry, J. J. B.; Taylor, R. J.; Turner, A.; Weir, A. N. *Angewandte Chemie-International Edition* **2000**, *39*, 4063-4067.

38 Singh, R. S.; Mukherjee, K.; Banerjee, R.; Chaudhuri, A.; Hait, S. K.; Moulik, S. P.; Ramadas, Y.; Vijayalakshmi, A.; Rao, N. M. *Chemistry-a European Journal* **2002**, *8*, 900-909.

39 Langer, R. *Nature* **1998**, *392*, 5-10.

40 Simoes, S.; Slepushkin, V.; Duzgunes, N.; de Lima, M. C. P. *Biochimica Et Biophysica Acta-Biomembranes* **2001**, *1515*, 23-37.

41 Kichler, A.; Zauner, W.; Ogris, M.; Wagner, E. *Gene Therapy* **1998**, *5*, 855-860.

42 Reddy, J. A.; Low, P. S. *Journal of Controlled Release* **2000**, *64*, 27-37.

43 Eaton, M. A. W.; Baker, T. S.; Catterall, C. F.; Crook, K.; Macaulay, G. S.; Mason, B.; Norman, T. J.; Parker, D.; Perry, J. J. B.; Taylor, R. J.; Turner, A.; Weir, A. N. *Angewandte Chemie-International Edition* **2000**, *39*, 4063-4067.

44 Wolff, J. A.; Malone, R. W.; Williams, P.; Chong, W.; Acsadi, G.; Jani, A.; Felgner, P. L. *Science* **1990**, *247*, 1465-1468.

45 Hickman, M. A.; Malone, R. W.; Lehmannbruinsma, K.; Sih, T. R.; Knoell, D.; Szoka, F. C.; Walzem, R.; Carlson, D. M.; Powell, J.

S. *Human Gene Therapy* **1994**, *5*, 1477-1483.

46 Gumbleton, M. *Advanced Drug Delivery Reviews* **2001**, *49*, 281-300.

47 Shaw, D. J. *Introduction to colloid and surface chemistry.*; 3rd Edition ed.; Butterworths: London, **1980**.

48 Moroi, Y. *Micelles : theoretical and applied aspects*; Plenum Press: New York, **1992**.

49 *Liposomes a Practical Approach*; New R, R., C, Ed.; Oxford University Press: Oxford, **1990**.

50 Zhigaltsev, I. V.; Maurer, N.; Wong, K. F.; Cullis, P. R. *Biochimica Et Biophysica Acta-Biomembranes* **2002**, *1565*, 129-135.

51 Byk, G.; Wetzer, B.; Frederic, M.; Dubertret, C.; Pitard, B.; Jaslin, G.; Scherman, D. *Journal of Medicinal Chemistry* **2000**, *43*, 4377-4387.

52 Pichon, C.; LeCam, E.; Guerin, B.; Coulaud, D.; Delain, E.; Midoux, P. *Bioconjugate Chemistry* **2002**, *13*, 76-82.

53 Wetzer, B.; Byk, G.; Frederic, M.; Airiau, M.; Blanche, F.; Pitard, B.; Scherman, D. *Biochemical Journal* **2001**, *356*, 747-756.

54 Eggers, K.; Fyles, T. M.; Montoya-Pelaez, P. J. *Journal of Organic Chemistry* **2001**, *66*, 2966-2977.

55 Le Garrec, D.; Taillefer, J.; Van Lier, J. E.; Lenaerts, V.; Leroux, J. C. *Journal of Drug Targeting* **2002**, *10*, 429-437.

56 Bisby, R. H.; Mead, C.; Morgan, C. G. *Photochemistry and Photobiology* **2000**, *72*, 57-61.

57 Bondurant, B.; Mueller, A.; O'Brien, D. F. *Biochimica Et Biophysica Acta-Biomembranes* **2001**, *1511*, 113-122.

58 Park, J. M.; Aoyama, S.; Zhang, W. B.; Nakatsuji, Y.; Ikeda, I. *Chemical Communications* **2000**, 231-232.

59 Ohya, Y.; Okuyama, Y.; Fukunaga, A.; Ouchi, T. *Supramolecular Science* **1998**, *5*, 21-29.

60 Bisby, R. H.; Mead, C.; Morgan, C. C. *Biochemical and Biophysical Research Communications* **2000**, *276*, 169-173.

61 Yaroslavov, A. A.; Udalykh, O. Y.; Melik-Nubarov, N. S.;

Kabanov, V. A.; Ermakov, Y. A.; Azov, V. A.; Menger, F. M. *Chemistry-a European Journal* **2001**, *7*, 4835-4843.

62 Eccleston, M. E.; Kuiper, M.; Gilchrist, F. M.; Slater, N. K. H. *Journal of Controlled Release* **2000**, *69*, 297-307.

63 Turk, M. J.; Reddy, J. A.; Chmielewski, J. A.; Low, P. S. *Biochimica Et Biophysica Acta-Biomembranes* **2002**, *1559*, 56-68.

64 Shi, G. F.; Guo, W. J.; Stephenson, S. M.; Lee, R. J. *Journal of Controlled Release* **2002**, *80*, 309-319.

65 Thomas, J. L.; You, H.; Tirrell, D. A. *Journal of the American Chemical Society* **1995**, *117*, 2949-2950.

66 Liang, E.; Hughes, J. *Biochimica Et Biophysica Acta-Biomembranes* **1998**, 1369, 39-50.

67 Budker, V.; Gurevich, V.; Hagstrom, J. E.; Bortzov, F.; Wolff, J. A. *Nature Biotechnology* **1996**, *14*, 760-764.

68 Isaacs, N. S. *Physical Organic Chemistry*, Longman Scientific and Technical, **1987**.

69 Parker, D ; Perry, J. J. B. Unpublished Work. **1999**.

70 Smith, R.M.; Martell, A.E. *Critical Stability Constants*, **1975** Vol-2.

71 Waldner, A. *Synthetic Communications* **1989**, *19*, 2371-2374.

72 Matsui, J.; Mitsuishi, M.; Miyashita, T. *Macromolecules* **1999**, *32*, 381-386.

73 Ren, X. Z.; Li, G. Z.; Wang, H. L.; Zhai, L. M.; Sui, W. P.; Xu, X. Y. *Chemical Journal of Chinese Universities-Chinese* **1995**, *16*, 1295-1297.

74 Backer, C. A.; Whitten, D. G. *Journal of Physical Chemistry* **1987**, *91*, 865-869.

75 Turro, N. J.; Okubo, T. *Journal of Physical Chemistry* **1982**, *86*, 159-161.

76 Winnik, F. M.; Regismond, S. T. A. *Colloids and Surfaces A-Physicochemical and Engineering Aspects* **1996**, *118*, 1-39.

77 Ren, X. Z.; Li, G. Z.; Wang, H. L.; Xu, X. H. *Colloids and Surfaces A-Physicochemical and Engineering Aspects* **1995**, *100*, 165-172.

78 Ananthapadmanab, K. P.; Goddard, E. D.; Turro, N. J.; Kuo, P. L. *Langmuir* **1985**, *1*, 352.

79 Zheng, X. L.; Meng, Z. Y.; Cao, W. X. *Acta Polymerica Sinica* **2000**, 386-390.

80 Li, F.; Li, G. Z.; Wang, H. Q.; Xue, Q. J. *Colloids and Surfaces A-Physicochemical and Engineering Aspects* **1997**, 127, 89-96.

81 Blandamer, M. J.; Cullis, P. M.; Soldi, L. G.; Rao, K. C.; Subha, M. C. S. *Journal of Thermal Analysis* **1996**, *46*, 1583-1588.

82 CurveExpert 1.3 software obtained from http://www.ebicom.net/~dhyams/cvxpt.htm

83 Prosser, R. S.; Bryant, H.; Bryant, R. G.; Vold, R. R. *Journal of Magnetic Resonance* **1999**, *141*, 256-260.

84 Jasanada, F.; Nepveu, F. *Tetrahedron Letters* **1992**, *33*, 5745-5748.

85 de Namor, A. F. D.; Tanaka, D. A. P. *Journal of the Chemical Society-Faraday Transactions* **1998**, *94*, 3105-3110.

86 Geraldes, C.; Delgado, R.; Urbano, A. M.; Costa, J.; Jasanada, F.; Nepveu, F. *Journal of the Chemical Society-Dalton Transactions* **1995**, 327-335.

87 Parker, D.; Pulukkody, K.; Smith, F.C.; Batsanov, A.; Howard, J.A.K. *Journal of the Chemical Society, Dalton Transactions.* **1994**, 689-693.

88 Yun-Ming, W.; Yueh-Ju, W.; Reu-Sheng, S.; Gin-Chung, L.; Wen-Chen, L.; Ju-Hsiou, L. *Polyhedron* **1999**, *18*, 1147.

89 Georgopoulou, A. S.; Ulvenlund, S.; Mingos, D. M. P.; Baxter, I.; Williams, D. J. *Journal of the Chemical Society, Dalton Transactions* **1999**, 547.

90 Aime, S.; Benetollo, F.; Bombieri, G.; Colla, S.; Fasano, M.; Paoletti, S. *Inorganica Chimica Acta* **1997**, *254*, 63.

91 Bligh, S. W. A.; Chowdhury, A. H. M. S.; McPartlin, M.; Scowen, I. J.; Bulman, R. A. *Polyhedron* **1995**, *14*, 567.

92 Wang, Y.-M.; Wang, Y.-J.; Sheu, R.-S.; Liu, G.-C.; Lin, W.-C.; Liao, J.-H. *Polyhedron* **1999**, *18*, 1147.

93 Bulman, R.A.; Jobanputra, N.; Kuroda, R.; McKinnon, A.; Sadler, P.J. *Inorganic Chemistry* **1987**, *26*, 2483

94 Noll, B.C.; Marusak, R.A. *Acta Crystallographica Section C-Crystal Structure Communications* **1992**, *48*, 969.

95 Ulvenlund, S.; Georgopoulou, A. S.; Mingos, D. M. P.; Baxter, I.; Lawrence, S. E.; White, A. J. P.; Williams, D. J. *Journal of the Chemical Society-Dalton Transactions* **1998**, 1869-1878.

96 Das, A.; Mahato, K. K.; Chakraborty, T. *Physical Chemistry Chemical Physics* **2001**, *3*, 1813-1818.

97 Lakowicz, J. R. *Principals of Fluorescence Spectroscopy*; 2nd ed.; Klewer Academic / Plemum Publishers: New York, **1999**.

98 Turro, N. J. *Modern Molecular Photochemistry*; University Science Books:, 1991.

99 Williams J. A. G.; *Luminescent Behaviour of Macrocycle Metal Complexes* (Durham Univ. Ph.D. thesis **1995**)

100 Outten, C. E.; O'Halloran, T. V. *Science* **2001**, *292*, 2488-2492.

101 Menger, F. M.; Lee, J. J. *Journal of Organic Chemistry* **1993**, *58*, 1909-1916.

102 Fang, X. L.; Yang, C. F. *Journal of Colloid and Interface Science* **1999**, *212*, 242-251.

103 Kim, W. J.; Yang, S. M. *Langmuir* **2000**, *16*, 6084-6093.

104 Xia, Y.; Goldmints, I.; Johnson, P. W.; Hatton, T. A.; Bose, A. *Langmuir* **2002**, *18*, 3822-3828.

105 Zhang, W.; Liu, H. Z.; Chen, J. Y. *Biochemical Engineering Journal* **2002**, *12*, 1-5.

106 Chidambaram, N.; Burgess, D. J. *Colloids and Surfaces A-Physicochemical and Engineering Aspects* **2001**, 181, 271-278.

107 Image taken from http://www.private.uni-jena.de/~b7drma/pc_samples/dmpc_liposome_cryo1.html

108 Driessen, A. J.; van den Hooven, H. W.; Kuiper, W.; van de Kamp, M.; Sahl, H. G.; Konings, R. N.; Konings, W. N. *Biochemistry* **1995**, *34*, 1606-1614.

109 Thomas, J. A.; Buchsbaum, R. N.; Zimniak, A.; Racker, E. *Biochemistry* **1979**, *18*, 2210-2218.

110 Nicol, F.; Nir, S.; Szoka, F. C. *Biophysical Journal* **2000**, *78*, 818-829.

111 Parente, R. A.; Nir, S.; Szoka, F. C. *Biochemistry* **1990**, *29*, 8720-8728.

112 Diagram modified from one displayed by Molecular Probes, Inc. at http://www.probes.com/handbook/

113 Ortiz, A.; Aranda, F. J.; Gomez-Fernandez, J. C. *Biochimica et Biophysica Acta* **1987**, *898*, 214

114 Jerchel D.; Hieder J.; Wagner H. *Justus Liebigs Annalen der Chemie.* **1958**, *613*, 153-170.

115 Tanner, D. D.; Meintzer, C. P.; Tsai, E. C.; Oumarmahamat, H. *Journal of the American Chemical Society* **1990**, *112*, 7369-7372.

116 Tanner, D. D.; Oumarmahamat, H.; Meintzer, C. P.; Tsai, E. C.; Lu, T. T.; Yang, D. *Journal of the American Chemical Society* **1991**, *113*, 5397-5402.

117 Nakayama, J.; Kawamura, T.; Kuroda, K.; Fujita, A. *Tetrahedron Letters* **1993**, *34*, 5725-5728.

118 Tanner, D. D.; Meintzer, C. P.; Dionarian, N.; Singh, H.; Tsai, E. C.; Oumarmahamat, H. *Journal of the American Chemical Society* **1990**, *112*, 2736-2739.

119 Schubert, U. S.; Eschbaumer, C.; Weidl, C. H. *Synlett* **1999**, 342-344.

120 Windscheif, P. M.; Vogtle, F. *Synthesis-Stuttgart* **1994**, 87-92.

121 Sakamoto, T.; Ohsawa, K. *Journal of the Chemical Society-Perkin Transactions* 1 **1999**, 2323-2326.

122 Wladner, A. *Synthetic Communications* **1989**, *19*, 2371-2374.

123 Moynehan, T. M. *Journal of the Chemical Society* **1962**, 2637-2645.

124 Vorbrueggen H; Krolikiewicz K. *Synthesis* **1983**, *4*, 316-319.

125 Nakatsuji, Y.; Nakamura, T.; Yonetani, M.; Hajime;, Y.; Okahara, M. *Journal of the American Chemical Society* **1988**, *110*, 531-538.

126 Belanger, A.; Brassard, P. *Canadian Journal of Chemistry* **1975**, *53*, 19-200.

127 Waldner, A. *Helvetica Chimica Acta* **1988**, *71*, 486-492.

Appendices

Appendix 1

X-ray Structural Data for 01srv205 (5-hexylpyridine-2-carboxamide)

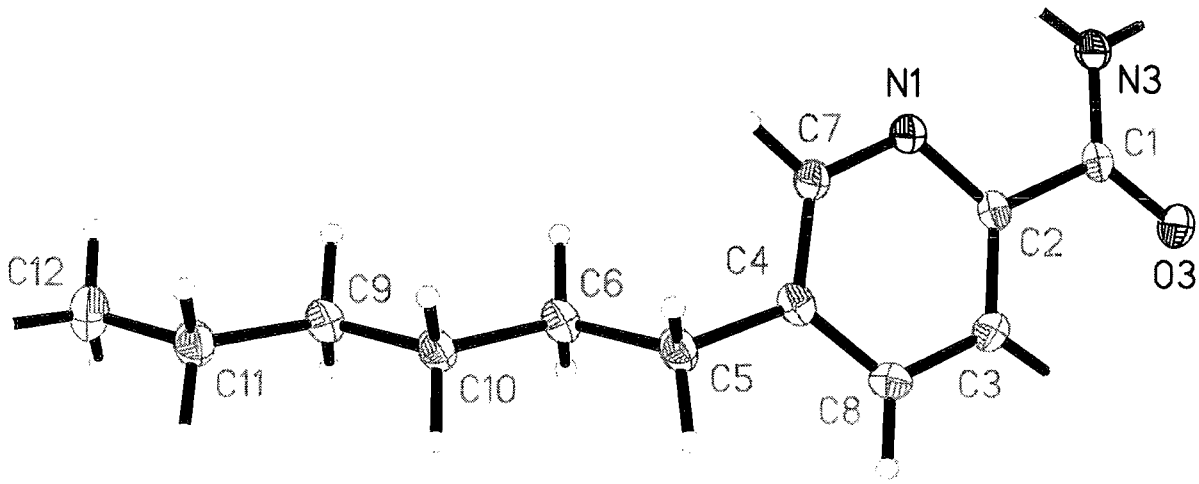

Table 1. Crystal data and structure refinement for 01srv205.

Identification code	01srv205	
Empirical formula	$C_{12}H_{12}NO_2$	
Formula weight	202.23	
Temperature	120(2) K	
Wavelength	0.71073 Å	
Crystal system	Monoclinic	
Space group	P2(1)/c	
Unit cell dimensions	a = 14.0716(12) Å	α= 90°.
	b = 5.6413(5) Å	β= 108.364(2)°.
	c = 15.1563(13) Å	γ= 90°.
Volume	1141.87(17) $Å^3$	
Z	4	
Density (calculated)	1.176 Mg/m^3	
Absorption coefficient	0.081 mm^{-1}	
F(000)	428	
Crystal size	0.20 x 0.15 x 0.15 mm^3	
Theta range for data collection	1.52 to 28.58°.	
Index ranges	-18<=h<=18, -7<=k<=7, -20<=l<=19	
Reflections collected	12220	
Independent reflections	2910 [R(int) = 0.0796]	
Completeness to theta = 28.58°	99.4 %	
Absorption correction	None	
Max. and min. transmission	. and .	
Refinement method	Full-matrix least-squares on F^2	
Data / restraints / parameters	2910 / 0 / 208	
Goodness-of-fit on F^2	1.043	
Final R indices [I>2sigma(I)]	R1 = 0.0455, wR2 = 0.0993	
R indices (all data)	R1 = 0.0836, wR2 = 0.1211	
Extinction coefficient	.	
Largest diff. peak and hole	0.300 and -0.265 $e.Å^{-3}$	

Table 2. Atomic coordinates (x 10^4) and equivalent isotropic displacement parameters ($Å^2$x 10^3) for 01srv205. U(eq) is defined as one third of the trace of the orthogonalized U^{ij} tensor.

	x	y	z	U(eq)
O(3)	4170(1)	4510(2)	11791(1)	25(1)
N(3)	4786(1)	1179(3)	11333(1)	22(1)
N(1)	4041(1)	2542(2)	9520(1)	20(1)
C(4)	3084(1)	5270(3)	8334(1)	19(1)
C(2)	3858(1)	3949(3)	10165(1)	18(1)
C(1)	4295(1)	3234(3)	11173(1)	18(1)
C(3)	3305(1)	6017(3)	9947(1)	22(1)
C(5)	2710(1)	5868(3)	7309(1)	22(1)
C(9)	1055(1)	2615(3)	5068(1)	22(1)
C(6)	1996(1)	4008(3)	6719(1)	22(1)
C(8)	2908(1)	6679(3)	9017(1)	23(1)
C(10)	1752(1)	4457(3)	5677(1)	21(1)
C(7)	3652(1)	3218(3)	8631(1)	21(1)
C(11)	864(1)	3002(3)	4031(1)	24(1)
C(12)	178(2)	1137(4)	3429(1)	31(1)

Table 3. Bond lengths [Å] and angles [°] for 01srv205.

O(3)-C(1)	1.2368(19)	C(8)-C(4)-C(7)	116.95(14)
N(3)-C(1)	1.332(2)	C(8)-C(4)-C(5)	123.46(15)
N(1)-C(7)	1.341(2)	C(7)-C(4)-C(5)	119.58(14)
N(1)-C(2)	1.345(2)	N(1)-C(2)-C(3)	123.10(14)
C(4)-C(8)	1.387(2)	N(1)-C(2)-C(1)	117.84(13)
C(4)-C(7)	1.398(2)	C(3)-C(2)-C(1)	119.06(14)
C(4)-C(5)	1.513(2)	O(3)-C(1)-N(3)	123.95(14)
C(2)-C(3)	1.384(2)	O(3)-C(1)-C(2)	120.02(14)
C(2)-C(1)	1.511(2)	N(3)-C(1)-C(2)	116.01(13)
C(3)-C(8)	1.394(2)	C(2)-C(3)-C(8)	118.90(15)
C(5)-C(6)	1.532(2)	C(4)-C(5)-C(6)	113.53(13)
C(9)-C(10)	1.524(2)	C(10)-C(9)-C(11)	113.39(14)
C(9)-C(11)	1.524(2)	C(10)-C(6)-C(5)	112.51(13)
C(6)-C(10)	1.528(2)	C(4)-C(8)-C(3)	119.46(15)
C(11)-C(12)	1.522(2)	C(9)-C(10)-C(6)	113.86(13)
		N(1)-C(7)-C(4)	124.72(15)
C(7)-N(1)-C(2)	116.86(14)	C(12)-C(11)-C(9)	113.07(14)

Table 4. Anisotropic displacement parameters ($Å^2 x\ 10^3$) for 01srv205. The anisotropic displacement factor exponent takes the form: $-2\pi^2[\ h^2\ a^{*2}U^{11} + ... + 2\ h\ k\ a^*\ b^*\ U^{12}\ ]$

	U^{11}	U^{22}	U^{33}	U^{23}	U^{13}	U^{12}
O(3)	30(1)	29(1)	15(1)	-4(1)	6(1)	3(1)
N(3)	25(1)	27(1)	13(1)	1(1)	4(1)	5(1)
N(1)	21(1)	22(1)	16(1)	-2(1)	4(1)	2(1)
C(4)	17(1)	22(1)	17(1)	2(1)	3(1)	-3(1)
C(2)	16(1)	21(1)	16(1)	0(1)	3(1)	-2(1)
C(1)	17(1)	23(1)	14(1)	-1(1)	3(1)	-3(1)
C(3)	26(1)	22(1)	19(1)	-4(1)	6(1)	2(1)
C(5)	24(1)	23(1)	16(1)	3(1)	2(1)	0(1)
C(9)	22(1)	24(1)	17(1)	2(1)	4(1)	-1(1)
C(6)	22(1)	25(1)	18(1)	3(1)	3(1)	-1(1)
C(8)	23(1)	20(1)	24(1)	1(1)	4(1)	4(1)
C(10)	21(1)	22(1)	17(1)	2(1)	3(1)	1(1)
C(7)	23(1)	25(1)	15(1)	-2(1)	5(1)	3(1)
C(11)	28(1)	24(1)	18(1)	1(1)	6(1)	-1(1)
C(12)	37(1)	33(1)	20(1)	-4(1)	6(1)	-6(1)

Table 5. Hydrogen coordinates ($x\ 10^4$) and isotropic displacement parameters ($Å^2 x\ 10^3$) for 01srv205.

	x	y	z	U(eq)
H(3)	2540(13)	8140(30)	8855(12)	24(5)
H(12)	553(14)	4580(30)	3842(13)	28(5)
H(11)	1360(13)	1010(30)	5247(12)	25(5)
H(7)	2297(13)	2410(30)	6852(12)	24(5)
H(9)	2403(15)	4450(30)	5502(13)	32(5)
H(16)	454(16)	-420(40)	3572(15)	45(6)
H(2)	3216(14)	6930(30)	10448(14)	31(5)
H(1)	3806(14)	2220(30)	8188(14)	34(5)
H(8)	1455(13)	6080(30)	5531(12)	24(5)
H(13)	1525(15)	2980(30)	3907(13)	35(5)
H(6)	1348(14)	3990(30)	6896(13)	29(5)
H(14)	-498(16)	1130(40)	3546(14)	40(6)
H(4)	2406(14)	7470(40)	7241(13)	32(5)
H(5)	3319(15)	6050(30)	7087(14)	35(5)
H(10)	406(14)	2560(30)	5192(13)	32(5)
H(15)	87(17)	1390(40)	2776(16)	49(6)
H(18)	4884(15)	420(40)	10847(15)	37(6)
H(17)	5048(16)	690(40)	11925(16)	43(6)

Appendix 2

Data used in the calculation of CMC and CAC values.

Pyridine-2-methylamine compounds [29] and [30]

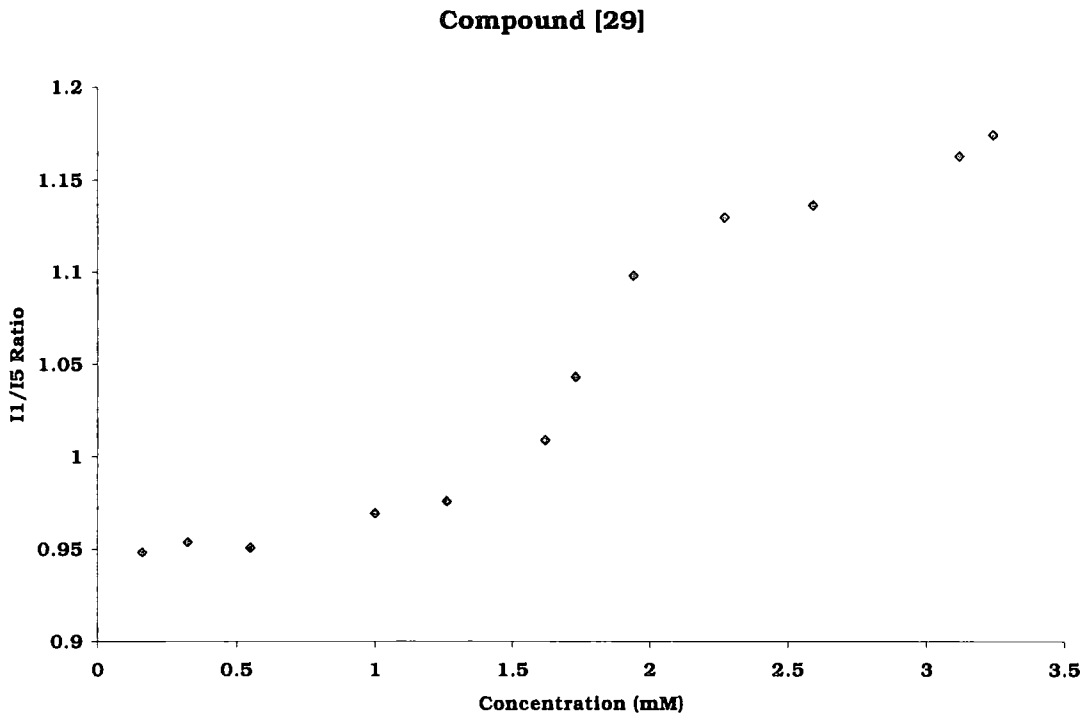

Concentration (mM)	I_1/I_5 Ratio
0.16	0.948
0.32	0.954
0.55	0.951
1.00	0.969
1.26	0.976
1.62	1.009
1.73	1.043
1.94	1.098
2.27	1.129
2.59	1.136

Compound [30]

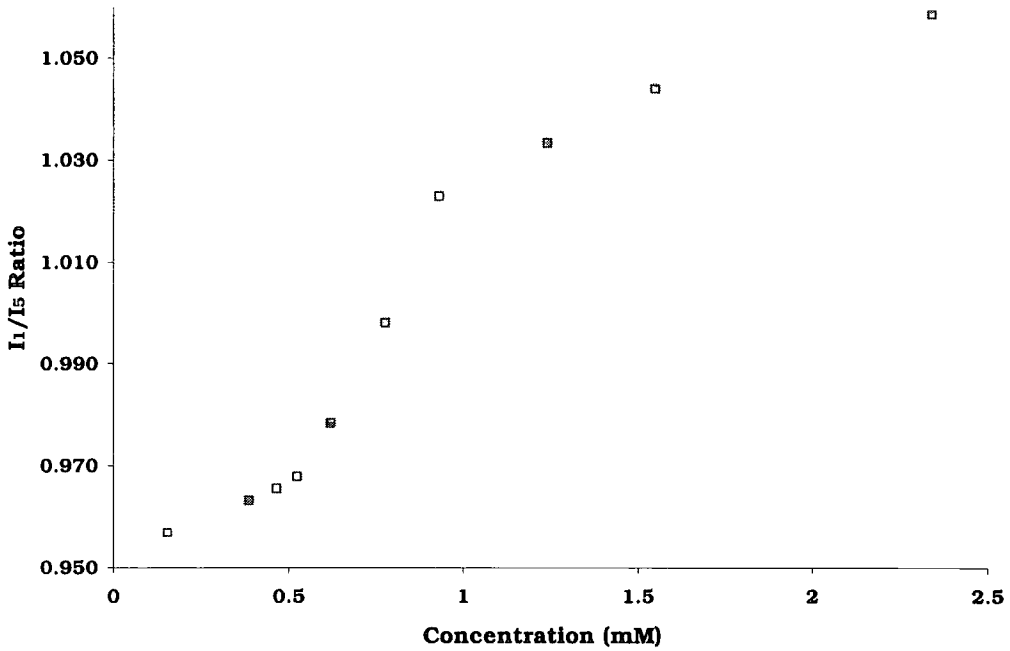

Concentration (mM)	I_1/I_5 Ratio
0.155	0.957
0.387	0.963
0.465	0.966
0.524	0.968
0.620	0.978
0.775	0.998
0.930	1.023
1.240	1.033
1.549	1.044
2.341	1.059

EDTA Diamide Compounds [33], [34] and [35]

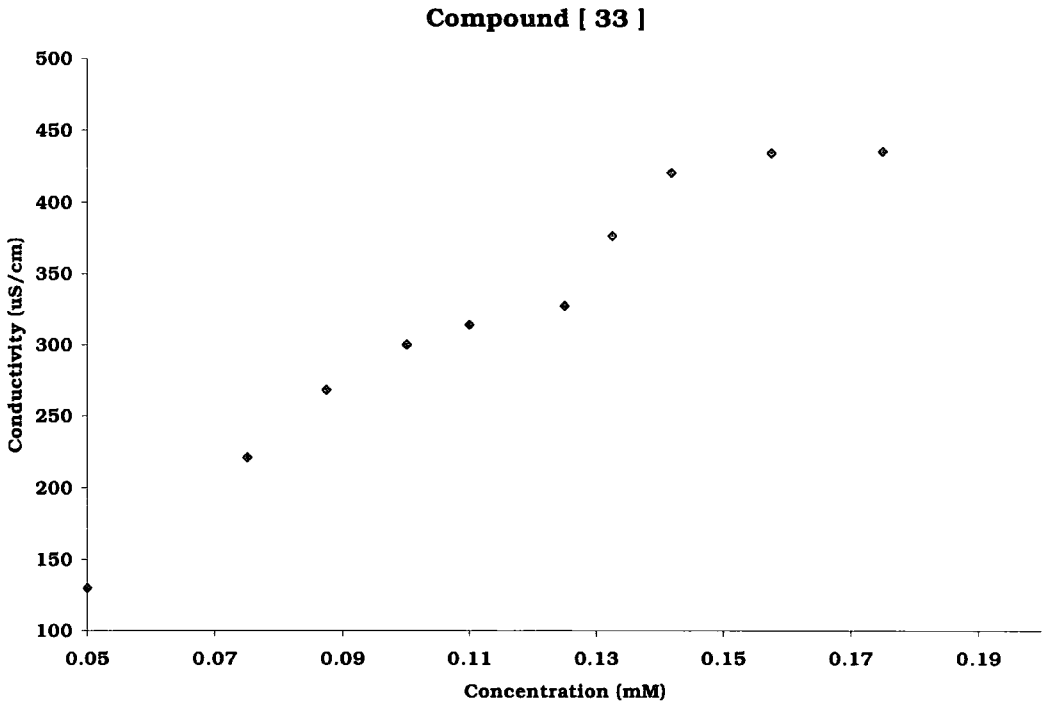

Concentration (mM)	Condictivity (μScm^{-1})
0.050	130
0.075	221
0.087	268
0.100	300
0.110	314
0.125	327
0.133	376
0.142	420
0.157	434
0.175	435

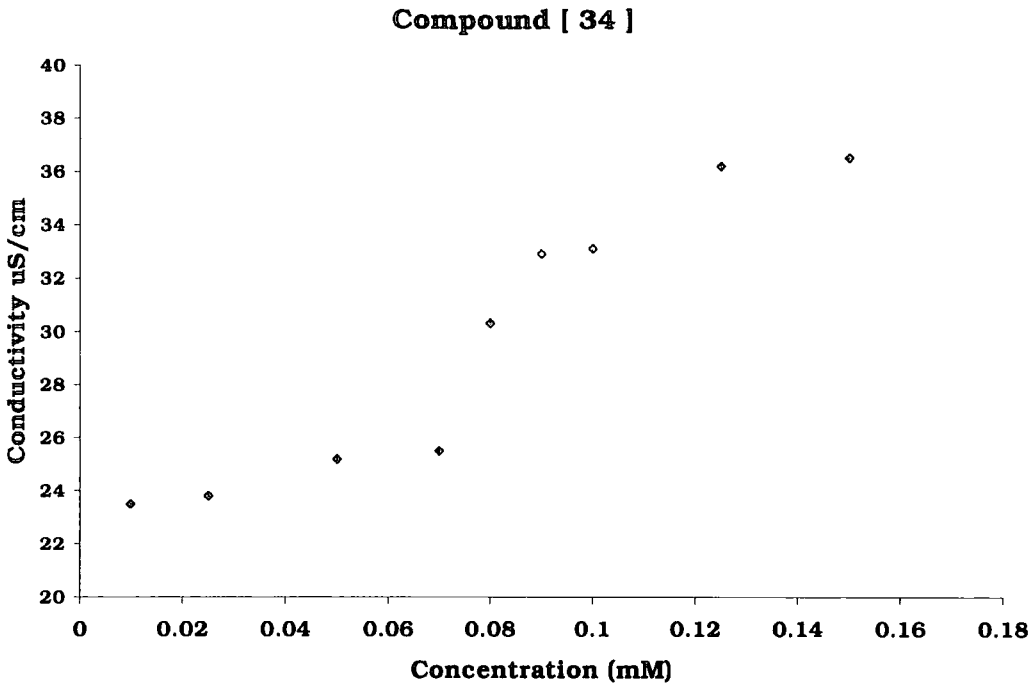

Concentration (mM)	Condictivity (μScm^{-1})
0.010	23.5
0.025	23.8
0.050	25.2
0.070	25.5
0.080	30.3
0.090	32.9
0.100	33.1
0.125	36.2
0.150	36.5

Compound [35]

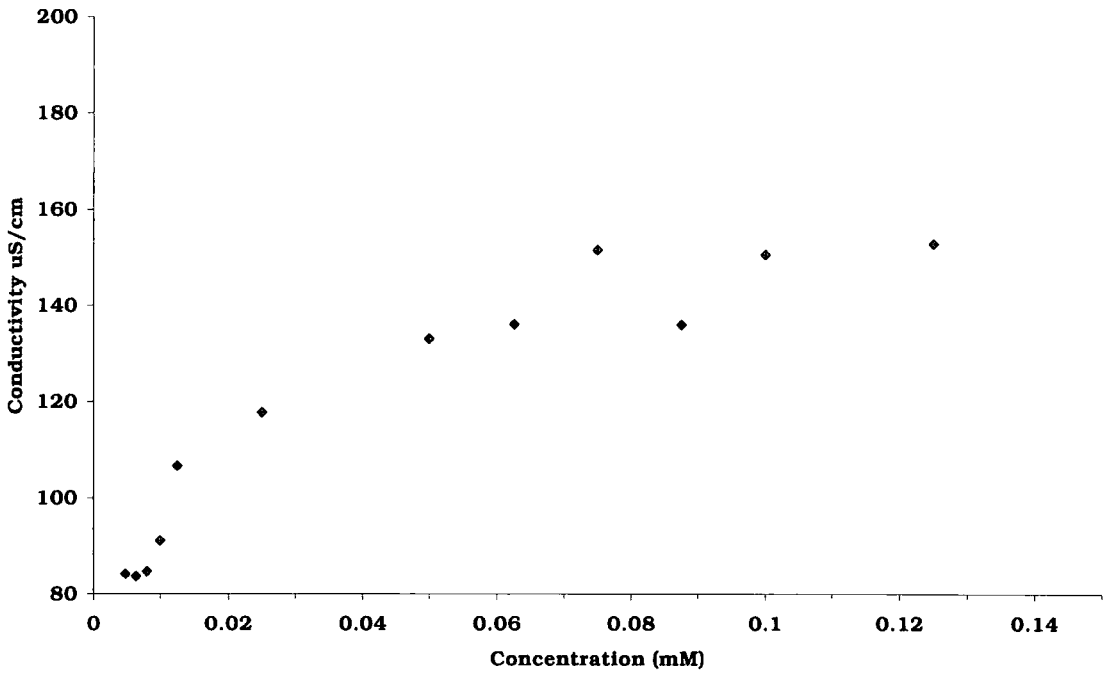

Concentration (mM)	Condictivity (μScm^{-1})
0.0048	84.20
0.0064	83.70
0.0080	84.70
0.0100	91.10
0.0125	106.7
0.0250	117.7
0.0500	133.1
0.0625	136.1
0.0750	151.4

Appendix 3

Courses Lectures and Seminars Attended by the Author October 1999 – October 2002

Lecture Courses Attended 1999/2000

Organometallics in Synthesis

Separation Methods

Practical Spectroscopy

Mass Spectroscopy and NMR Techniques

Departmental Seminars Attended 1999/2002

1999

October 13	Professor G. Fleet, University of Oxford Sugar Lactone and Amino Acids
October 20	Professor S. Lincoln, University of Adelaide Aspects of Complexation and Supramolecular Chemistry
November 10	Dr. I. Samuel, Department of Physics, University of Durham Improving Organic Light Emitting Diodes by Molecular, Optical and Device Design
November 18	Dr. G. Siligardi, Kings College London The Use of Circular Dichrosim to Detect and Characterise Biomolecular Interactions in Solution.
November 23	Professor B. Caddy Trace evidence - a challenge for the forensic scientist
December 8	Professor D. Crout, Department of Chemistry, University of Warwick More than Simply Sweet: Carbohydrates in Medicine and Biology

2000

January 19	Dr. P.R. Fielden, UMIST Miniaturised Chemical Analysis (Lab-on-a-Chip): Functional or Merely Fashionable?

January 26	Professor S. Flisch, University of Edinburgh The challenges involved in protein glycosylation - synthesis of glycan chains and selective attachment to proteins
January 25	Professor B. Meijer From Supramolecular Architecture Towards Functional Materials
March 1	Professor D. Tildsley, Unilever (Head of Research) Computer Simulation of Interfaces: Fact and Friction
March 8	Professor J. Courtieu, Universite de Paris-Sud, Orsay Chiral Recognition through NMR in Liquid Crystal Solvents: an Order Affair
May 5	Professor R. Hochstrasser, University Pennsylvania, USA Ultrafast Molecular and Protein Dynamics seen through their Vibrations
October 25	Dr S.F. Campbell, Former Senior Vice President of Pfizer Science, art and drug discovery. A personal perspective
November 7	Dr C. Ludman, Durham University Explosions - A demonstration lecture
November 8	J.P.L. Cox, Bath University Cosmic: a universal, DNA-based language for communicating with aliens and other intelligent lifeforms
November 29	Professor T. George Truscott, University of Keele Life, Death and the Carotenoids
December 5	Dr D. Kelly, Cardiff University The chemistry of sexual attraction
December 6	Professor Richard Compton, University of Oxford Dual activation approaches to electroanalysis: ultrasound, microwaves and laser activation

2001

January 10	Professor S. P. Armes School of Chemistry, Physics and Environmental Science, University of Sussex Micelles, reversed micelles and shell-crosslinked micelles based on tertiary amine methacrylates
January 23	Professor C. Sterling, Sheffield University Why should the public bother with science anyway?
January 24	Dr Andrew de Mello, Department of Chemistry, Imperial College, London Chemical Integrated Circuits: organic synthesis and analysis on a small scale
February 21	Professor Rob Richardson Department of Physics, University of Bristol Liquid Crystals of All Shapes and Sizes
October 9	Dr Roy S Lehrle, Birmingham Forensics, Fakes and Failures
October 31	Dr Colin Raston, School of Chemistry, Univ of Leeds Towards benign supramolecular chemistry: synthesis - self organisation
November 6	Dr Cliff Ludman, Durham University Explosions - a demonstration lecture
November 20	Professor Peter Atkins A Century of Physical Chemistry
November 21	Dr Roy Copely, GlaxoSmithKline Crystallography in the Pharmaceutical Industry
November 27	Professor Ian G M Cowie, Herriot-Watt University Cellulose - An old polymer with new applications In association with The North East Polymer Association
December 5	Dr Mike Eaton, Celltech Drugs of the Future

2002

February 26	Dr Mike Griffin, Forensic Science Service, Metropolitan Police Smack, Crack, Speed and Weed: A forensic chemists tale
March 12	Professor David Williams, Cardiff Beer and Health: 7000 years of history

Graduate Colloquia, comprising talks by third-year postgraduate students, have been attended each year.

Conferences Attended

Stereochemistry at Sheffield

University of Sheffield 1999

RSC Organic Reaction Mechanisms Group. Winter Meeting 2002

"Mechanistic Aspects of the Design of Bioactive Materials"

University of Manchester January 3 2002

RSC Perkin Group Meeting
University of York April 2002